A role for integrin-linked kinase in oligodendrocyte mediated myelination of the central nervous system

John-Paul Michalski

Thesis submitted to the Faculty of Graduate and Postdoctoral Studies in partial fulfillment of the requirements for the Ph.D. degree in Neuroscience

Department of Neuroscience

Faculty of Medicine

University of Ottawa

ABSTRACT

The interplay between oligodendrocyte (OL) and extracellular matrix (ECM) is critical to the proper maturation of this unique cell type. Recent work has established the β1 integrin-signaling pathway, a mediator for ECM/OL interactions, as an essential component of myelin sheath formation in the central nervous system (CNS). A major downstream effector of β1 integrin is integrin-linked kinase (ILK), an adaptor and structural platform protein. Herein, we (1) generated a model system to study ILK *in vivo* and (2) employed the model to elucidate ILK's role in regulating OL biology.

To assess the importance of ILK in OL-mediated myelination, we ablated ILK in primary OLs. ILK loss delayed morphological maturation and led to filamentous actin accumulation in the processes and cell body. Further, we noted an upregulation in RhoA activity, with pathway inhibition rescuing an OL subset. We next moved our studies *in vivo*. First, we assessed the *proteolipid protein* promoter's utility as OL-specific Cre driver. Protocols established, we generated an ILK conditional knockout line (*Ilk cKO*). Ultrastructural analysis of *Ilk cKO* optic nerves revealed increased number of amyelinated nerve fibers at P14 with subsequent recovery by P28. The observed transient defects were due neither to a loss nor a gain in total number of mature or progenitor OLs. To rationalize recovery, we grew ILK-depleted OLs on an "inert" substrate. Here, while morphology improved, ILK-depleted OLs were characterized by enlarged and sluggish growth cones as well as microtubule disorganization.

Taken together, our data suggests a role for ILK in regulating the morphological maturation of OLs both *in vitro* and *in vivo*, the loss of which results in defective OL

branching and membrane formation with phenotype and subsequent recovery dependent upon niche complexity.

TABLE OF CONTENTS

LIST OF TABLES

CHAPTER 2: THE PROTEOLIPID PROTEIN PROMOTER AS OLIGODENDROCYTE LINEAGE DRIVER

LIST OF FIGURES

CHAPTER 1: GENERAL INTRODUCTION

CHAPTER 2: THE PROTEOLIPID PROTEIN PROMOTER AS OLIGODENDROCYTE LINEAGE DRIVER

CHAPTER 3: INTEGRIN-LINKED KINASE REGULATES OLIGODENDROYTE-MEDIATED MYELINATION OF THE CNS

CHAPTER 4: INTEGRIN-LINKED KINASE REGULATES OLIGODENDROCYTE CYTOSKELETON, GROWTH CONE, AND ADHESION DYNAMICS

CHAPTER 5: GENERAL DISCUSSION

ABBREVIATIONS

AKT: also known as PKB or protein kinase B
APC: adenomatous polyposis coli
Arp2/3: actin-related protein 2/3
BrdU: 5-bromo-2'-deoxyuridine
C: central
CC: corpus callosum
Cdc42: cell division control protein 42 homolog
CER: cerebellum
CNP: 2'3'-cyclic nucleotide 3'phosphodiesterase
CNS: central nervous system
COR: cortex
Cre: causes recombination
DAPI: 4',6-diamidino-2-phenylindole
DIV: days *in vitro*
DR: dorsal root
DRGN: dorsal root ganglion neuron
E: embryonic
ECM: extracellular matrix
EGFP: enhanced green fluorescent protein
ER: estrogen receptor
F-actin: filamentous actin
FAK: focal adhesion kinase
FOV: field of view
GFAP: glial fibrillary acidic protein
GFP: green fluorescent protein
GL: granular layer
GM: grey matter
GSK3β: glycogen synthase kinase 3 beta
IGL: internal granular layer
ILK: integrin-linked kinase
$ILK^{fl/fl}$: ILK floxed homozygote
ILKcKO: integrin-linked kinase conditional knockout
ILKcKO;mT/mG: integrin-linked kinase conditional knockout; TdTomato-EGFP
IPP: ILK/PINCH/Parvin complex
Kid: kidney
LINGO-1: leucine rich repeat and Ig domain containing 1
Liv: liver
Ln-2: laminin-2
MAG: myelin-associated glycoprotein
MBP: myelin basic protein
mT/mG: tdTomato-EGFP (membrane-targeted)
NeuN: neuronal nuclei
NF-200: neurofilament-200
Nrg1: neuregulin-1
N-WASP: neuronal Wiskott-Aldrich Syndrome protein

OL: oligodendrocyte
ON: optic nerve
OPC: oligodendrocyte precursor cell
P(#): postnatal
P: peripheral
PCL: Purkinje cell layer
PFA: paraformaldehyde
PIX: PAK-interacting exchange factor
PINCH: particularly interesting Cys-His rich protein
PIP3: phosphatidylinositol 3,4,5-triphosphate
PLL: poly-L-lysine
PLP: proteolipid protein
PNS: peripheral nervous system
PSA-NCAM: polysialylated Neural Cell Adhesion Molecule
Rac1: ras-related C3 botulinum toxin substrate 1
RhoGTPases: Rho family of small guanosine triphosphatases
RhoA: ras homolog gene family, member A
ROCK: Rho-associated kinase
RT-PCR: reverse transcription-polymerase chain reaction
SC: spinal cord
Spln: spleen
Sr-PLP: somal-restricted PLP
SVZ: subventricular zone
T: transitional
TA: tibialis anterior
TAT-Cre: His-TAT-NLS-Cre recombinase
TdTomato: tandem dimer Tomato
VR: ventral root
VZ: ventricular zone
WASP: Wiskott-Aldrich Syndrome protein
WAVE1: WASP family verprolin-homologous protein 1
WM: white matter
WMT: white matter tract
WT: wild-type

AUTHORIZATION

Figure 1.1 Simplified schematic depicting oligodendrocyte development, figure taken. This figure was taken from (O'Meara et al., 2011a). No permission is required from the publisher or authors (of which I am one), as it falls under the Creative Commons Attribution license.

Figure 1.2.A. Myelin ultrastructure, figure taken and adapted. This figure was adapted from an open access article in PLOS Pathogens, and the Creative Commons Attribution license applies. No permission is required from the authors or publisher, only citation: (Roussarie et al., 2007).

Figure 1.2.B. Myelin ultrastructure, figure taken and adapted. This figure was adapted from two sources; (Nave, 2010a) permission given under license #: 3398470819018 and (Baumann and Pham-Dinh, 2001) which itself adapted the image from (Bunge, 1968). In neither case was permission for reprint required.

Figure 1.3. Myelin sheath genesis, figure taken and adapted. The figure from (Snaidero et al., 2014) was adapted with permission under license #: 3398460355942.

Chapter 2. This is an open access article, and the Creative Commons Attribution license applies. No permission is required from the authors or publisher, only citation: (Michalski et al., 2011).

Chapter 3. The Journal of Neuroscience adopted a License to Publish form. Authors therefore retain material copyright. As well, after 6 months, it falls under the terms for Creative Commons Attribution license. A citation is required: (O'Meara et al., 2013).

ACKNOWLEDGMENTS

I look back on my time in the laboratory as some of the best and most formative years of my life. And while the research holds its own merits, it is the people – family and friends, and those I met along the way – who truly define my experience.

I would like to thank my supervisor, Dr. Rashmi Kothary, for all his advice and support, in times both good and bad. He taught me to think critically, ask questions, and to persist, even in the face of adversity. Thank you Rashmi.

To my labmates, past and present, you were, and remain, great colleagues and friends. You challenged me, you inspired me, and then we drank lots of coffee together. You put a smile on my face every morning, even if, and when, you rolled your eyes. Thank you Carrie Anderson, Ariane Beauvais, Bruno Pinheiro, Sabrina Gibeault, Dr. Hong Liu, Armin Yazdani, Marc-Oliver Deguise, Yves De Repentigny, Dr. Kevin Young, Dr. Lyndsay Murray, Sarah Cummings, Samantha Kornfeld, Dr. James Knight, Mehdi Eshraghi, Dr. Scott Ryan, Anisha Lynch-Godrei, Dr. Karen Lee, Dr. Dina Shafey, Dr. Melissa Bowerman and Dr. Tadasu Sato. And finally, *the core:* Ryan O'Meara, Dr. Andrew Ferrier, Dr. Justin Boyer and Kunal Bhanot.

I would also like to thank the members of my advisory committee, Dr. Steffany Bennett, Dr. Ruth Slack, and Dr. Antonio Colavita, for engaging and lively conversations.

I am grateful to the Multiple Sclerosis Society of Canada, the Canadian Institute of Health Research and the Ontario Graduate Scholarship for support provided throughout my doctoral work.

Last, but certainly not least, my family. To my sister Thea, watching you grow up, and getting married, has been a source of joy. To my brother Nick, your no-

nonsense approach to life has somehow found its way into my research (I think). And to my mum and dad, I love you. This is for you.

Chapter 1
General Introduction

Introduction

Unique to vertebrate biology is the production of myelin by glial cells (Nave, 2010a). In the central nervous system (CNS), oligodendrocytes (OL) are the glial-subtype responsible. Axonal ensheathment by myelin membrane is critical for high efficiency conduction along nerve fibers. Today, we take this knowledge for granted. It is easy to forget, that until the mid-1950's, some researchers believed the myelin sheath to be an axonal creation, and not the natural product of glia (Geren and Raskind, 1953; Geren, 1954; Nave, 2010a). This notion of glia as playing second fiddle, unfortunately, persisted. Often viewed as little more than "glue" holding the nervous system together, OLs have had difficulty in ridding themselves of this namesake and driving interest in the scientific community. Only recently have researchers begun to truly dissect and understand this unique cell type. Advances in imaging technology and model systems have allowed scientists unprecedented access to the OLs inner workings. From roles in axonal maintenance, survival and adaptation (Nave, 2010b; Fünfschilling et al., 2012; Lee et al., 2012b; Gibson et al., 2014; Tomassy et al., 2014) to extracellular matrix (ECM) guided differentiation (Colognato and Tzvetanova, 2011; Lau et al., 2013) and, recently, the precise underpinnings of myelin sheath morphogenesis (Snaidero et al., 2014) our understanding and appreciation of OLs has never been greater.

Here, I begin by introducing the reader to general aspects of OL development – taking the OL from simple bipolar progenitor to fully mature myelin-producing cell. I then focus and finish on a specific aspect of OL biology; its interaction with the ECM and subsequent regulation by the integrin-signaling pathway.

Oligodendrocytes in CNS myelination

From start to finish, the life of an OL is defined by three distinct phases: (1) the birth, migration, and proliferation of oligodendrocyte precursor cells (OPCs), a process occurring in waves, followed by (2) morphological differentiation – the OL establishes an expansive network of processes – and (3) axonal contact, leading to ensheathment and generation of compact myelin around target axons (Figure 1.1).

Oligodendrocyte precursor cells (OPCs)

CNS birthing of the OL lineage occurs in distinct waves through time and space. In the spinal cord, OLs begin life as migrating precursors originating in the ventral ventricular zone at E12.5 (Lu et al., 2002; Richardson et al., 2006). A second wave, though much smaller, follows from the dorsal ventricular zone approximately two days later, with a third, smaller still, arriving postnatally (Cai et al., 2005; Fogarty et al., 2005; Vallstedt et al., 2005; Sevc et al., 2014). Similarly, in the brain, three separate OPC waves (also beginning at E12.5) eventually define the mature OL population. These temporal migrations compete one with the other for space (Kessaris et al., 2006). Importantly, for ideas presented in our own work, these cells clearly display compensatory redundancy – when any single wave is destroyed, OPCs present before or after fill the void and development proceeds unaffected (Kessaris et al., 2006). Interestingly, the idea of "oligodendrocytes at war", either as competition between populations or individual cells, appears thematic of OL biology (Richardson et al., 2006). For example, the CNS produces an overabundance of OPCs across all regions during development. A large percentage then die during the myelination process, as the cells "fight" for limited axonal/astrocytic survival factors (Barres et al., 1992; Trapp et

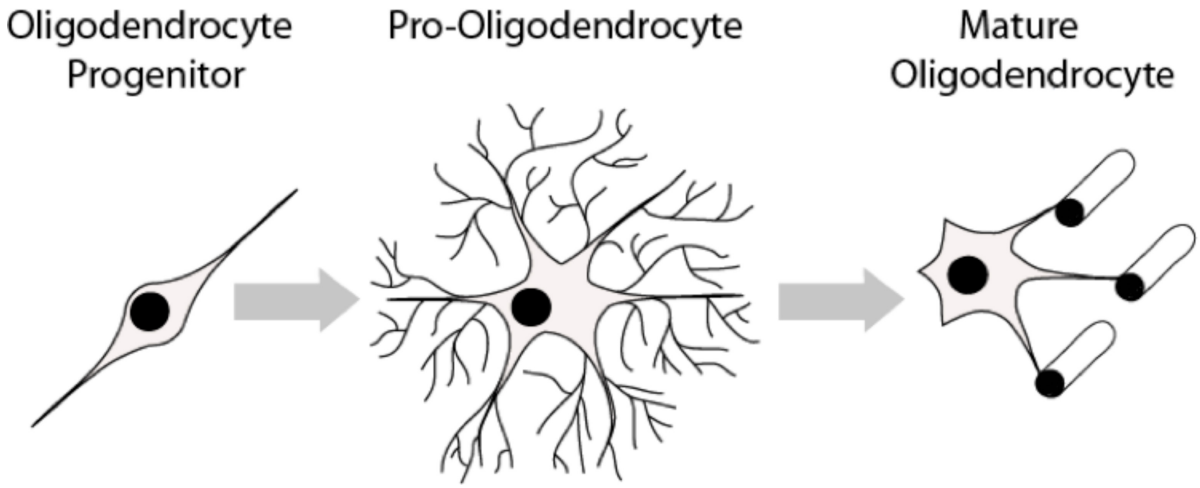

Figure 1.1. Simplified schematic depicting oligodendrocyte development. The OL begins life as a migrating bipolar cell. As it matures, the OL extends a branched network. First primary, then secondary and tertiary processes appear, generating a highly complex cellular morphology. Processes contact nude axons, triggering a myelination event. The OL membrane wraps the axon in concentric layers, while cytoplasm is simultaneously expelled and mature myelin is generated. The final product is a myelin internode, an insulating membrane necessary for signal propagation along the axon. For more on myelin sheath generation, see Figure 1.2 and 1.3. (Taken from (O'Meara et al., 2011a)).

al., 1997; Barres and Raff, 1999). In zebrafish, OPC laser ablation results in local expansion of neighboring progenitors. Through process extension, OPCs first sample then settle the vacated space, thereby maintaining a progenitor landscape primed for myelination (Kirby et al., 2006). Clearly, mechanisms have evolved which allow effective myelination capacity even under duress. As we will see, we can expand the idea to include mature myelin-producing OLs, as they race, one against the other, for denuded axons.

A substantial number of OPCs persist in the adult brain. Here, they comprise the largest population of dividing cells, each subsisting within its own unique non-overlapping domain (Dawson et al., 2003; Hughes et al., 2013). Again, in the vein of competition and balance, recent work from the Bergles laboratory beautifully captures the adult OPC population in a state of controlled equilibrium (Hughes et al., 2013). With the aid of reporter mice and cranial windows, live recorded OPCs were shown to exist within unique spatial pockets, established through inter-repulsive cues with other progenitors. OPCs were highly exploratory, sampling their environment in search of unoccupied space. OPC loss led to rapid invasion/division by neighboring progenitors, ensuring a spatially crafted balance in the aged brain (similar to what is seen during development (Kirby et al., 2006)). It paints the picture of a web-like network, with unique micro-domains strung throughout. Pulling on any "string" triggers local, or in the case of injury, global reverberations, thereby forcing a response – be it proliferation, migration or repair.

While functional nuances for the progenitor cells abound, (and remain highly debated) they are generally thought responsible for myelin maintenance, both in normal and diseased brains (Rivers et al., 2008; Kang et al., 2010; Young et al., 2013). In the non-diseased brain, OPCs are actively recruited for myelin remodeling, and possibly, *de novo* myelination (Young et al., 2013). Here, they replace naturally dying OLs, generating myelin

for white matter tract maintenance following turnover, or, in the case of *de novo*, are thought to be molded in response to adaptive neural plasticity. In support of *de novo* adaptation, stimulated, and therefore electrically active neurons have recently been shown capable of driving OPC proliferation and oligodendrogenesis *in vivo*. The change in myelin capacity within the activated circuit, in this case, the premotor cortex, led to motor improvement (Gibson et al., 2014).

Intriguingly, relative to developmental "early" OPCs, "late" adult OPCs are capable of myelinating a greater number of axons but to a lesser degree (Young et al., 2013). Remyelination, often the focus of disease research, is also characterized by an overall decrease in myelin capacity (Blakemore and Murray, 1981; Franklin and Ffrench-Constant, 2008). Researchers have therefore suggested that the observed decrease in myelination capacity following a demyelinating event is not necessarily injury-related, but, rather, showcases the aged cells increasingly limited potential to myelinate (Young et al., 2013).

Oligodendrocytes: from immature to mature myelin-producing cell

OPC differentiation is a relationship with increased complexity. The cell is required to produce an astronomic volume of membrane over its lifetime. It is this mixture of complexity and expansion, first in branching and then membrane, that allows a single mature OL to produce upwards of 50 myelin sheaths (Chong et al., 2012). The gamut of differentiation, presented in a simplified manner, occurs as follows: in early stages, the OL extends multiple highly ramified processes that contact nude axons and trigger myelination. Process tips are dynamic, and while once considered simple filopodia, there is now recognition within the field for "growth cone-like" structures directing, guiding and retracting the developing branched network (Fox et al., 2006). The OL process expands upon

axonal contact, wrapping the axon in concentric layers of membrane. The membrane compacts, expelling cytoplasm, and mature myelin is born (Snaidero et al., 2014). Individual myelin segments, still connected to the OL soma, are termed internodes. Unlike most schematics depicting sheaths as uniform and ordered, internodes originating from a single OL vary wildly in orientation and length even among neighboring OLs (Chong et al., 2012). The unmyelinated space between internodes forms the node of Ranvier (often referred to simply as "nodes") (Figure 1.2A). It is here that axonal signal propagation and current flow are maintained through membrane depolarization by high density voltage-gated sodium channels, as the signal hops from node to node (Nave, 2010a).

Myelin compaction

Compact myelin itself has a rather unique architecture as classically captured through electron micrographs. Here, concentric layers of compacted myelin encircle the axon. The innermost layer consists of an uncompacted inner tongue, and the outermost a similar uncompacted outer tongue (although, as we will see later, the inner tongue, and not the outer, is the engine driving radial myelination). The myelin's lateral edge forms cytoplasm-heavy paranodal loops, which align and define the myelin-nodal border (see Figure 1.2 for detailed schematic of myelin structure) (Nave, 2010a).

Myelin compaction is driven in large part by myelin basic protein (MBP). Often compared to a spring, the protein binds opposing inner membranes drawing the two faces together. MBP then clusters into a dense fibrillary network. Likened to nuclear pores, the clustering dams access, creating a threshold above which molecules of a certain size are unable to pass. Thus, local protein mobility and eventually concentrations are drastically

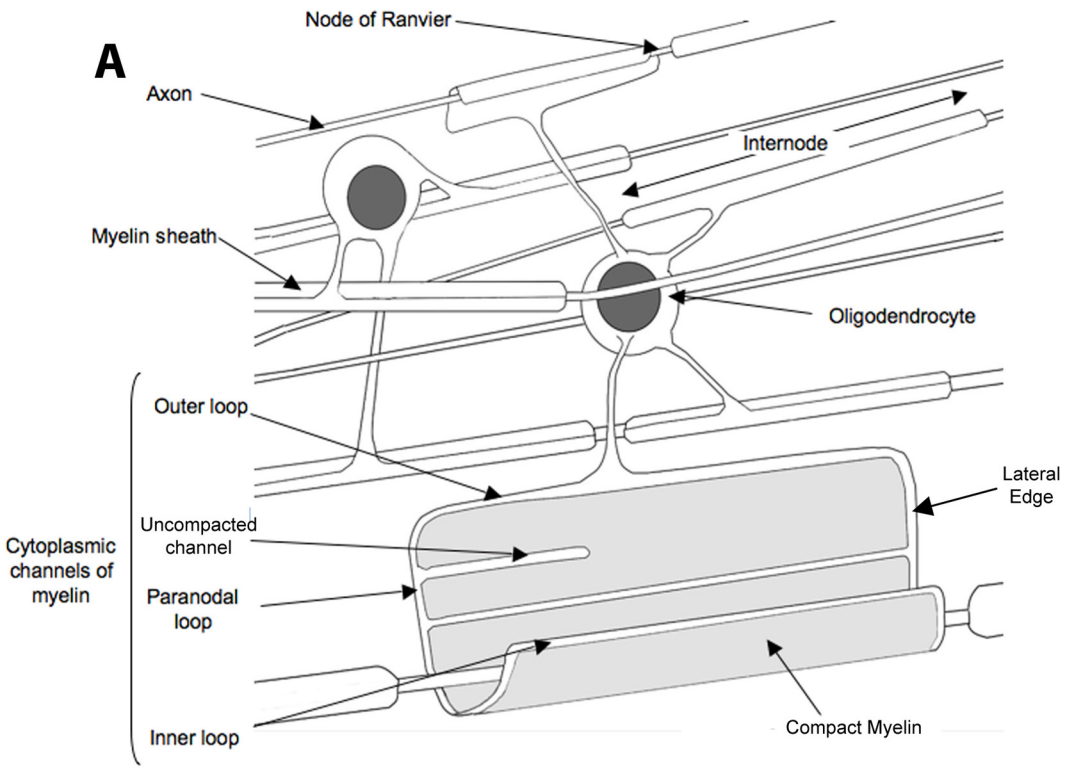
A
Node of Ranvier
Axon
Internode
Myelin sheath
Oligodendrocyte
Outer loop
Lateral Edge
Uncompacted channel
Cytoplasmic channels of myelin
Paranodal loop
Inner loop
Compact Myelin

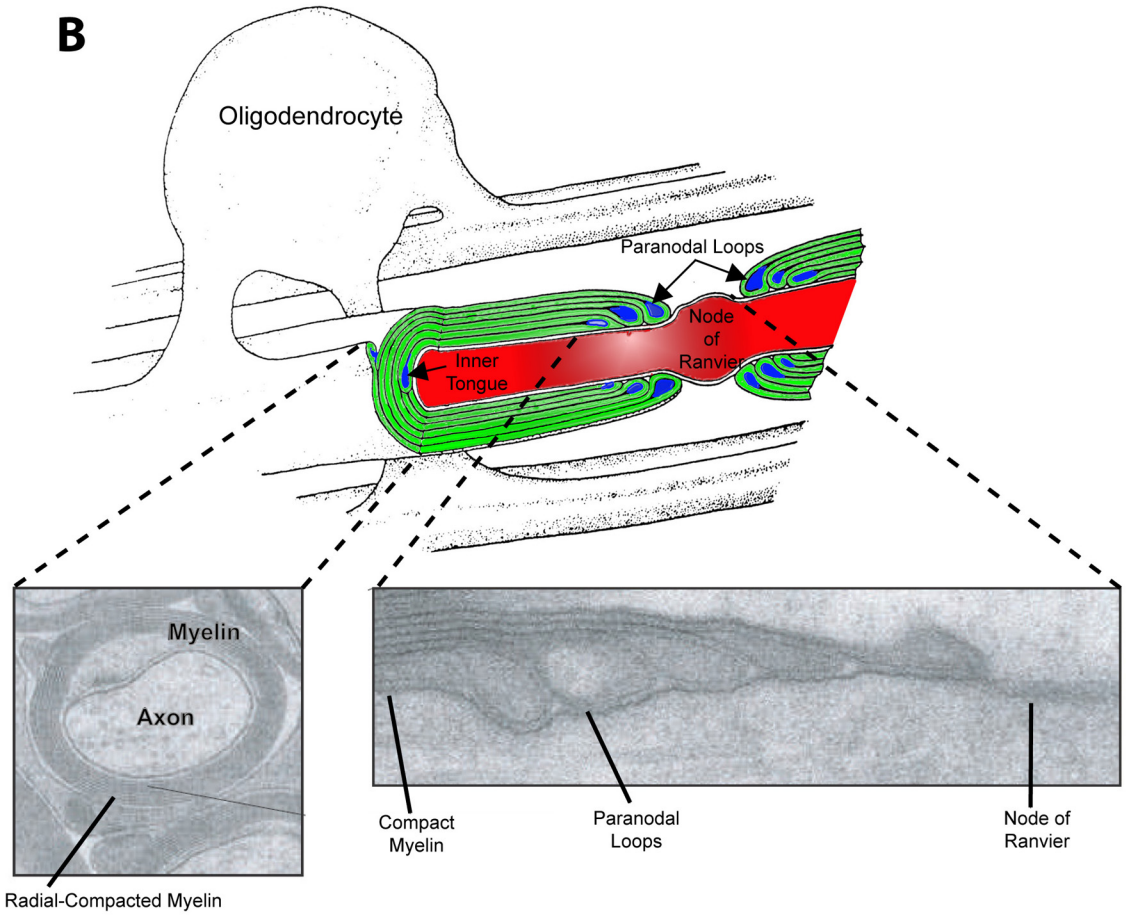
B
Oligodendrocyte
Paranodal Loops
Node of Ranvier
Inner Tongue
Myelin
Axon
Radial-Compacted Myelin
Compact Myelin
Paranodal Loops
Node of Ranvier

Figure 1.2. Myelin ultrastructure. A. A single oligodendrocyte extends multiple processes and forms internodes. Unmyelinated space between myelin segments generates nodes of Ranvier. Depicted are various uncompacted cytoplasmic channels within the unfurled sheath. The myelin contour is defined by a thin strip of uncompacted membrane. On either end is the lateral edge, which forms the paranodal loops. The central and leading edge form the inner loop/tongue. Recent evidence demonstrates cytoplasmic channels running through compacted myelin, allowing transport to the membrane's leading edge. **B.** Depicted in blue is cytoplasm from uncompacted regions - the inner tongue and paranodal loops. The paranodal loops align at the nodes of Ranvier. Condensed myelin is in green, and axon in red. Below are electron micrographs representing structures on display in schematic (Figure A taken and adapted from (Roussarie et al., 2007), Figure B top taken and adapted from (Baumann and Pham-Dinh, 2001) and bottom (Nave, 2010a).

reduced (Aggarwal et al., 2011, 2013; Bakhti et al., 2014). MBP deficient mice, an extremely well-studied dysmyelination model, do not produce compact myelin (Readhead et al., 1987; Schain et al., 2014).

Unsurprisingly, compact myelin is relatively devoid of cytoskeleton (Bauer et al., 2009; Aggarwal et al., 2011; Snaidero et al., 2014). In the absence of actin and tubulin, engines of morphological change (as well as most other proteins), the sheath appears in the desired static state. Although, as we shall see, this is somewhat of an illusion – the engine can be rekindled and myelin profiles can change in response to a shifting environment (Gibson et al., 2014; Snaidero et al., 2014).

The cytoskeleton in oligodendrocytes and myelin membrane

Such radical morphological change, from bipolar to myelin producing cell, demands a dynamic cytoskeleton. The OL houses two major cytoskeletal components: microtubules and microfilaments (the latter will hereafter be referred to as F-actin) (Bauer et al., 2009). Independently or in tandem, they form adaptive structures and give rise to an underlying architecture prepared for rapid and sustained growth. Both components are expressed to varying degrees and within distinct regions at all stages of morphological differentiation *in vitro* (due to their ubiquitous nature, direct assessment *in vivo* is rare). In the coming section, we will explore their role in process outgrowth and myelin membrane formation, as well as describe numerous regulatory proteins governing their function.

The cytoskeleton: F-actin and microtubules

In the immature OL, F-actin is highly concentrated at the process's leading edge. The edge itself appears similar to a growth cone's; it is formed of lamellipodia and filopodia, the latter extruding the surface (Rumsby et al., 2003; Fox et al., 2006). Splayed microtubules sit behind this highly active front. They invade from the more stable primary processes, themselves replete with bundled microtubules (Lunn et al., 1997; Song et al., 2001; Bauer et al., 2009). As the OL matures, and morphological complexity increases, microtubules display increasingly high levels of acetylated α-tubulin, leading to long term stability for both microtubule and the process it inhabits (Song et al., 2001; Lee et al., 2005; Li et al., 2007). Taken together, cytoskeletal-mediated growth can be envisioned as follows: an F-actin rich OL "growth cone" leading the way, laying down a "track" for microtubules and the process to follow. As the cell matures, tubulin is acetylated, microtubules are stabilized, and the dense branched network maintained (Lunn et al., 1997; Song et al., 2001; Bauer et al., 2009).

As discussed, a shift from process outgrowth to membrane production results in a progressively sparse cytoskeleton. Following membrane compaction (in culture), F-actin is relegated to the cells periphery, a region containing uncompacted membrane, (a potential correlative for cytoplasm heavy structures *in vivo*, such as the inner tongue) (Dyer and Benjamins, 1989a; Bauer et al., 2009; Aggarwal et al., 2011; Snaidero et al., 2014). Microtubules hold out longer, forming a dense pattern of cytoplasm rich tendrils that snake between larger pockets of compact membrane (Dyer and Benjamins, 1989a, 1989b; Boggs and Wang, 2001). However, as the membrane continues to mature, microtubules are removed and the final product, a fully compact myelin sheath, is relatively devoid of both cytoskeletal components (Dyer and Benjamins, 1989a; Boggs and Wang, 2001, 2004; Bauer et al., 2009; Aggarwal et al., 2011).

The cytoskeleton: F-actin and microtubule regulating proteins

The OL's leading edge is home to numerous F-actin assembly and remodeling proteins, such as the Arp2/3 complex, N-WASP, WAVE1, myosin II and the small Rho GTPases Rac1, Cdc42 and RhoA (Song et al., 2001; Fox et al., 2006; Kim et al., 2006; Bacon et al., 2007; Wang et al., 2012). Bit by bit, researchers have identified often unique and opposing roles for each, demonstrating a malleable and responsive OL cytoskeleton.

The WASP family members N-WASP and WAVE1, through interactions with Arp2/3, generate branched F-actin networks at the cell's leading edge (Ridley, 2011). WAVE1 deficient OLs form fewer processes, and those formed lacked discernable tip lamellipodia (a growth cone-like structure was lacking) (Kim et al., 2006). *In vivo*, WAVE1 loss translated as fewer myelinated axons, while myelin thickness remained unaffected (Kim et al., 2006). Similarly, chemical inhibition of N-WASP (unable to activate Arp2/3) led to defects in OPC process extension and filopodia retraction. The cells also failed to initiate axonal ensheathment in chemically treated optic nerves (Bacon et al., 2007). Surprisingly, loss of either Rac1 or Cdc42 did not manifest any overt morphological defects in culture. Instead, OL-specific conditional knockouts displayed abnormal cytoplasmic accumulation in the myelin membrane's inner tongue (Thurnherr et al., 2006). These seemingly anomalous findings fit with recent work describing myelin's F-actin rich inner tongue (one of the only structures sporting this cytoskeletal component in actively developing myelin *in vivo*) (Snaidero et al., 2014). During active myelination the tongue is swollen and, as the myelin and animal matures, the tongue shrinks and F-actin is lost (Snaidero et al., 2014). Control of tongue size is dependent on phosphatidylinositol 3,4,5-triphosphate (PIP3) levels, a pathway that governs spatial activation of Rho GTPases (Snaidero et al., 2014; Hanna and El-Sibai, 2013). Regulation of Rac1 and/or Cdc42 levels or localization could therefore provide a

mechanism for controlling tongue morphology through F-actin reorganization. It remains to be seen whether they are directly involved, although their loss, leading to tongue swelling, strongly suggests it.

In stark contrast, RhoA, through its downstream effector Rho-associated kinase (ROCK), inhibits OL morphogenesis (Wolf et al., 2001; Liang et al., 2004; Kippert et al., 2009; Rajasekharan et al., 2010; Wang et al., 2012). RhoA/ROCK's role as morphogenic inhibitor is largely attributable to its activation of myosin II, which, in turn, leads to actomyosin based hyper-contractility (Wang et al., 2008, 2012; Kippert et al., 2009). The RhoA/ROCK/myosin II pathway is thought to act as gatekeeper for myelinating events – differentiation is triggered through downregulation of RhoA/ROCK's activity, which loosens contractile forces and allows the OL to extend and eventually form membrane (Bauer and Ffrench-Constant, 2009; Rajasekharan et al., 2010; Wang et al., 2012).

Microtubule associating and/or binding proteins are also present in the OL (Bauer et al., 2009). One of the more intriguing is 2',3'-cyclic nucleotide 3'phosphodiesterase (CNP), a canonical myelin protein required for process outgrowth (Lee et al., 2005). Often used as a general marker for immature OLs, CNP binds tubulin heterodimers and drives microtubule assembly (Lee et al., 2005). Strikingly, when exogenously expressed in nonglial cells, radical morphological change ensues; the cells extend highly branched OL-like processes, microtubules bundle along the process length, and the F-actin network undergoes complete reorganization. In the case of actin, stress fibers are lost and growing processes, tipped with F-actin rich lamellipodia and filopodia, are formed (Lee et al., 2005).

Fortunately, CNP's high level expression is normally restricted to myelinating cells, as it appears necessary for a relentless drive to growth (Lee et al., 2005; Bauer et al., 2009). In nascent myelin, CNP is localized to "loose" uncompacted wraps (Yin et al., 1997;

Snaidero et al., 2014). Overexpression leads to exuberant process outgrowth and myelin production, followed by myelin compaction failure (Gravel et al., 1996; Yin et al., 1997). Recently, researchers have proposed a necessary equilibrium between CNP's drive for growth and MBP's desire to compact and stabilize the membrane (Snaidero et al., 2014). By playing one against the other, the OL ensures copious generation of "active" and "loose" membrane followed closely by membrane zippering, a final act in establishing compact myelin.

Mechanisms of myelination

The past decade has seen advances in imaging technology and techniques, as well as transgenic modeling, advances that have generated remarkable insight into the mechanical underpinnings of OL biology. Below I detail some of the more interesting findings as they relate to myelin sheath genesis, OL adaptability and sculpting of the myelin landscape.

All wrapped up: mechanics of radial ensheathment and adaptive change

For the longest time, myelin wrapping was taken for granted. While we were aware of the final product – compact layers of myelin – concepts for mechanics involved were often best guesses or suppositions. Questions, such as the identity of the sheath's leading edge, or initial direction of growth – inward or outward, radial or lateral – were left unanswered. Over the years, various models have been proposed, chief among them the "carpet-crawler" (Bauer et al., 2009; Snaidero et al., 2014). Here, the OL process, having contacted an axon, spreads laterally, stretching the length of the to-be-formed internode. Then, like rolling a carpet, the membrane loops under itself with progressive radial layers

built one atop the other. Newer models both support and contradict varying aspects of the "carpet-crawler" (Pedraza et al., 2009; Sobottka et al., 2011). Contention focused on whether myelin (1) wraps first as a relatively thin structure, and then expands laterally across the axon, (2) laterally first, as seen in the "carpet-crawler" model, followed by radial wrapping or (3) a mixture of the two. Like so much in life, the answer appears to be a little of both.

In a study published this year in *Cell*, Snaidero and colleagues reconcile conflicting points of view and offer a comprehensive vision for wrapping mechanics (Snaidero et al., 2014). The difference-maker, again, rests largely with imaging technology and improved experimental technique. Whereas those before used primarily fluorescent microscopy, the authors employed pressure-freezing technology to preserve exquisite resolution of fine myelin structure. Three-dimensional myelin sheaths were then reconstructed from serial electron micrographs, and sheath minutiae explored. The authors were able to track the ensheathment process from beginning to end (see Figure 1.3). As they describe, OLs first form a triangular membrane at axonal point of contact. Membrane expansion and wrapping then proceeds in a coordinated bi-directional motion: both radially and laterally. Driving radial ensheathment is an F-actin rich inner tongue, originating at the initial point of contact. The tongue pushes under pre-existing membrane, and remains juxtaposed with the axolemma, wrapping the axon in progressive layers. In tandem, all myelin being generated moves laterally. The lateral edge, similar to the inner tongue, remains uncompacted and in constant contact with the axon. As myelination progresses, each layer's lateral edge halts at the nodal border, leading to the sequential generation of paranodal loops one behind the other (Figure 1.3E). Membrane compaction then begins in the outermost layers, moving inexorably inwards as the system matures. The unprecedented resolution also allowed

identification of cytoplasmic channels running throughout compacted myelin (Figure 1.3C). The channels were shown to traffic materials for sustained growth at the leading edge. The authors also demonstrated capacity within the system for inner tongue reactivation and cytoplasmic channel reappearance, leading to thickening of the pre-existing myelin. The effect is PIP3-dependant, a pathway whose members are capable of driving OL maturation, as well as inducing hypermyelination in the adult brain (Flores et al., 2008; Narayanan et al., 2009; Goebbels et al., 2010; Snaidero et al., 2014).

That mature OLs retain the capacity to drive further ensheathment fits perfectly the picture of white matter as adaptive and plastic. Recent evidence suggests reshaping of the myelin landscape occurs not only through *de novo* events or replacement of dying OLs (see section on OPCs), but through plasticity in the myelin sheath itself. In mice, forced activation of motor neuronal circuitry by means of optogenetic stimulation leads to increased myelin thickness in the stimulated region (these were the same experiments that demonstrated increased OPC proliferation and oligodendrogenesis discussed previously) (Gibson et al., 2014). A gain in associated motor outcome was also dependent on increased myelin thickness – it was lost when the OLs ability to produce myelin membrane was inhibited (although, it must be noted, the authors were unable to decidedly prove whether the thicker myelin was not simply the result of *de novo* myelination of previously unmyelinated axons) (Gibson et al., 2014). In contrast, areas of the pre-frontal cortex are thinly myelinated when mice are kept in isolation during critical periods of development (Makinodan et al., 2012). A similar thinning of myelin is observed in isolated adult mice, with social re-introduction leading to up-regulation of myelin gene expression (Liu et al., 2012). It is clear that OLs and the myelin they produce carry the tools to respond to shifts in higher order systems. Alterations in myelin thickness could mold signal speed in response to social and motor

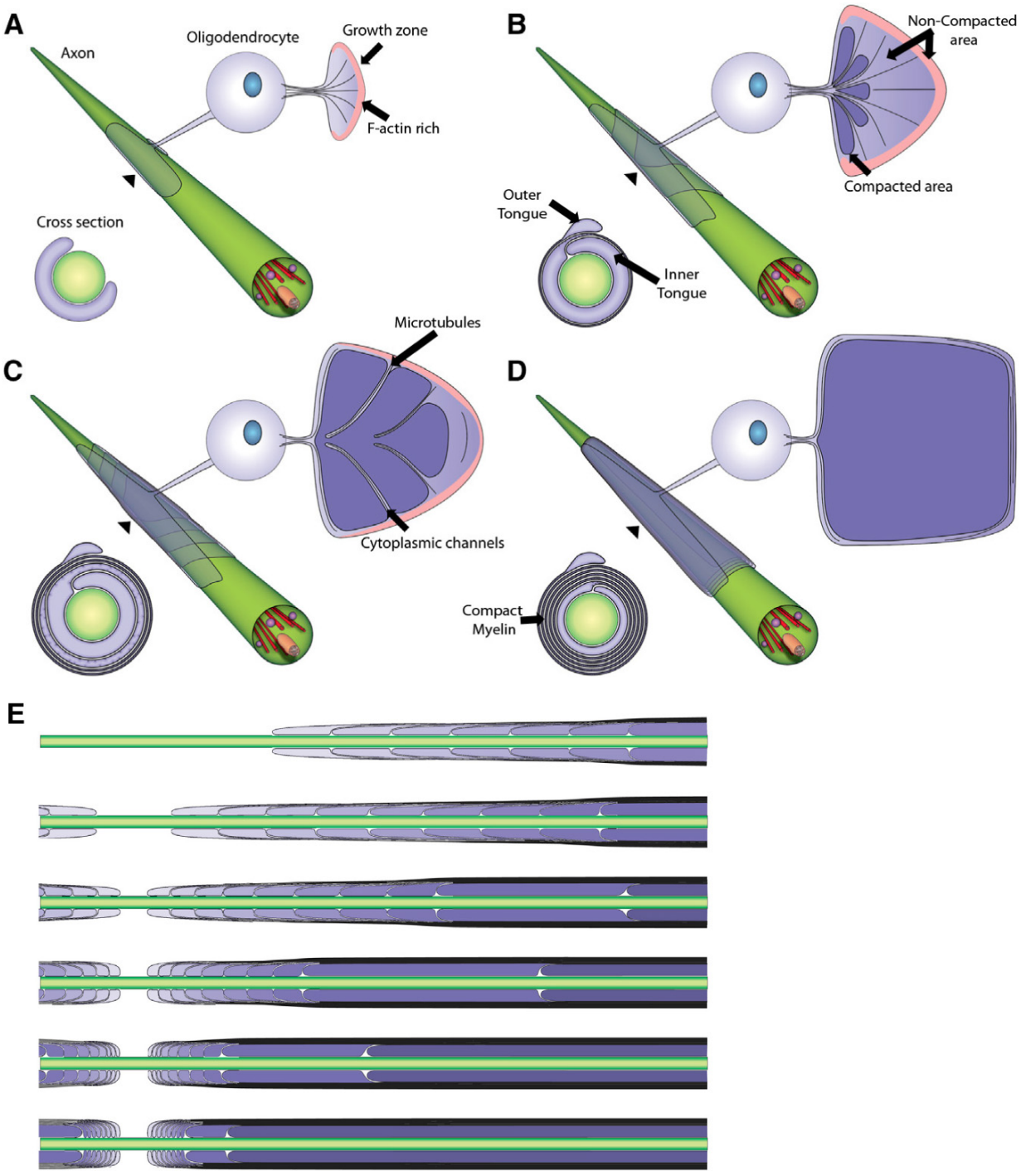

Figure 1.3. Myelin sheath genesis. A. The OLs process, having contacted the axon, forms a triangular-shaped membrane. This forward edge is responsible for myelin growth and gives rise to the inner tongue **B.** Growth proceeds in two directions: radially and laterally through leading and lateral edges of the developing membrane. The leading edge, now the inner

tongue, pushes under previously laid membrane and continues to encircle the axon. Myelin compaction begins in the outermost membrane layers. **C.** Cytoplasmic domains run through compacted myelin. Components for membrane building can be delivered along microtubule tracts to the distal leading edge. **D.** In fully mature myelin, the vast majority of cytoplasmic domains are removed. The uncompacted inner tongue, lateral edges and outer tongue remain. All other cytoplasm has been expelled. **E.** Lateral expansion and alignment of myelin layers at node. Over time, the paranodes are formed from the lateral edges. (Taken and adapted from Snaidero et al., 2014).

adaptation, adding another layer of control to an already highly refined system.

To myelinate or not: deciding to form internodes

But what of switches regulating OL development: specifically, how does an OL choose to myelinate an axon? It is an interesting question, as OLs undergo almost all phases of differentiation when cultured in isolation, and importantly, in the absence of axons. In fact, OLs are more than willing to myelinate fixed "dead" axons or engineered nanonofibers (Rosenberg et al., 2008; Lee et al., 2012a, 2013). Further, the "dead" axons are myelinated to the same extent as the living, suggesting that dynamic exchange between OL and axon is not necessary for myelination to proceed (Rosenberg et al., 2008; Lee et al., 2012a). This data points to a system whereby OLs are relatively autologous in their drive to undergo differentiation, and will produce myelin given a suitable scaffold. But this is not to say myelination occurs without reason or is "brainless". First, axon size regulates temporal order of myelination, with larger axons preceding smaller, both *in vivo* and in nanofiber cultures (Almeida et al., 2011; Lee et al., 2012a). A single OL will also myelinate more small axons relative to large (Almeida et al., 2011). In deciding which axons to myelinate, the OL further displays incredible adaptability. When zebrafish are manipulated to produce a greater number of large axons, OLs respond in kind by producing a greater number of sheaths (Almeida et al., 2011). This effect is not due to complementary increase in OL number, rather, normal myelination is achieved through adaptive change in OL morphology – the same OL simply extends more processes (although, it must be said, a massive increase in total axon number does seem to precipitate a concomitant increase in OL number (Burne et al., 1996)). There is also clear competition for axonal space between neighboring OLs – by reducing OL density, the number of internodes generated by any given OL increases (Chong

et al., 2012). The effect seems mediated by repulsive OL membrane bound cues, which allow for coordinated non-overlapping internode formation. Loss of one such cue, Nogo-A, results in increased myelination potentiation with associated exuberant myelin internode formation *in vivo* (Chong et al., 2012). Importantly, even here, the final global myelination pattern in the adult is no different with or without the restrictive cue. Rather, it leads to premature myelin expansion with an associated decrease in total mature OL number. This effect is most likely due to a percentage of the population rendered redundant as they are outcompeted for denuded axons by uninhibited neighbors.

But just how plastic is internode formation? While evidence overwhelmingly suggests ongoing myelination throughout life, the question remains: can mature OLs continue to generate internodes as the CNS requires? Recent live imaging experiments suggest that this is not the case. Instead, dynamic internode formation (the time allocated an OL to lay its first and last sheath) is limited to a temporal window – approximately 5 hours in zebrafish – after which time, barring a small number of myelin sheath retractions, internode number and OL morphology remain static (Czopka et al., 2013). Even when the ability of OLs to generate internodes is altered (increased and decreased) through manipulation of Fyn kinase – a key integrator of multiple axo-glial signaling pathways regulating OL myelination potential through RhoA/ROCK – still the time constraint is in effect (Umemori et al., 1994; Liang et al., 2004; Laursen et al., 2009; Rajasekharan et al., 2009; Wake et al., 2011; Czopka et al., 2013). Coupled with the data on shifting myelin sheath thickness in the adult brain (see previous section), a general model emerges: newly generated OLs (both in developing and adult organisms) can adapt to their environment and produce the requisite number of sheaths within a relatively narrow time frame. Subsequent adaptive requirements placed on the

mature OL, say, in response to social and motor behavioral change, can then be made through alterations to the myelin sheath itself.

Sculpting the myelin landscape

The OL is clearly an adaptive cell, able to respond even when presented shifting axonal numbers and size. But myelination is also a process of pruning and sculpting, a fine-tuning of the OLs underlying need to myelinate, as seen through distinct myelin patterning and profiles in the brain (Tomassy et al., 2014). It therefore becomes a question of balance; playing factors that inhibit and cut from the growing OL against local cues that serve to boost speed or extent of myelination. Many such signals have been identified and studied, for example, ligands and secreted molecules present on axons and/or the OL itself, as well as molecules in the OLs environment (the ECM). Some are inhibitory, such as Nogo-A (which we have already discussed) (Chong et al., 2012), LINGO-1 (Mi et al., 2005), and PSA-NCAM (Charles et al., 2000). Loss of any results in premature and exuberant myelination (Charles et al., 2000; Mi et al., 2005, Chong et al, 2012). Then there are the enhancers and drivers of myelination. While no single molecule has yet been named a master regulator, there is direct evidence for various axonal ligands or secreted substances, such as glutamate and/or Neuregulin-1 (Nrg1), in regulating OL differentiation and extent of myelination (Brinkmann et al., 2008; Wake et al., 2011; Makinodan et al., 2012). Glutamate ties in nicely with a paradigm for circuit activation, wherein stimulation and axon firing, resulting in the neurotransmitters release, signals to the OL that the axon is ready to myelinate (Charles et al., 2000; Wake et al., 2011). Nrg1's story in the CNS is slightly more convoluted. For Schwann cells (the peripheral nervous system's myelinators), Nrg1 is absolutely critical for myelination (Michailov et al., 2004; Taveggia et al., 2005). However, defying expectations, a

similar narrative did not evolve in the CNS. While controversial, disruption of the Nrg1 pathway had minimal impact on overall CNS myelination (Brinkmann et al., 2008). Rather, it was its overexpression that gave rise to a phenotype: an increase in total number of myelinated axons (which the authors attribute to increased internodal length) coupled with hypermyelination (more myelin wraps) (Brinkmann et al., 2008). Interestingly, the later observation supports recent findings for mice kept in isolation (see previous section "All wrapped up"). Isolation leads to myelin thinning in the prefrontal cortex, a phenomenon replicated by loss of Nrg1's receptor, ErbB3 (Makinodan et al., 2012). Further, social isolation itself led to decreased Nrg1 expression (Makinodan et al., 2012). However, the signals discussed above appear mostly to enhance myelination, or lead to subtle shifts, rather than dictate the process. Other systems of management must be at play – a necessity to account for the array of adaptive behavior required during myelination. Among these, the integrin-signaling pathway, governing the interaction between OL and cellular milieu, has come to the fore as a critical regulator of OL development.

The integrin-signaling pathway in oligodendrocytes

The interaction between ECM and OL, its role in mediating initiation and extent of myelination, has garnered much attention (Colognato and Tzvetanova, 2011). Key among these is activation of the integrin signaling pathway by ligands present in the local environment (Figure 1.4) (Colognato et al., 2004; Lee et al., 2006; Câmara et al., 2009; Laursen et al., 2009; O'Meara et al., 2011a). In the coming sections, we will explore discoveries at all levels of the pathway as they relate to OL-mediated myelination.

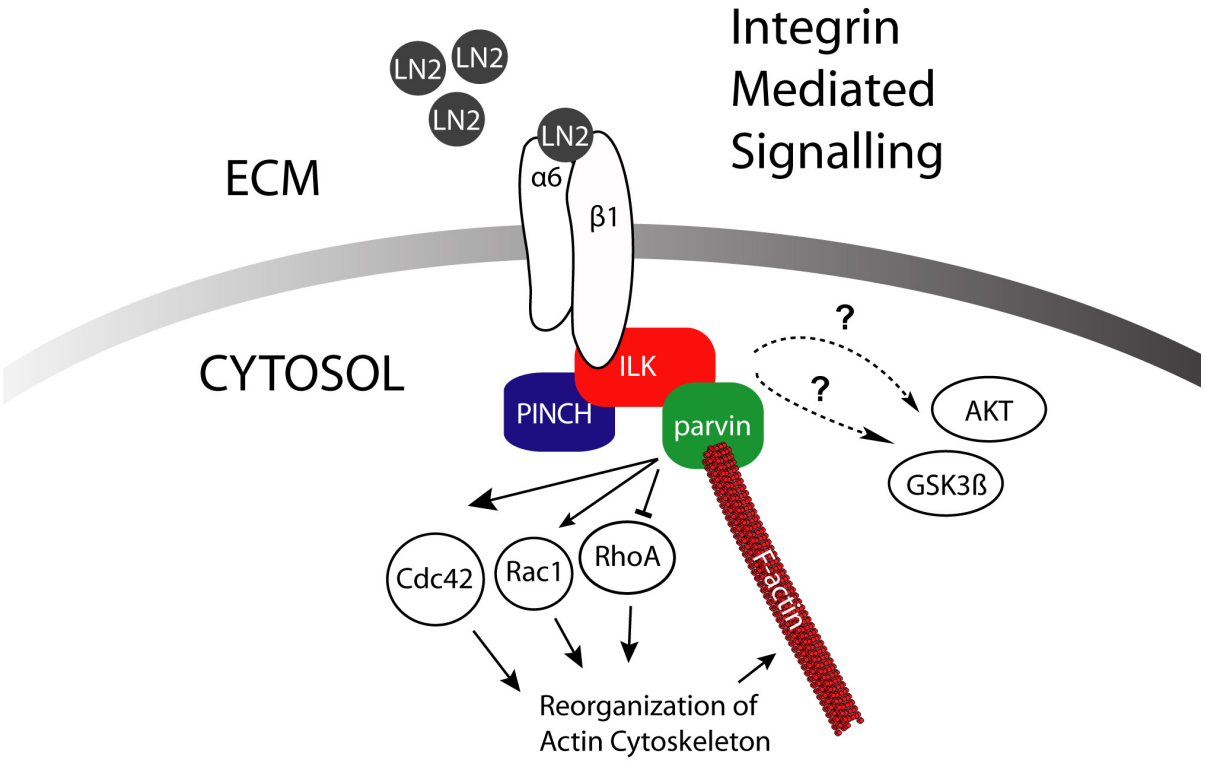

Figure 1.4. The integrin-signaling pathway in oligodendrocytes. Ln-2 present in the ECM binds α6β1 integrin leading to receptor activation. ILK, along with obligate binding partners PINCH and parvin, binds β1 integrin's cytoplasmic tail. Here, it acts as a link between integrins and cytoskeleton. For example, ILK can recruit proteins leading to the activation or suppression of various Rho GTPases. ILK is also purported to have kinase activity, with AKT and GSK3β as substrates. However, more recent evidence suggests ILK is a pseudokinase, and instead controls phosphorylation levels through recruitment of other proteins to the growing complex.

Integrating signals: laminin-2 and fibronectin

Integrins, some of the most well-studied adhesion-mediating receptors in biology, are responsible for bridging the gap between ECM and cellular cytoskeleton. Existing as heterodimeric proteins – composed of α and β subunits – they act as signal transducers, both to and from the cell. As transducers, integrin activation modulates a slew of intracellular signaling pathways, with far reaching consequences for the cell and environment (Hynes, 2002). In the OL, they have been shown as important across a spectra of processes, from proliferation and survival, to morphological differentiation and myelination (reviewed in O'Meara et al., 2011a).

OLs express five distinct heterodimeric units; the first three, αvβ1, αvβ3, and αvβ5 appear transient, with levels tied to a specific timeframe in OL development. The fourth, αvβ8, is expressed early and late in the differentiation process, with a brief dip as morphological complexity increases. The fifth and final member, α6β1, is present throughout the differentiation gamut (Milner and Ffrench-Constant, 1994; Milner et al., 1997 O'meara et al., 2011a).

Each α and β subunit has three primary domains; an extracellular and transmembrane domain, as well as a short cytoplasmic tail. Integrin's extracellular domain extrudes from the cell's surface, where it binds target ligands present in the ECM (Hynes, 2002). The two most interesting targets with regard to OL biology are fibronectin and laminin-2 (Ln-2). Fibronectin can bind all integrin receptors present on the OL save α6β1, which is unique to Ln-2 (O'Meara et al., 2011a). Interestingly, in OLs, these two molecules function in opposition, with fibronectin inhibiting and Ln-2 promoting differentiation.

As stated, fibronectin's role in OL differentiation is staunchly antagonist. OLs grown on the substrate are characterized by decreased process branching and perturbed.

myelinogenesis in culture (Maier et al., 2005; Sisková et al., 2009; Lafrenaye and Fuss, 2010). Further, fibronectin, normally absent from the adult brain, is deposited at high levels in demyelinated lesions (as seen in patients suffering from multiple sclerosis) (van Horssen et al., 2005, 2007). The molecule also forms aggregates in chronically demyelinated lesion sites (Stoffels et al., 2013). When these same aggregates were injected into chemically induced lesions, remyelination stalled, as local OLs failed to differentiate (Stoffels et al., 2013).

Then there is Ln-2. Expressed along axonal tracts undergoing myelination, this molecule is responsible for OL survival (Colognato et al., 2002), process outgrowth and myelin membrane formation *in vitro* (Buttery and Ffrench-Constant, 1999; Eyermann et al., 2012), as well as myelination capacity *in vivo*, specifically, myelin internode formation and myelin thickness (Chun et al., 2003; Relucio et al., 2009, 2012). Intriguingly, when OLs were grown on both fibronectin/Ln-2, fibronectin was shown to override Ln-2 and prevent morphological differentiation (Baron et al., 2014). The effect was mediated by sulfatide, a galactolipid with Ln-2 binding affinity (Baron et al., 2014). When OLs were cultured on Ln-2 alone, sulfatide clustered with integrins, and was necessary for the Ln-2-induced increase in morphological complexity. Fibronectin prevented sulfatide clustering, and thus, when layered with Ln-2, potentially prevented the interaction between integrins and sulfatide necessary for Ln-2-induced differentiation (Baron et al., 2014). The authors also note, with interest, the ability to override fibronectin's inhibition of OL morphological maturation through sulfatide targeted-antibodies. It suggests a paradigm – both during normal development and in the diseased brain – of substrate hierarchy, one that could possibly be overcome through sulfatide inhibition (the authors suggest sulfatide antibodies as therapy) (Baron et al., 2014). Unfortunately, if used as a therapeutic, it then becomes a question of

finding the right balance, as sulfatide loss would block both fibronectin inhibition (more myelin) as well as Ln-2-induced differentiation (less myelin) (Baron et al., 2014).

A role for α6β1

The identification of α6β1 as Ln-2 mediating receptor in OLs (Buttery and Ffrench-Constant, 1999) sparked a flurry of study into the heterodimer's overarching role in CNS myelination. Here was evidence for one of the most well-studied families of adhesion molecules – integrins – driving morphological change and myelin membrane formation in OLs. When the α6 subunit was shown as important for OL survival and a switch to differentiation (Colognato et al., 2002), but not necessarily myelin production (Relvas et al., 2001), the focus fell on integrin's β1 subunit. With its cytoplasmic tail acting as both signal transducer and hub for a variety of signaling and adaptor proteins, it made for an exciting candidate.

To dissect β1's potential role in OL-mediated myelination, various transgenic lines were generated with the goal of knocking-out or disrupting the protein's function *in vivo*. Like so much in science, however, differences in transgenic approach led to conflicting results. Our own laboratory-created mice expressed a dominant-negative form of β1 integrin (lacking the cytoplasmic tail). The truncated protein's expression was restricted to the OL lineage through use of the *proteolipid protein* (*Plp*) promoter (Lee et al., 2006) (though, as we will see in Chapter 2, *Plp* as promoter, like so many others, is not OL lineage restricted early in development). These mice suffered a decrease in number of mature OLs, concomitant with a loss in total number of myelinated fibers (amyelination), and decreased myelin thickness. The same year, Benninger et al., employing an OL specific knockout model – recombination of a floxed *β1* gene by *CNP* promoter driven Cre recombinase (*CNP*

is another OL-lineage specific promoter) – demonstrated the polar opposite; no overt defect in myelin thickness nor in number of myelinated axons (Benninger et al., 2006). Rather, the authors noted a decrease in OL survival. The discrepancy between the two is striking – conclusions drawn as to the protein's necessity for CNS myelination are in stark contrast. Why the disparity? A likely explanation lies in the discovery of transient phenotypes following disruption of the integrin signaling pathway in OLs (they only manifest during early postnatal periods) (Câmara et al., 2009; Forrest et al., 2009; our own work, O'Meara et al., 2013). This would go a long way to explaining why Benninger and colleagues did not observe an overt phenotype following integrin loss, as they primarily assessed more mature mice.

Compensation with age could possibly be regulated through dystroglycan, a second Ln-2 receptor recently identified in OLs (Colognato et al., 2007). Similar to β1 integrin loss, dystroglycan-depleted OLs have defective process outgrowth and branching, and decreased potential to generate myelin membrane (Colognato et al., 2007; O'Meara et al., 2011a; Eyermann et al., 2012). The idea follows; with β1 integrin compromised, the OL instead mediates similar functional requirements through dystroglycan. The two Ln-2 receptors can be viewed as functionally redundant over time. To fully resolve the possibility, a double knockout for both β1 integrin and dystroglycan would be telling.

Today, following nearly a decade of study, general consensus clearly supports a role for β1 integrin in OL mediated myelination (Barros et al., 2009; Câmara et al., 2009; O'Meara et al., 2011a). Even so, small differences abound. It now seems a question of whether β1 integrin affects the OLs ability to trigger myelination (Câmara et al., 2009) or myelin thickness (Barros et al., 2009). Although each model introduces its own complexities, the answer is most likely that β1 integrin has the potential for both. Each study (including

those that came before) manages to disrupt the pathway within a unique framework at a time when the OL, as highly adaptive as we know it can be, cannot immediately compensate. Viewed this way, incongruences can be attributed to inherent differences in promoter used (whether it drives expression very early or late in OL maturation), knockout versus dominant-negative (dominant-negative models are susceptible to unintended secondary consequences), and the developmental window at which time myelination was assessed.

Intriguingly, the story appears to have an additional layer; in line with my own work, small caliber axons are preferentially affected following disruption of β1 integrin signaling (Lee et al., 2006; Câmara et al., 2009). This selectivity will be discussed in more detail in Chapter 3, as ILK loss replicates the phenotype.

Signaling through β1 integrin: FAK and ILK in oligodendrocyte development

Integrins themselves do not directly interact with the cytoskeleton. Rather, following receptor-ligand binding, protein complexes are recruited to their cytoplasmic tails, forming focal adhesions. It is through these complexes that the cell triggers the myriad of responses necessary to respond to environment cues (O'Meara et al., 2011a). In the context of α6β1 integrin, two of the most studied complex members are focal adhesion kinase (FAK) and ILK. Through recruitment to β1 integrin's cytoplasmic tail, these two proteins are often at the center of dynamic cytoskeletal and signaling change.

FAK

FAK governs varying aspects of cellular biology, from migration and adhesion to cellular morphology, in large part through changes wrought to the underlying cytoskeleton

(Mitra et al., 2005). First identified in the OL in 2000 (Kilpatrick et al., 2000), FAK is now considered important for multiple facets of OL differentiation; from formation and outgrowth of primary processes to governance of morphological maturation and myelination capacity *in vivo* (Hoshina et al., 2007; Câmara et al., 2009; Forrest et al., 2009; Lafrenaye and Fuss, 2010). With direct relevance to β1 integrin (as well as my own work, see Chapter 3), conditional OL-specific FAK knockouts are characterized by a transient amyelination phenotype (Forrest et al., 2009; Câmara et al., 2009). As the animal ages, the phenotype fades, suggesting a delay and accompanying compensation as the system adjusts. Again, the finding's significance and mechanism, as it relates to my own work, will be discussed in Chapter 3.

FAK also appears to have unique and opposing roles in determining OL morphology based on ECM component presented and the OL's developmental stage. As previously described, fibronectin inhibits OL maturation while Ln-2 enhances. FAK was required both for fibronectin induced inhibition and Ln-2 induced growth when substrates were presented in isolation (Lafrenaye and Fuss, 2010). However, similar to previous findings (where fibronectin outcompetes Ln-2 (Baron et al., 2014)), when substrates were combined, FAK predominantly signaled through fibronectin. In this context, FAK knockdown increased the OLs morphological complexity (Lafrenaye and Fuss, 2010). Intriguingly, if OLs were cultured from an older brain, and therefore considered more developmentally advanced, the effect was reversed. In "older" OLs, FAK in mixed substrate cultures transduced signals predominately from Ln-2 and not fibronectin. FAK knockdown now inhibited OL maturation. These findings exemplify the ability of a single molecule to intercalate between layers of growth and inhibition. It hints at the complexities inherent to adaptive integrin

signaling, adaptations required as the OL responds to a shifting matrix in the developing brain.

ILK

In a similar vein to FAK, ILK mediates a slew of cellular processes in large part through interactions with the cytoskeleton, as well as activation of intracellular signaling pathways (Wickström et al., 2010b). ILK acts primarily as adapter and structural platform, linking the cytoskeleton and ECM through integrin binding, thereby allowing force transmission from the cell to environment (Ghatak et al., 2013). By engaging the ECM and generating force, the cell creates traction, an essential first step in morphological growth and migration.

ILK is composed of three domains: a four ankyrin repeat domain on the N-terminal, a central pleckstrin homology-like domain, and a kinase-like domain at the C-terminal (Legate et al., 2006). ILK binds β1 integrin's cytoplasmic tail through its kinase-like domain, as well as α and β parvin. Through its N-terminal, ILK interacts with PINCH (particularly interesting Cys-His rich protein). Together, these three proteins (ILK, PINCH and parvin), form an obligate heterotrimeric complex, dubbed IPP (Legate et al., 2006). Loss of any member results in degradation of the remaining partners (Legate et al., 2006). ILK itself does not directly bind F-actin. Rather, it engages the actin cytoskeleton, generally, in one of two ways; either (1) by recruiting proteins capable of direct F-actin interaction, such as its obligate binding partner parvin, or (2) through activation of dynamic actin remodelers such as RhoA, Rac1 and Cdc42 (Mishima et al., 2004; Boulter et al., 2006; Legate et al., 2006; Kogata et al., 2009; Ghatak et al., 2013). Recent work has also described ILK as important for microtubule dynamics. Similar to its function in microfilaments, ILK does not directly

bind microtubules. Instead, it recruits microtubule binding proteins, and, together, they anchor microtubules at the membrane, thereby ensuring stable and polarized microtubule architecture (Wickström et al., 2010a; Akhtar and Streuli, 2013; Ghatak et al., 2013). In line with ILK's primary role as a cytoskeletal-linker protein, ILK deletion results in peri-implantation lethality, with cells characterized by massive F-actin disorganization/accumulation and adhesion failure (Sakai et al., 2003).

But what of ILK's kinase-like domain? Does it possess catalytic activity? The debate as to whether the protein should be classified as pseudokinase – that its kinase activity is a manufactured illusion of other recruited kinases – or is a true kinase, rages on (Wickström et al., 2010b; Fukuda et al., 2011; Hannigan et al., 2011; Ghatak et al., 2013). Regardless, either directly or indirectly, ILK does appear necessary for the phosphorylation of both AKT and GSK3β (Delcommenne et al., 1998; Legate et al., 2006).

With regard to OL function, not much is known. "Kinase-inactive" dominant-negative ILK attenuates Ln-2 driven myelin membrane production in culture (Chun et al., 2003). However, following this one study, no further attempt was made to uncover functional responsibilities in OLs. We therefore set out to fully elucidate ILK's role in OL-mediated myelination of the CNS.

Research Plan

The integrin signaling pathway is essential for OL driven myelin sheath formation in the CNS. Studies have shown integrin-linked kinase (ILK) to be a major structural binding partner of β1 integrin. Through our work, we will assess the functional importance of ILK in signaling CNS myelination. Understanding key steps in the modulation of myelination is critical as we move towards a better understanding of this unique cell type.

We **hypothesize** that the ILK signaling pathway plays an important role in CNS myelination. Project **specific aims** are:

1. **Characterize *Plp* driven Cre-recombinase as a useful model for OL-specific knockouts, and the subsequent study of ILK loss *in vivo***
2. **Assess morphological and ultrastructural changes in CNS myelination and measure impact of ILK depletion on downstream signaling pathways**
3. **Examine a role for ILK in OL development independent of Ln-2 pathway activation**

Chapter 2

The Proteolipid Protein Promoter as Oligodendrocyte Lineage Driver

The Proteolipid Protein Promoter Drives Expression Outside of the Oligodendrocyte Lineage During Embryonic and Early Postnatal Development

John-Paul Michalski[1,2,*], Carrie Anderson[1,*], Ariane Beauvais[1], Yves De Repentigny[1] and Rashmi Kothary[1,2,3,#]

[1]Ottawa Hospital Research Institute, Ottawa, ON, Canada K1H 8L6

[2]Department of Cellular and Molecular Medicine, University of Ottawa, Ottawa, ON, Canada K1H 8M5

[3]Department of Medicine, University of Ottawa, Ottawa, ON, Canada K1H 8M5

[*]These authors contributed equally to the manuscript

To whom correspondence should be addressed

Published in *PLoS ONE*, 2011, 6(5): e19772.

Author Contributions

Conceived and designed the experiments: J-PM, RK. Performed the experiments: J-PM (Figures 2.2, 2.3, 2.4, 2.5, 2.6, 2.7, 2.8, all tables and all supplemental), CA (Figures 2.1 and 2.7), AB (assisted with Figures 2.2, 2.3, 2.4, 2.5 and tables). CA and YDR generated the *Plp-Cre* line. J-PM, CA, and AB analyzed the data. J-PM and CA wrote the paper and RK revised and edited the manuscript.

Abstract

The *proteolipid protein* (*Plp*) gene promoter is responsible for driving expression of one of the major components of myelin – PLP and its splice variant DM-20. Both products are classically thought to express predominantly in oligodendrocytes. However, accumulating evidence suggests *Plp* expression is more widespread than previously thought. In an attempt to create a mouse model for inducing oligodendrocyte-specific gene deletions, we have generated transgenic mice expressing a Cre recombinase cDNA under control of the mouse *Plp* promoter. We demonstrate *Plp* promoter driven Cre expression is restricted predominantly to mature oligodendrocytes of the central nervous system (CNS) at postnatal day 28. However, crosses into the $Rosa26^{LacZ}$ and *mT/mG* reporter mouse lines reveal robust and widespread Cre activity in neuronal tissues at E15.5 and E10.5 that is not strictly oligodendrocyte lineage specific. By P28, all CNS tissues examined displayed high levels of reporter gene expression well outside of defined white matter zones. Importantly, our study reinforces the emerging idea that *Plp* promoter activity is not restricted to the myelinating cell lineage, but rather, has widespread activity both during embryonic and early postnatal development in the CNS. Specificity of the promoter to the oligodendrocyte cell lineage, as shown through the use of a tamoxifen inducible *Plp-*$CreER^t$ line, occurs only at later postnatal stages. Understanding the temporal shift in *Plp* driven expression is of consequence when designing experimental models to study oligodendrocyte biology.

Introduction

Proteolipid protein (PLP), a tetraspan membrane protein, is the most abundant component of CNS myelin. It is encoded by a highly conserved 17 Kb gene (*Plp*) containing seven exons. By means of an alternate splicing event, a second protein, DM-20, is also generated. *Plp*, though active at low levels during embryonic development, is expressed maximally in mature myelinating cells, while *DM-20* is expressed earlier during embryonic development in both neural, and subsequently, oligodendrocyte progenitors (Timsit et al., 1995; Spassky et al., 1998; Delaunay et al., 2008). Together, PLP and DM-20 play an important role in regulating proper oligodendrocyte maturation and myelin compaction/stability over time (Klugmann et al., 1997; Nadon and West, 1998).

The *Plp* promoter and its regulatory elements, located in exon 1 and intron 1 of the gene, were previously shown to dictate expression specifically to oligodendrocytes (Wight et al., 1993; Fuss et al., 2000, 2001) and Schwann cells (Puckett et al., 1987; Mallon et al., 2002) at various stages of development. Although the promoter is generally considered oligodendrocyte lineage specific, accumulating evidence suggests a *Plp* expression pattern outside of defined white matter zones; included are both glial and neuronal CNS subpopulations, implying a role for *Plp* in activities independent of myelination (Jacobs et al., 2003, 2004; Le Bras et al., 2005; Tuason et al., 2008; Guo et al., 2009; Miller et al., 2009).

To study *Plp* promoter driven expression patterns across time in CNS tissues, we have generated and characterized transgenic mice expressing full length Cre cDNA under control of the mouse *Plp* promoter (*Plp-Cre*). We did not necessarily expect the transgene

to completely faithfully mimic the endogenous *Plp* gene expression due to the phenomenon of position-effect in transgenic mice, but rather we wished to test whether such cassettes can provide cell specificity in a temporal fashion. These mice demonstrate a transient spatio-temporal expression pattern for *Plp-Cre*. As expected, at P28 the *Plp* promoter drove Cre expression predominantly in mature oligodendrocytes; however, by crossing the *Plp-Cre* line to either the *Rosa26*^{LacZ} (Soriano, 1999) or the *mT/mG* (Muzumdar et al., 2007) reporter mice, a more promiscuous expression pattern was observed during embryonic and early postnatal stages of development. Specificity of the promoter to the oligodendrocyte cell lineage, as shown through the use of a tamoxifen inducible *Plp-CreER*^{t} line (Doerflinger et al., 2003), occurs only at later postnatal stages.

Our work reinforces previous studies supporting a role for the *Plp* promoter in the nervous system outside of myelinating cell lineages, particularly early in development. Consequently, the promoter construct should be used with caution in studies requiring genetic modifications strictly in myelinating cells, especially when embryonic and early postnatal time points are involved.

Materials and Methods

Ethics Statement: The mice were cared for according to the Canadian Council on Animal Care (CCAC) guidelines. Ethical approval for experiments conducted was obtained from the University of Ottawa Animal Care Committee under protocol approval OGH-118 and OGH-119.

Transgenic and Reporter Mice: The *Cre* cDNA (kindly provided by Dr. Robin Parks, Ottawa Hospital Research Institute) was inserted into the *Plp* promoter cassette, consisting of exon 1 and intron 1 of the mouse *Plp* gene (Fuss et al., 2000). The resulting transgene construct was microinjected into one-cell mouse embryos. Tail biopsies were obtained from potential founder mice, DNA was extracted and transgenic mice were identified by PCR amplification using sense oligo 5' TGG GTG TTG GTT TTT GGA GA 3' (specific to the *Plp* promoter) and antisense oligo 5' CGC ATA ACC AGT GAA ACA GCA 3' (specific to the *Cre* cDNA). Positive founder mice were bred with C57BL/6 mice (obtained from Charles River) to establish two independent transgenic lines. *Plp-CreER*^{t} mice were kindly provided by Dr. Brian Popko (Doerflinger et al., 2003). One mg of tamoxifen (20 µL of a 50 mg/ml solution) was administered intraperitoneal once a day for 5 consecutive days to P16 mice. A single 1 mg injection was given to P4 mice. Cre protein distribution was assessed by crossing transgenic mice into the *Rosa26*^{LacZ} reporter line (Soriano, 1999) or to a floxed stop tdTomato-EGFP (*mT/mG*) fluorescent reporter mouse line (Muzumdar et al., 2007). Animals homozygous for the *Rosa26*^{LacZ} or *mT/mG* locus were crossed to mice heterozygous for the *Cre* transgene, generating a final line of mice heterozygous for both the *Cre* and respective reporter transgenes. The genotype of offspring mice was confirmed by PCR.

***RT-PCR Analysis*:** For reverse transcription-polymerase chain reaction (RT-PCR) analysis, RNA was isolated from transgenic P4 and P28 tissues from the two *Plp-Cre* founder lines. To produce cDNA, equal amounts of RNA were reverse-transcribed in a standard reaction with MuLV reverse transcriptase (Invitrogen). PCR amplification using the sense oligo 5' CCT TCC AGC TGA GCA AAG TC 3' (specific to *Plp* exon 1), and the antisense oligo 5' CGC ATA ACC AGT GAA ACA GCA 3' (specific to the *Cre* cDNA) yielded a 440 nucleotide fragment. Primers were chosen to flank the intronic region of the construct to selectively amplify the RNA transcript and prevent amplifying any contaminating genomic DNA. The reaction began with a 3 min incubation time at 94°C followed by 30 cycles of 45 sec at 94°C, 45 sec at 55°C, 1 min at 68°C, with a final extension time of 10 min at 68°C. Amplification of actin cDNA served as a control. The PCR products were electrophoresed on a 1.5% agarose gel containing ethidium bromide, and amplified fragments were visualized under UV transillumination.

Immunohistochemistry: Mice were anesthetized with avertin and perfused transcardially with 4% paraformaldehyde (PFA). Brains, spinal cords and optic nerves were dissected in PBS, fixed with 4% PFA overnight at 4°C, cryoprotected in 30% sucrose overnight at 4°C, then frozen in a 1:1 mixture of 30% sucrose:OCT (Sakura, CA). Cryostat sections of 10 μm thickness were obtained and stored at -20°C until use. Sections were postfixed in 70% ethanol for 5 min, rinsed with PBS for 10 min, and incubated in warm citrate buffer (10 mM citric acid, 26 mM NaOH, pH 6) for 10 min. Sections were then blocked using TBLS (0.5 mM Tris-HCl pH 7.4, 0.0085% NaCl, 0.01% BSA, 0.009% L-lysine, and 10% sodium azide) with 20% goat serum and 0.3% Triton-X-100 for 1 hour. Primary

antibodies for CC-1 (1:10, Abcam, MA), GFAP (1:500, chemicon), Ng2 (1:250, Millipore), NeuN (1:100, Chemicon), and Cre (1:100, Novagen) were diluted in TBLS and incubation was for 1 hour at RT and overnight at 4°C, respectively. Secondary antibodies were used at a dilution of 1:200 (Invitrogen), and Hoechst counterstain at 1:10,000. Slides were mounted with a fluorescence mounting medium (Dako North America, Inc.) and sections analyzed by fluorescence microscopy using a Zeiss Axioplan microscope or Zeiss Confocal microscope (LSM 510 Meta DuoScan). Cells were considered to be Cre positive only if they had a clear nuclear staining pattern co localizing with DAPI. All images for co labeling analysis were done using the Zeiss Confocal microscope set at a 1 μm slice capture.

***β-galactosidase staining*:** Heterozygous male *Plp-Cre* or *Plp-CreER*^{t} mice were bred with female *Rosa26*^{LacZ} homozygotes. The Cre positive offspring should harbor cells expressing a functional Cre-recombinase enzyme; hence allowing expression of *lacZ* driven by the ROSA26 promoter. Cre-positive *Rosa26*^{LacZ} heterozygous progeny were analyzed for β-galactosidase enzyme activity, with Cre-negative *Rosa26*^{LacZ} heterozygotes serving as controls. Mice were anesthetized with avertin and perfused transcardially using 0.2% glutaraldehyde with 1.25 mM EGTA pH 7.3 and 2 mM $MgCl_2$ in PBS. Tissues (brain, spinal cord, sciatic nerve, optic nerve) or embryos were then postfixed in 0.2% glutaraldehyde solution for 1 to 4 additional hours at 4°C, then rinsed 3 times with PBS. Tissues were incubated from 2 hours to overnight at 37°C in X-Gal staining solution consisting of 5 mM potassium ferricyanide, 5 mM potassium ferrocyanide, 2 mM $MgCl_2$, 0.02% Nonidet P-40, and 1 mg/ml of 5-bromo-4-chloro-3-indolyl-β-D-galactopyranoside

(X-Gal) in 0.1 M phosphate buffer, pH 8. Samples were then washed 3 times with PBS and whole mount photographs were taken.

Results

Generation of Plp-Cre transgenic mice

To direct oligodendrocyte specific expression, full-length *Cre* cDNA was placed under control of the mouse *Plp* promoter (Figure 2.1A). The promoter region consists of exon 1 and intron 1 of the *Plp* gene, shown previously to be sufficient for mimicking the endogenous *Plp* activity (Fuss et al., 2000). Six of 29 potential founders tested positive for the transgene construct with two successfully breeding and transmitting the transgene to subsequent generations (Figure 2.1B). From these two founders, independent lines 627 and 633, described herein, were generated.

The Plp-Cre transgenic mice display CNS-specific expression

Specificity of *Plp-Cre* expression to CNS tissues in lines 627 and 633 was initially assessed by RT-PCR. To compare early and later stage transgene expression, total RNA was isolated from selected tissues at P4 and P28. At P28, both lines exhibited a CNS-specific expression pattern, with transcripts detected in, for example, spinal cord, cerebellum and cortex (Figure 2.1C). At P4, transgene expression was also detected in CNS tissues (Figure 2.1C). However, at this stage, mice from line 627 also expressed the Cre transgene in kidney, liver, and skeletal muscle (Figure 2.1C). Nevertheless, it should be noted that for the purpose of this study the transgene was consistently expressed at higher levels in CNS tissues relative to all other tissues examined.

A

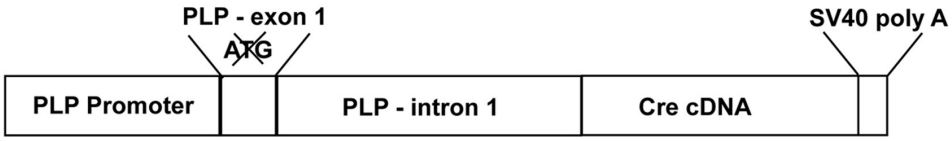

B

Transgene	Mice born	Number of founder mice	Transgenic strains established
PLP Cre	29	6	2

C

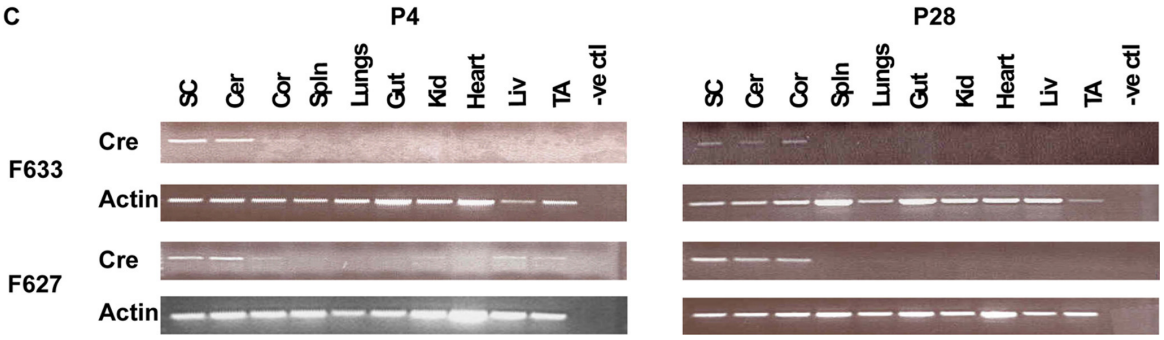

Figure 2.1. Schematic and expression profile of *Plp-Cre* transgene. A. Schematic representation of the *Plp-Cre* transgene construct. The mouse *Plp* promoter is used to drive expression of the *Cre* cDNA. The initiating ATG within exon 1 has been mutated to prevent initiation of translation within the promoter region. **B.** Summary of *Plp-Cre* transgenic mice generated. **C.** RT-PCR analysis of the tissue expression profile of the *Plp-Cre* transgene for both founder lines. At P28, both lines adhered to a strictly CNS-specific expression pattern, with transcripts detected in the spinal cord, cerebellum and cortex. At P4, the transgene transcript in line F633 was detected solely in CNS tissues, whereas line F627 displayed a more widespread expression pattern, with transcripts also detected in kidney, liver and TA muscle. SC = spinal cord, Cer = cerebellum, Cor = cortex, Spln = spleen, Kid = kidney, Liv = liver, TA = tibialis anterior muscle. Actin mRNA amplification was used as control.

Plp-Cre transgene expression displays selectivity to oligodendrocytes in later postnatal stage mice

Immunocytochemistry was performed to assess specificity of Cre protein expression to oligodendrocytes. Cerebellar, spinal cord, and optic nerve sections from P4 and P28 *Plp-Cre* transgenic mice and their wild type littermates were examined. An antibody against CC-1 was used as a marker for mature oligodendrocytes. In both *Plp-Cre* lines (627 and 633), all neural tissues examined at P28 expressed the Cre protein. The majority of Cre-positive cells also labeled positive for CC-1 (see Table 2.1), indicating specificity of the *Plp* promoter to mature oligodendrocytes at this stage in postnatal development (spinal cord Figure 2.2D-I, cerebellum Figure 2.3D-I, and optic nerve Figure S2.1D-I). As expected, we did not detect any Cre-positive cells in tissues from WT littermates (Figure 2.2A-C, Figure 2.3A-C, and Figure S2.1A-C). There were a few faintly labeled Cre-positive cells that also co-labeled with the astrocytic marker GFAP (Figure 2.2J, Figure 2.3J and Figure S2.1J) as well as with Ng2, a marker for oligodendrocyte progenitor cells (OPCs) (Figure 2.2K, Figure 2.3K and Figure S2.1K) (summarized in Table 2.1). In comparison, there were no Cre-positive cells that co-labeled with NeuN, a marker for mature neurons, in the tissues examined (Figure 2.2L and 2.3L).

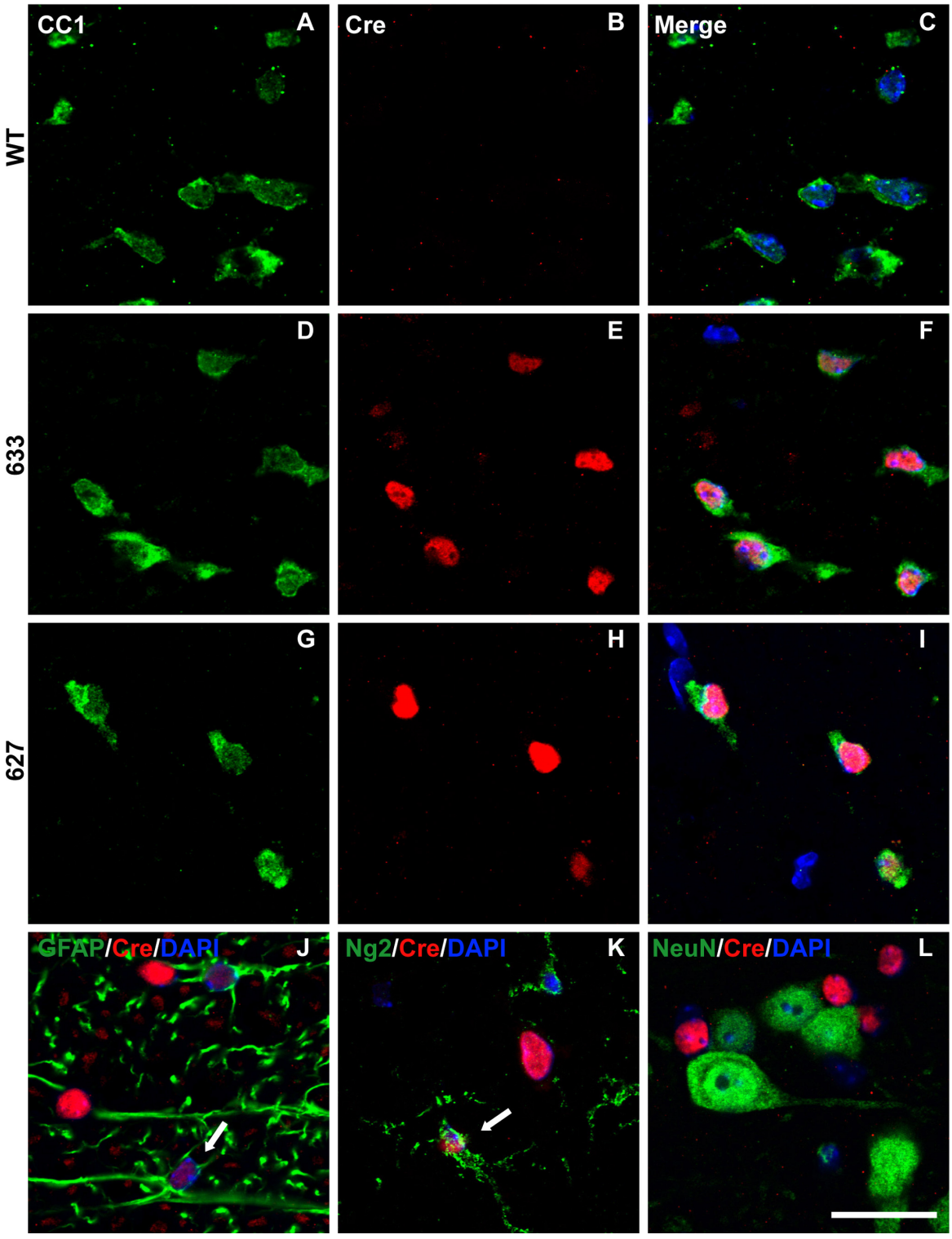

Figure 2.2. Cre-recombinase is predominantly expressed in oligodendrocytes of P28 *Plp-Cre* mouse spinal cord. A-I. Ventral white matter regions were double-stained with antibodies specific to CC-1 as a marker for mature oligodendrocytes (green), Cre (red)

and counterstained with DAPI. Cre was not detected in WT spinal cord sections (B). Sections from transgenic mice of both F633 (D-F) and F627 (G-I) lines exhibited a similar pattern of Cre expression. High levels of Cre recombinase protein was detected in the CC1-positive oligodendrocytes. **J.** Ventral white matter region stained for GFAP (green) as a marker for astrocytes, Cre (red) and counterstained with DAPI. A small number of Cre-positive cells co-labeled with GFAP (arrow). **K.** Ventral white matter region stained for Ng2 (green) as a marker for OPCs, Cre (red) and counterstained with DAPI. A small number of Cre-positive cells co-labeled with Ng2 (arrow). **L.** Ventral grey matter region stained for NeuN (green) as a neuronal marker, Cre (red) and counterstained with DAPI. There were no NeuN positive cells that co-labeled with Cre. Scale bar = 20 μm.

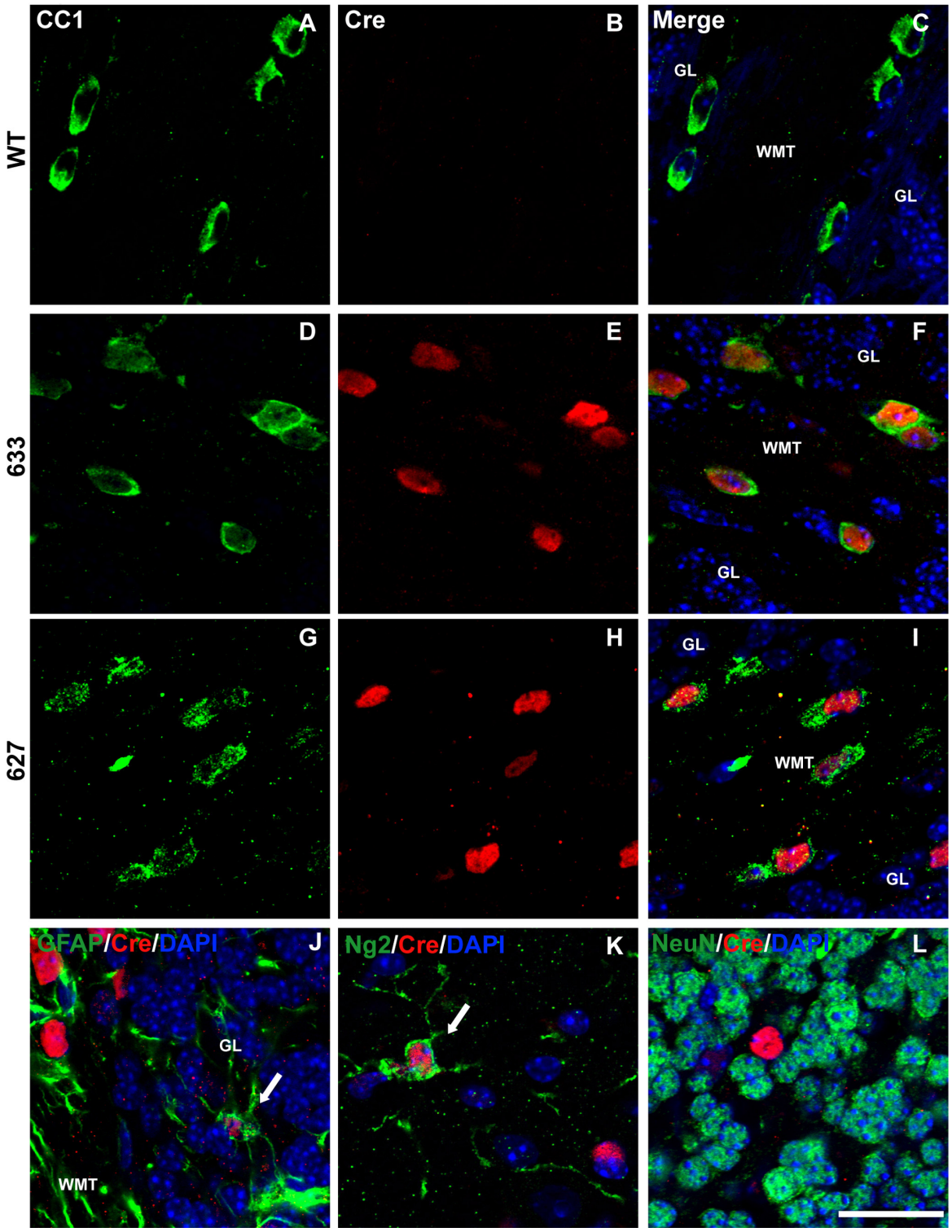

Figure 2.3. Cre-recombinase is predominantly expressed in oligodendrocytes of P28 *Plp-Cre* mouse cerebellum. A-I. Cerebellar sections were double-stained with antibodies specific to CC-1 as a marker for mature oligodendrocytes (green), Cre (red) and

counterstained with DAPI. Cre was not detected in WT cerebellar sections (B). Sections from transgenic mice of both F633 (D-F) and F627 (G-H) lines exhibited a similar pattern of Cre expression. High levels of Cre recombinase protein was detected in the CC1-positive oligodendrocytes. **J.** Cerebellar section stained for GFAP (green) as a marker for astrocytes, Cre (red) and counterstained with DAPI. A small number of weakly stained Cre-positive cells co-labeled with GFAP (arrow). **K.** Representative example within the molecular layer of cerebellar section stained for Ng2 (green) as a marker for OPCs, Cre (red) and counterstained with DAPI. A small number of weakly stained Cre-positive cells co-labeled with Ng2 (arrow). **L.** Representative example within granular layer of cerebellar section stained for NeuN (green) as a neuronal marker, Cre (red) and counterstained with DAPI. There were no NeuN positive cells co-labeled with Cre. GL = granular layer, WMT = white matter tract. Scale bar = 20 μm.

Table 2.1. Distribution of Cre-positive cell types in P28 *Plp-Cre* CNS tissues

	% of CC-1+ cells that are Cre+[a]	% of Cre+ cells that are CC-1+[a]	% of Cre+ cells that are Ng2+	% of Cre+ cells that are GFAP+[a]	% of Cre+ cells that are NeuN+
Spinal Cord	88.9% ±5.4	95.8% ±6.8	10.8% ±0.7	10.6% ±2.2	0
Cerebellum	86.0% ±4.8	90.0% ±9.2	5.8% ±4.3	8.6% ±5.8	0
Optic Nerve	91.2% ±6.4	88.7% ±2.8	3.8% ±2.5	3.3% ±0.2	n.d.

[a] There are most likely Cre-positive cells which stain for GFAP and CC-1. These cells are assumed to be GFAP astrocytes, and not oligodendrocytes.

n.d. = not determined

At P4, Cre protein was detected in both spinal cord (Figure 2.4, Figure S2.2-3) and cerebellum (Figure 2.5, Figure S2.4-5) of *Plp-Cre* transgenic mice. However, unlike the situation at the P28 stage, Cre expression was often more widespread, with many Cre-positive cells outside of the oligodendrocyte lineage, especially in the cerebellum (see Table 2.2).

In the spinal cord, the most intensely stained Cre-positive cells localized predominantly to emerging white matter tracts, and co-labeled with the oligodendrocyte marker CC-1 (Figure 2.4A-B, G-H, Figure S2.2A-C). Approximately a third of Cre-positive cells co-labeled with Ng2 (Figure 2.4C-D, I-J, Figure S2.2D-F). However, a considerable number of Cre-positive cells also were positive for the astrocyte marker GFAP, both in white and grey matter regions (Figure 2.4E-F, K-L, Figure S2.2G-I). As the cumulative percentage of Cre-positive cells expressing markers for CC-1 and GFAP exceeds 100%, it is suggested that GFAP positive cells are often also labeled by CC-1 at P4 (these cells would be considered astrocytes) (see Table 2.2). There was no co-labeling of Cre-positive cells with the neuronal marker NeuN at this time point (Figure S2.3).

In the P4 cerebellum, CC-1 positive cells were localized to the deep central white matter region, the zone of initial myelination. Approximately half (see Table 2.2) of the central white matter region's Cre-positive cells were CC-1 positive (Figure 2.5A-B, G-H, Figure S2.4A-C). Cre-positive cells within the region also co-labeled with Ng2 (Figure 2.5C-D, I-J, Figure S2.4D-F), and a small number with GFAP (Figure S2.5). Most striking was the Cre staining pattern in the developing granular, Purkinje and molecular cell layers. Almost no CC-1 positive cells were identified and less than 10% of Cre-positive cells within this region co-stained for Ng2 in both transgenic lines (data not shown). Approximately half (see Table 2.2) of all Cre-positive cells co-labeled with

NeuN (Figure 2.5E-F, K-L, Figure S2.4G-I), suggesting a large population of neurons within the granular, Purkinje and molecular cell layers in which the *PLP* promoter is active at P4.

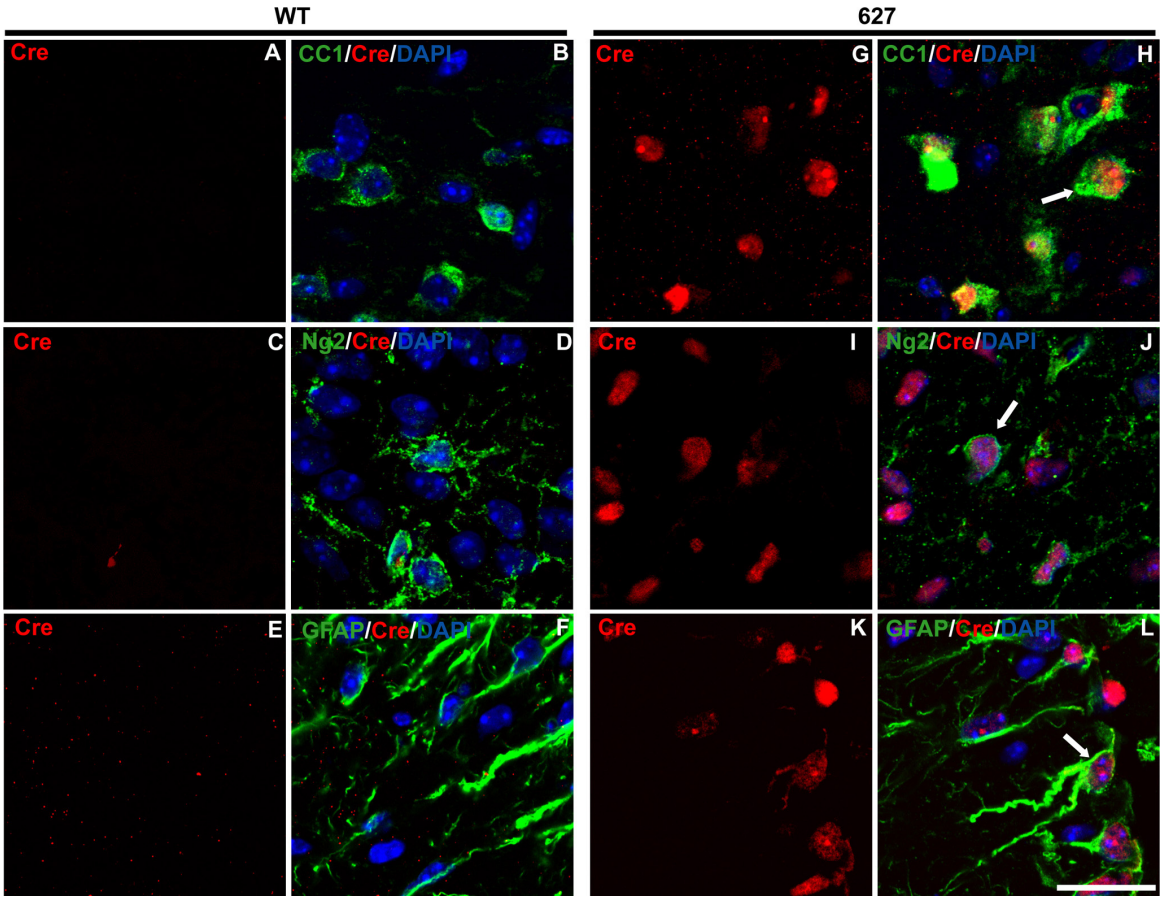

Figure 2.4. Cre-recombinase is expressed both in and outside the oligodendrocyte lineage in spinal cords of P4 *Plp-Cre* mice. A-L. Ventral spinal cord sections from WT and *Plp-Cre* line 627 mice were double-stained with antibodies specific to Cre (red) and either CC-1 (green) as a marker for mature oligodendrocytes (A-B, G-H), Ng2 (green) as a marker for OPCs (C-D, I-J), or GFAP (green) as a marker for astrocytes (E-F, K-L), and counterstained with DAPI. Cre was not detected in WT sections (A-F). As expected, many Cre-positive cells were CC-1-positive, however, a large percentage also co-stained for Ng2 and GFAP. Examples of Cre and glial marker co-labeling are denoted by arrows. WM = white matter, GM = grey matter. Scale bar = 20 μm.

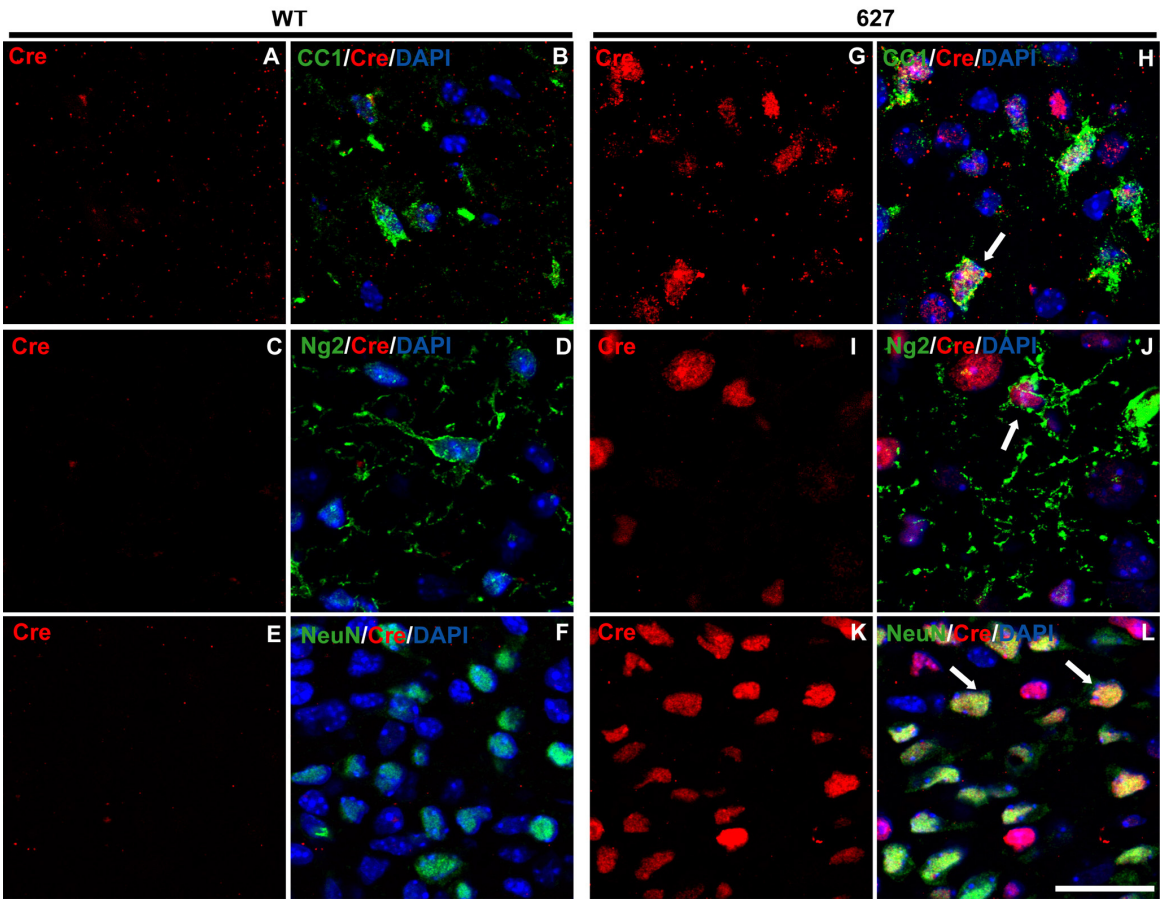

Figure 2.5. Cre-recombinase is expressed both in and outside the oligodendrocyte lineage in the cerebellum of P4 *Plp-Cre* mice. A-D, G-J. Deep cerebellar white matter regions from WT and *Plp-Cre* line 627 mice were double-stained with antibodies specific to Cre (red) and either CC-1 (green) as a marker for mature oligodendrocytes (A-B, G-H), or Ng2 (green) as a marker for OPCs (C-D, I-J) and counterstained with DAPI. Cre was not detected in WT sections (A-D). A large percentage of Cre-positive cells within the region co-stained for CC-1 and Ng2. **E-F, K-L.** Cerebellar sections of the developing granular layer from WT and *Plp-Cre* line 627 mice were double-stained with antibodies specific to Cre (red), the neuronal marker NeuN (green) and counterstained with DAPI. Cre was not detected in WT sections (E-F). Many Cre-positive cells co-stained for NeuN. Examples of Cre-positive cells co-labeling with neuronal or glial markers are denoted by arrows. Scale bar = 20 μm.

Table 2.2. Distribution of Cre-positive cell types in P4 *Plp-Cre* CNS tissues

	% of CC-1+ cells that are Cre+[a]	% of Cre+ cells that are CC-1+[a]	% of Cre+ cells that are Ng2+	% of Cre+ cells that are GFAP+[a]	% of Cre+ cells that are NeuN+
Spinal Cord	55.0% ±11.2	92.0% ±9.1	34.4% ±3.6	33.0% ±7.4	0
Cerebellum	80.6% ±6.8[b]	46.7% ±10.2[b]	21.4% ±6.6[b]	8.4% ±5.1[b]	53.3 ±14.4[c]

[a] There are most likely Cre-positive cells which stain for GFAP and CC-1. These cells are assumed to be GFAP astrocytes, and not oligodendrocytes. This is especially true for P4 spinal cord.

[b] Cells counted from deep central white matter region of cerebellum.

[c] Cells counted in developing region of cerebellar granular, Purkinje and molecular cell layers.

Inducible model demonstrates PLP promoter expression outside of oligodendrocytes during early postnatal development

The above results suggest a temporal shift in the promoter's expression pattern. To further validate the observed difference in *Plp* promoter activity between early (P4) and late (P28) postnatal time points, we took advantage of an existing line in which *Plp* drives expression of a Cre protein fused to a mutated estrogen receptor (*Plp-CreER*^{t}) (Doerflinger et al., 2003). This fusion necessitates activation of Cre by tamoxifen. The *Plp* promoter region, similar to our *Plp-Cre* transgenic mice, consists of exon 1 and intron 1 of the endogenous *Plp* gene, and as such, would be expected to drive Cre expression in an identical manner. The *Plp-CreER*^{t} mice were crossed to a ROSA26 reporter line (*Rosa26*^{LacZ}). *Rosa26*^{LacZ} mice express *lacZ* driven by the constitutively active ROSA26 locus promoter (Soriano, 1999). A floxed stop region is located upstream of the *lacZ* coding sequence, therefore necessitating Cre-mediated excision of the stop region to allow for *lacZ* expression. Tamoxifen is thus required to induce translocation of CreER^t from the cytoplasm into the nucleus thereby activating *lacZ* expression. For the *Plp-CreER*^{t} transgenic line, injections of tamoxifen were given at P16 and P4. The time points were chosen to reflect different stages of oligodendrocyte maturation and the observed temporal shift in *Plp* promoter patterning observed in our *Plp-Cre* mice; that of increasing specificity to the oligodendrocyte lineage as the animal matures from P4 to P28. Injections at P4 would allow for early postnatal *Plp* expression profiling, while the later P16 time point would reflect the increasing oligodendrocyte selectivity of the *Plp* promoter. P16 and P4 tamoxifen injected mice were analyzed at P60 and P28 respectively. Therefore, the reporter-positive cells observed at P60 and P28 are the

progenies of *Plp* promoter active cells at P16 and P4. The reporter-positive cells at the stages examined do not necessarily have *Plp* promoter activity.

The pattern of *lacZ* expression, as determined by β-galactosidase activity, in *Plp-CreER^{t};Rosa26^{LacZ}* mice differed depending on the time course of tamoxifen administration. In mice given the drug at P16, β-galactosidase expression was similar to that previously described (Doerflinger et al., 2003), localizing mainly to white matter tracts of the CNS (e.g. in the brain, spinal cord and optic nerve), but not in the PNS (e.g. sciatic nerve) (Figure 2.6A). In contrast, when tamoxifen was given to P4 *Plp-CreER^{t};Rosa26^{LacZ}* mice, β-galactosidase was expressed both in CNS and PNS tissues (Figure 2.6B). Also, β-galactosidase expression in P4 brains was not exclusive to CNS white matter tracts; in the cerebellum β-galactosidase was expressed in the Purkinje cell layer (PCL) and the internal granular layer (IGL) and was not observed in the corpus callosum. The β-galactosidase expression profile observed in the PCL and IGL of P4 injected mice corroborates nicely with our immunocytochemistry for Cre protein performed at the same time point (see Figure 2.5E-F, K-L). In both P16 and P4 tamoxifen injected mice, β-galactosidase was expressed in the olfactory bulb, most likely in olfactory ensheathing cells as reported previously (Dickinson et al., 1997).

These experiments suggest *Plp* promoter driven expression occurs outside of the oligodendrocyte cell lineage early in postnatal development, and demonstrates increased oligodendrocyte specificity as a result of cellular maturation.

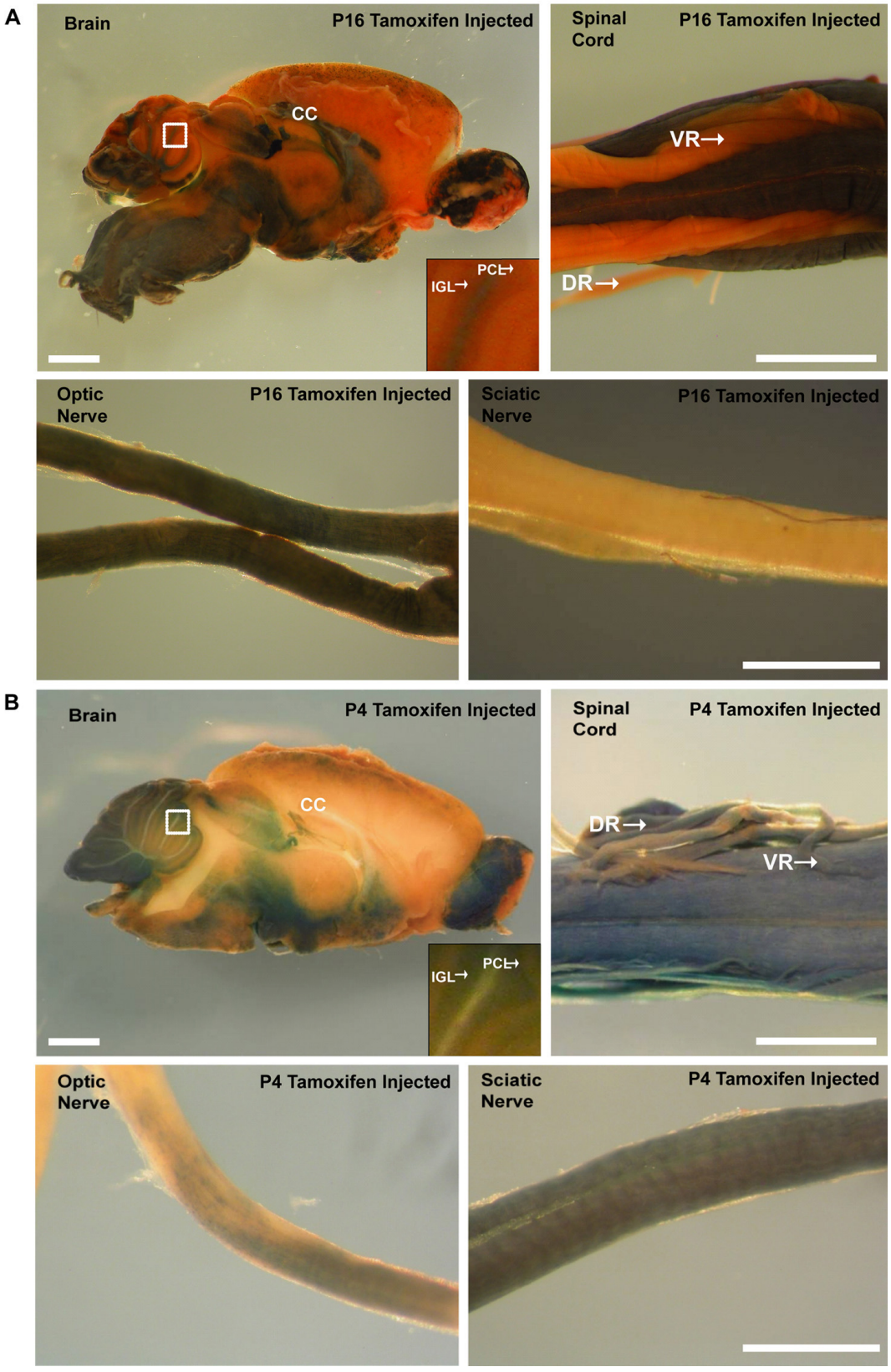

Figure 2.6. β-galactosidase expression in *Plp-CreER^{t};ROSA26^{LacZ}* mice given

tamoxifen at either P16 or P4. A. β-galactosidase expression in *Plp-CreER^t;ROSA26^{LacZ}* mice given tamoxifen at P16 and examined by whole mount X-gal staining at P60. In the brain, β-galactosidase activity is predominantly observed in white matter tracts. In the spinal cord, β-galactosidase activity is detected in the dorsal and ventral white matter tracts, but is absent from the ventral and dorsal roots. Finally, β-galactosidase activity is apparent throughout the length of the optic nerve, but not in the sciatic nerve. **B.** β-galactosidase expression in *Plp-CreER^t;ROSA26^{LacZ}* mice given tamoxifen at P4 and examined by whole mount X-gal staining at P28. In the brain, β-galactosidase activity is detectable outside of large white matter tracts. In the spinal cord, β-galactosidase activity is detectable in the dorsal and ventral white matter tracts, and is also present in the ventral and dorsal roots. Finally, β-galactosidase is expressed throughout the length of the optic nerve, albeit at a reduced level, and the sciatic nerve is now positive for β-galactosidase activity. CC = corpus callosum, PCL = Purkinje cell layer, IGL = internal granular layer, VR = ventral root, DR = dorsal root. Scale bars = 1 mm in A and B Brain, 500 μm in B Spinal Cord.

Plp-Cre transgene expression during embryonic and early postnatal development is not restricted to the myelinating cell lineage

To further assess both the temporal and spatial expression of Cre from early embryonic stages, we crossed our *Plp-Cre* transgenic mice to the *Rosa26*^{LacZ} line. Brain, spinal cord, and optic nerve tissues were examined from two early developmental time points (E10.5, E15.5). Cells marked by activation of the *lacZ* reporter gene would therefore suggest *Plp* promoter driven Cre expression either before or at the time of analysis.

β-galactosidase activity was detected in E10.5 whole mount embryos (Figure 2.7A). Robust staining was apparent throughout the telencephalon, optic stalk, mesencephalon, rhombencephalon, and spinal cord as well as in PNS derivatives of the neural crest (Figure 2.7A). As the progeny of these cells faithfully inherit the activated *lacZ* gene, it was not surprising to observe widespread β-galactosidase activity in the brains and spinal cords of E15.5 (Figure 2.7B) mice. No β-galactosidase expression was observed in either *Plp-Cre* or *Rosa26*^{LacZ} mice alone (data not shown).

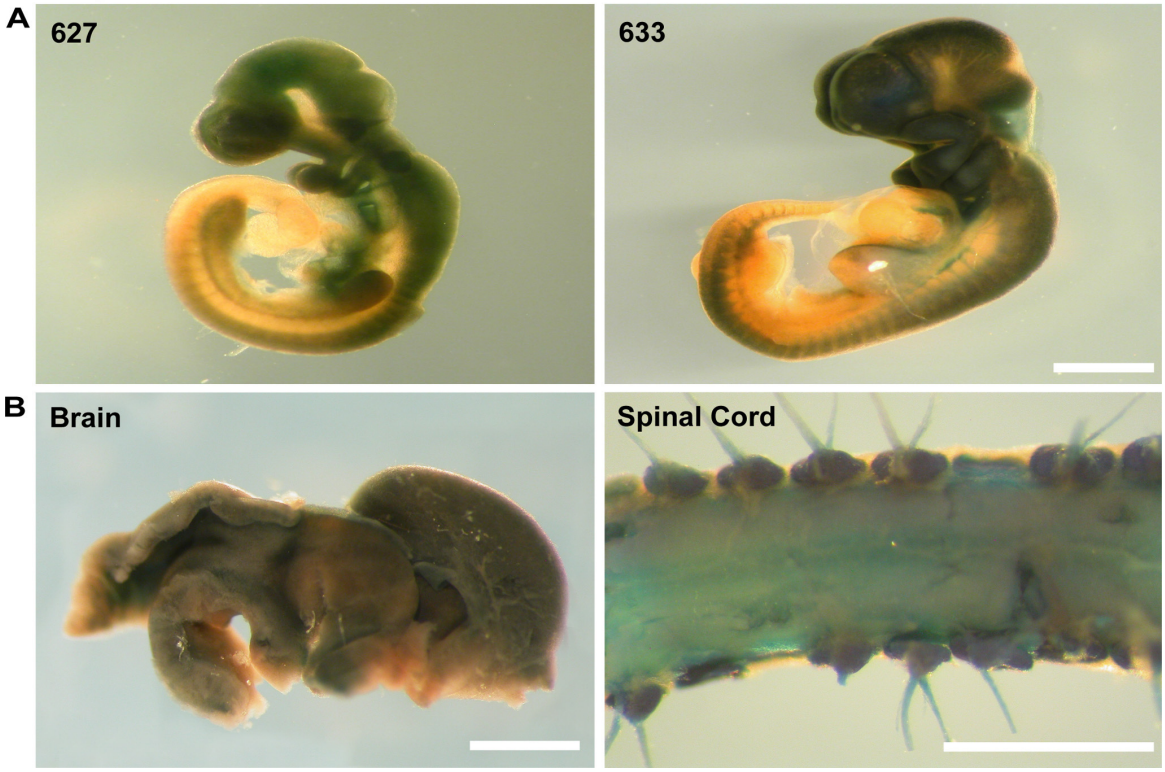

Figure 2.7. β-galactosidase expression outside of the oligodendrocyte lineage in CNS tissues of *Plp-Cre;ROSA26*^{LacZ} mice at E10.5 and E15.5. A. β-galactosidase expression in *Plp-Cre;ROSA26*^{LacZ} embryos at E10.5. Shown are representative examples of E10.5 embryos from lines F627 and F633 after whole mount X-gal staining. Both lines show β-galactosidase expression throughout the developing brain and spinal cord. **B.** β-galactosidase expression in *Plp-Cre;ROSA26*^{LacZ} mice at E15.5. Shown is an example of whole mount staining of tissues from line F633. β-galactosidase activity was detected throughout both the brain, and ventral and dorsal spinal cord. Scale bars = 2 mm in A and B Brain and Spinal Cord, 1 mm in A and B Optic nerve and Sciatic nerve.

To allow for higher resolution analysis of *Plp* promoter activity in CNS tissues at a later time point, *Plp-Cre* transgenic mice were crossed to a reporter line expressing *tomato red* and *EGFP* driven by the constitutively active ROSA26 locus (*mT/mG*). A floxed stop region located upstream of the *EGFP* coding sequence necessitates Cre-mediated excision to allow for *EGFP* expression. All cells in which excision of the stop region does not occur would express *tomato red* only. Brain and spinal cord sections from P28 *Plp-Cre;mT/mG* transgenic mice were analyzed. Similar to the *Plp-Cre;Rosa26*^{LacZ} double transgenic line, we observed high levels of EGFP expression throughout CNS tissues occurring outside of oligodendrocyte-rich regions (Figure 2.8B, C, D). Only very discreet zones remained tomato red positive, localizing predominantly to macro- and micro-vasculature in the cerebellum (Figure 2.8B), forebrain (Figure 2.8C), and spinal cord (Figure 2.8D) areas. A typical example of fluorescent patterning in the absence of Cre is shown as a control (Figure 2.8A).

Both the *Rosa26*^{LacZ} and *mT/mG* reporter lines clearly demonstrate *Plp* promoter driven Cre activity outside of the oligodendrocyte lineage, beginning as early as E10.5. By P28, with the exception of vasculature, almost all cell types within CNS tissues examined, either during embryonic and/or early postnatal development, have activated the *Plp* promoter region as denoted by high β-galactosidase or EGFP expression levels.

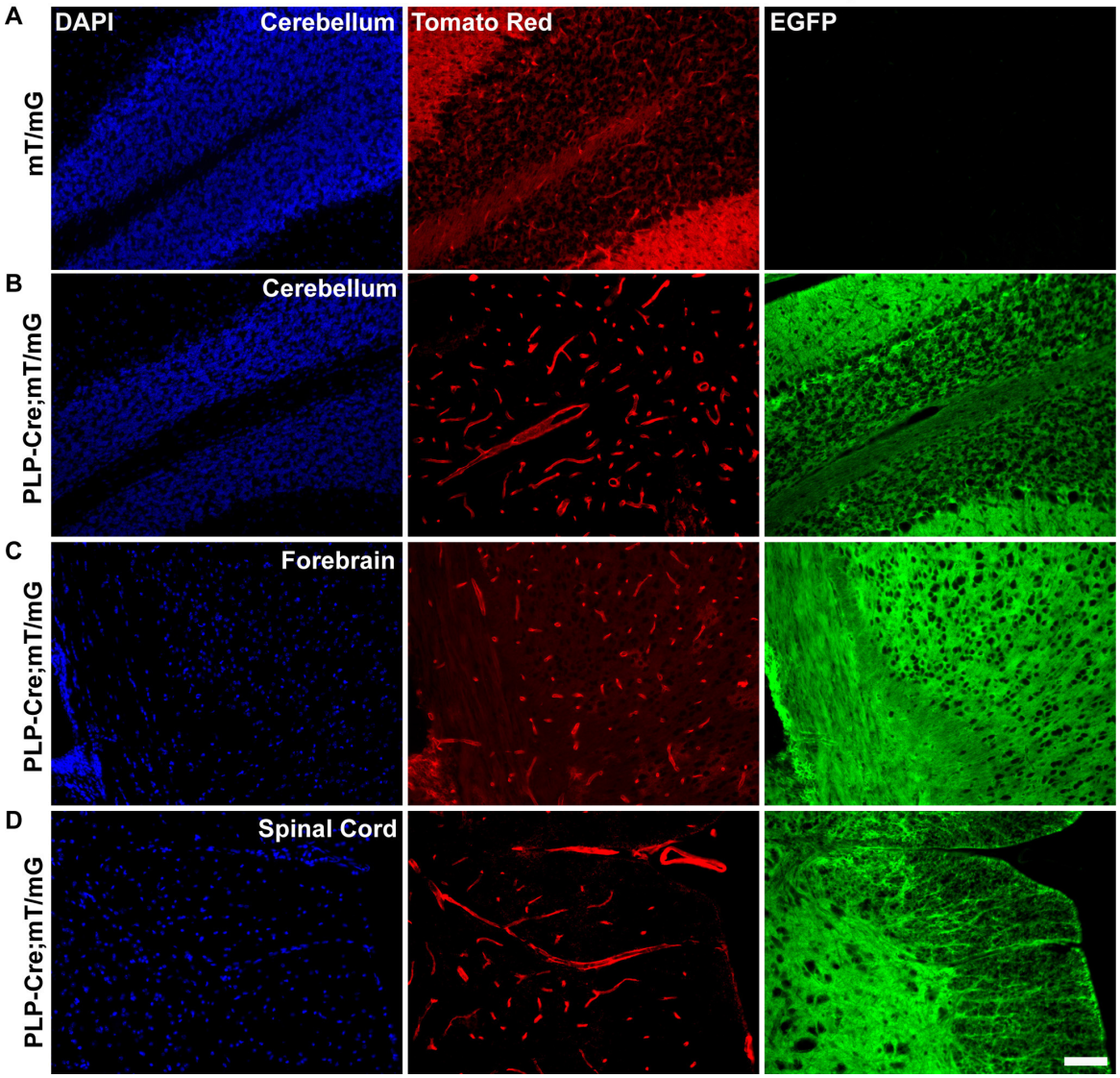

Figure 2.8. EGFP expression occurs outside of the oligodendrocyte lineage in CNS tissue of P28 *Plp-Cre;mT/mG* mice. A. Representative example of *mT/mG* reporter expression in the absence of Cre recombinase in sections of the cerebellum from non-transgenic mice. Only tomato red expression is detected and EGFP expression is absent. **B.** EGFP expression in cerebellum of *Plp-Cre;mT/mG* mice. EGFP is expressed throughout the cerebellum, including the granular, Purkinje and molecular layers. Non-recombined cells, marked by tomato red expression, are limited to the vasculature. **C.** EGFP expression in forebrain region of *Plp-Cre;mT/mG* mice. EGFP is detected throughout the region. Non-recombined cells, marked by tomato red expression, are

limited predominantly to vasculature. **D.** EGFP expression in spinal cord of *Plp-Cre;mT/mG* mice. EGFP is detected throughout the spinal cord including gray and white matter zones. Non-recombined cells, marked by tomato red expression, are limited to vasculature. Scale bar = 50 μm.

Discussion

Here we have characterized two independent transgenic mouse lines in which Cre recombinase is expressed under the control of the mouse *Plp* promoter. We demonstrate the *Plp* promoter cassette's capability to drive expression of a Cre recombinase transgene within the CNS, but in a more widespread pattern than initially anticipated. This was particularly true at early developmental stages when the transgene was expressed in neural tissues, and not restricted to the oligodendrocyte lineage, results corroborated by the work of others (Greenfield et al., 2006; Delaunay et al., 2008; Tuason et al., 2008; Miller et al., 2009). During this time, transgene expression was also localized to the PNS (sciatic nerve, ventral and dorsal roots), most likely in Schwann cells. It was only at late postnatal stages that the *Plp-Cre* transgene demonstrated a high level of oligodendrocyte specificity.

At the mRNA level, Cre expression was highly restricted to CNS tissues (within those examined) at early and late stages of postnatal development. At both P4 and P28, transgene expression was detected in cortex, cerebellum, and spinal cord. In addition, at P4, Cre transcript was also detected in the kidney, liver, skeletal muscle, and heart of mice from line 627, albeit at a level lower than that in neural tissues.

At the protein level in the optic nerve, spinal cord, and cerebellum of P28 transgenic mice Cre recombinase was predominantly in mature oligodendrocytes as identified by CC-1 staining. However, at P4, Cre protein expression was more widespread, localizing to granular (Figure 2.5E-F, K-L) and Purkinje cell layers within the cerebellum, and throughout spinal cord astrocytes. Previous studies have also identified *Plp* gene products in the external granular and Purkinje cell layers of the

developing mouse cerebellum, as well as in grey matter astrocytes of the developing spinal cord (Jacobs et al., 2003; Kang et al., 2010).

The fact that the *Plp-CreER*^{t} transgenic mice have an inducible Cre protein allowed for tracking of the *Plp* promoter activity from specific developmental stages onward. Indeed, the administration of tamoxifen at specific time points allowed us to follow the fate of cells that were *Plp* positive at the time of administration. The reporter-positive cells observed at later stages are the progeny of *Plp* promoter active cells at the time of tamoxifen administration. Mice given tamoxifen at P4 displayed the *Plp* promoter's promiscuity at this early time point, with the result that β-galactosidase reporter expression was detected in neuronal non-white matter regions at later time points. In stark contrast, the β-galactosidase expression profile in mice receiving tamoxifen at P16 was limited strictly to white matter zones at later stages of analysis. From these studies, a clear *Plp* promoter driven spatio-temporal patterning emerges for the CNS – that of neuronal inclusion early in postnatal development, with later stages defined by increased oligodendrocyte specificity.

Our transgene product, by analysis of *Plp-Cre;Rosa26*^{LacZ} mice, proved to be functional in a large range of cell types during embryogenesis. This is dramatically demonstrated in the crosses to the *mT/mG* reporter mice, in which, by P28 all but discreet zones of CNS vasculature expressed excision activated EGFP.

To better understand where and when the *Plp* promoter is active in the CNS, it is important to consider the products of the *Plp* gene. The promoter drives production of both PLP and its splice variant DM-20. The splice site is located within exon three of the gene, producing a transcript product lacking exon 3B (Nave et al., 1987). The protein structure of the smaller isoform DM-20 is identical to PLP except for the removal of

amino acids 116 through 150 (Macklin et al., 1987). DM-20 mRNA has been detected by RT-PCR in the murine neural tube and spinal cord during embryonic development, whereas the PLP transcript is the predominant postnatal isoform (Timsit et al., 1992; Dickinson et al., 1996). *In situ* hybridization experiments at E10 using a DM-20 anti-sense probe detected signal in both the CNS (neural tube within the diencephalic basal plate) and the PNS (trigeminal and spinal ganglia, and sympathetic ganglion chain) (Timsit et al., 1992, 1995). Other studies have confirmed this observation, demonstrating the presence of PLP/DM-20 RNA transcript as early as E9.5 (Ikenaka et al., 1992; Spassky et al., 1998). DM-20 is therefore clearly present in cells long before the appearance of defined mature or even precursor oligodendrocytes. Previous studies have shown DM-20 outside of the glial cell lineage, with expression detected in diverse cell types, including various neuronal cell lines such as G-26, B104, NG108-15, NG18-TG, Neuro2A, PC12, and P19 (Campagnoni et al., 1992; Ikenaka et al., 1992; Nadon et al., 1997). PLP/DM-20 transcripts and/or protein have also been found in cells of the thymus, spleen and testicles (Pribyl et al., 1996a, 1996b).

Recently, various groups have identified specific cellular subtypes within the murine CNS expressing *Plp* gene products at early embryonic and postnatal stages. One such study tracked the fate of $NG2^+$ oligodendrocyte progenitors co-labeling for *Plp* promoter driven EGFP (Guo et al., 2009). They demonstrated the ability of the progenitors to not only differentiate into myelinating oligodendrocytes, but also into astrocytes and neurons. Another study compared PLP/DM-20 transcript levels at P5 and adult stages, between whole murine cortex and isolated NG2-positive cells. PLP mRNA was detected in isolated NG2-positive cells at both time points, whereas DM-20 mRNA

was amplified from whole cortex only (Ye et al., 2003). Similar to our own experiments, Delauney and colleagues crossed *Plp-Cre* mice to a GFP reporter, subsequently identifying GFP-positive neuroepithelial cells at E9.5, with the expressing profile switching to reporter-positive radial glial cells by E13.5 (Delaunay et al., 2008).

Thus, it is clear that the two *Plp* gene products yield varying and different expression profiles, and can be generally classified as follows – *Plp,* while expressed early in various CNS cellular subtypes, is at its highest levels postnatally and in an oligodendrocyte-specific manner, while *DM-20* is preferentially expressed early and diffusely in the embryo. It is therefore important to recognize the possibility for *Plp* promoter driven transgene expression simply as a by-product through activation of factors normally involved in DM-20 regulation.

Interestingly, in 1999 a novel exon was discovered lying within intron 1 of the *Plp* gene. Termed exon 1.1, it produced a protein with an additional 12 amino acid leader sequence (Bongarzone et al., 1999). The additional sequence allowed for expression of two further *Plp* variants, termed sr-PLP and sr-DM-20. These proteins have been detected in oligodendrocytes, muscle, and to an even larger extent in neurons (Bongarzone et al., 1999; Jacobs et al., 2004; Miller et al., 2009). Two similar novel exons have recently been discovered in intron 1 of the human *Plp1* gene, giving rise to unique PLP isoforms (Sarret et al., 2010). The isoforms are expressed predominantly in neurons and to lesser extent in oligodendrocytes, beginning during human fetal development. The authors suggest a role for the proteins in axonal-glial communication, the disruption of which would account for neuronal dysfunction in humans carrying *Plp1* mutations.

The very early and widespread expression of our transgene product forces us to reconsider certain aspects of *Plp* gene regulation. Perhaps there are regulatory elements

activated differentially for each of the *Plp* derived isoforms, responsible for the specific spatial and temporal expression patterns observed during embryonic and postnatal development. Recent evidence suggests that this could indeed be the case. Within the *Plp* gene, six evolutionary conserved non-protein coding sequences were identified as *Plp/DM-20* enhancers, five of which were located within intron 1 (Tuason et al., 2008). When inserted as single copies driving expression of an *EGFPLacZ* reporter gene, each unique regulatory sequence matched characterized components of the *Plp* promoter's spatio-temporal expression profile as seen through a spectra of glial and neuronal lineage patterning.

The present study informs on *Plp* promoter functionality as a driver for both Cre and other transgene expression. Since the goal of many such studies is oligodendrocyte targeting within the CNS, it is important to better understand differences in gene regulation between *Plp* splice variants. Once more information is obtained deciphering the different regulatory elements governing expression of *Plp*/*DM-20* and sr-*Plp*/*sr-DM-20*, one could perhaps design a more specific promoter construct, which would allow for a postnatal, and more robust oligodendrocyte-specific expression of the requisite transgene. In the mean time, our work would stress that as long as one uses the tamoxifen inducible system (*Plp-CreER*^{t}) and induces Cre activity at adult stages, one can achieve oligodendrocyte specific excision of target genes.

Acknowledgments

We thank members of the Kothary laboratory for critical reading of the manuscript. We also thank Dr. Popko for the *Plp-CreER*^{t} mice, Dr. Wallace for the *ROSA26*^{LacZ} mice, and Dr. Bennett for the *mT/mG* mice. This work was supported by a grant from the Multiple Sclerosis Society of Canada to R.K. J-P.M. is supported by a Studentship from the Multiple Sclerosis Society of Canada. The funders had no role in study design, data collection, and analysis, decision to publish, or preparation of the manuscript.

Supporting Information

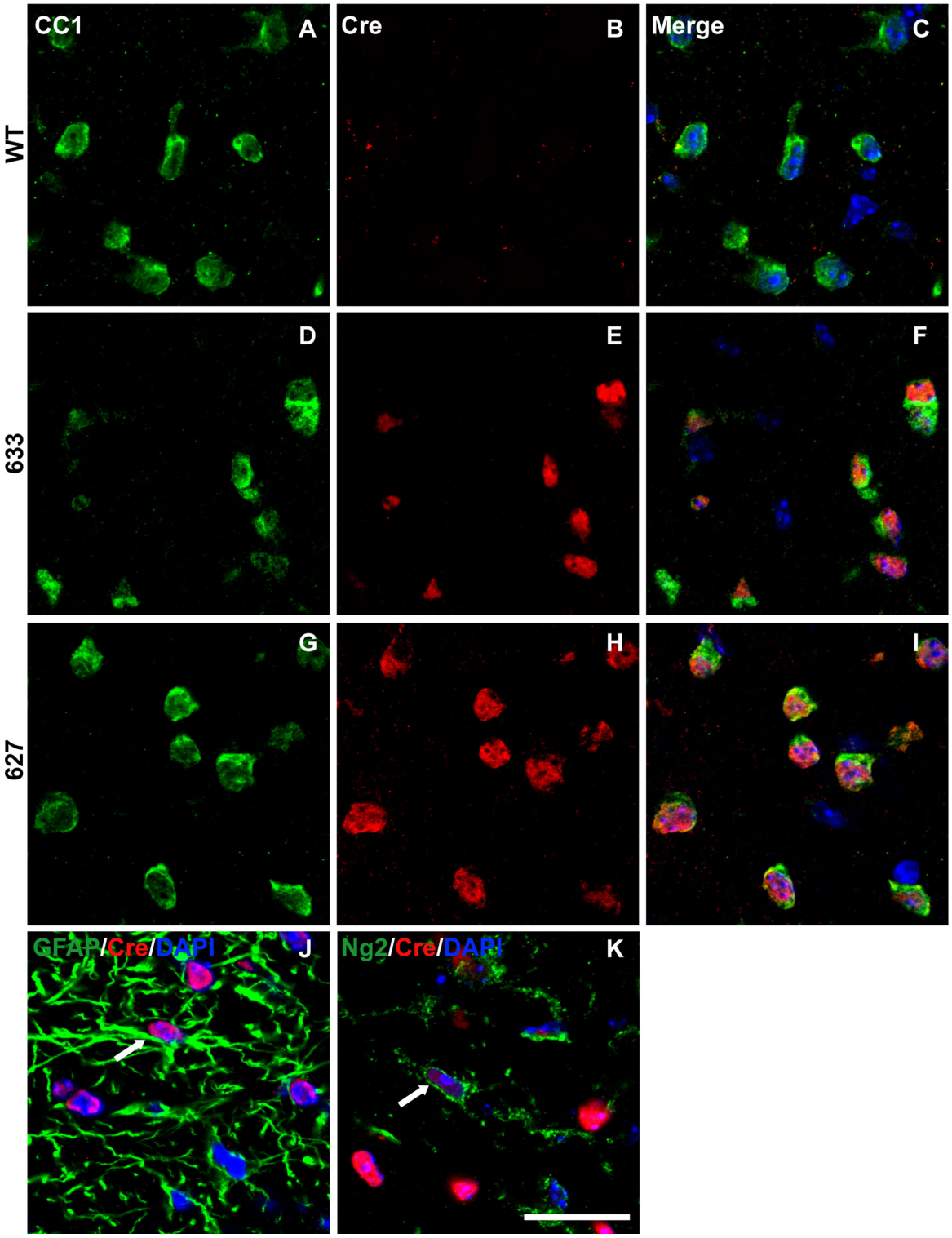

Figure S2.1. Cre-recombinase is predominantly expressed in oligodendrocytes of P28 *Plp-Cre* mouse optic nerves. A-I. Optic nerve sections were double-stained with

antibodies specific to CC-1 as a marker for mature oligodendrocytes (green), Cre (red) and counterstained with DAPI. Cre was not detected in WT optic nerve sections (B). Sections from transgenic mice of both F633 (D-F) and F627 (G-I) lines exhibited a similar pattern of Cre expression. High levels of Cre recombinase protein were detected in the CC1-positive oligodendrocytes. **J.** Optic nerve section stained for GFAP (green) as a marker for astrocytes, Cre (red) and counterstained with DAPI. A very small number of Cre-positive cells were also positive for GFAP. **K.** Optic nerve section stained for Ng2 (green) as a marker for OPCs, Cre (red) and counterstained with DAPI. A very small number of weakly stained Cre-positive cells co-labeled with Ng2 (arrow). Scale bar = 20 μm.

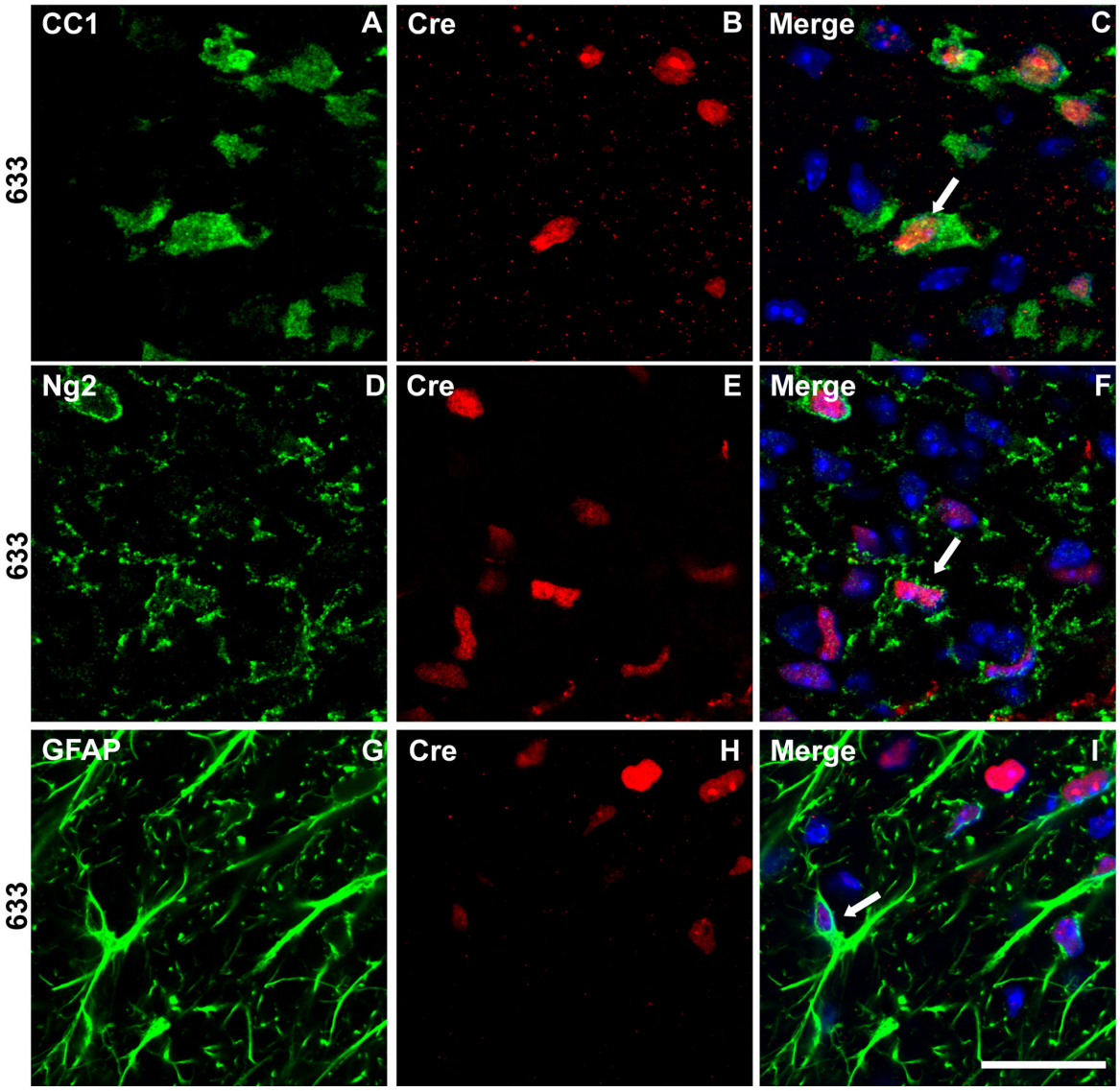

Figure S2.2. Cre-recombinase is expressed both in and outside of the oligodendrocyte lineage in the spinal cord of *Plp-Cre* mice from line 633. A-I. Ventral spinal cord sections from *Plp-Cre* line 633 mice were double-stained with antibodies specific to Cre (red) recombinase and either CC1 (green) for mature oligodendrocytes (A-C), Ng2 (green) for OPCs (D-F) or GFAP (green) for astrocytes (G-I) and counterstained with DAPI. Similar to line 627 many Cre-positive cells were CC-1-positive, however, a large percentage also co-stained for Ng2 and GFAP. Examples of

Cre and glial marker co-labeling are denoted by arrows. WM = white matter, GM = grey matter. Scale bar = 20 μm.

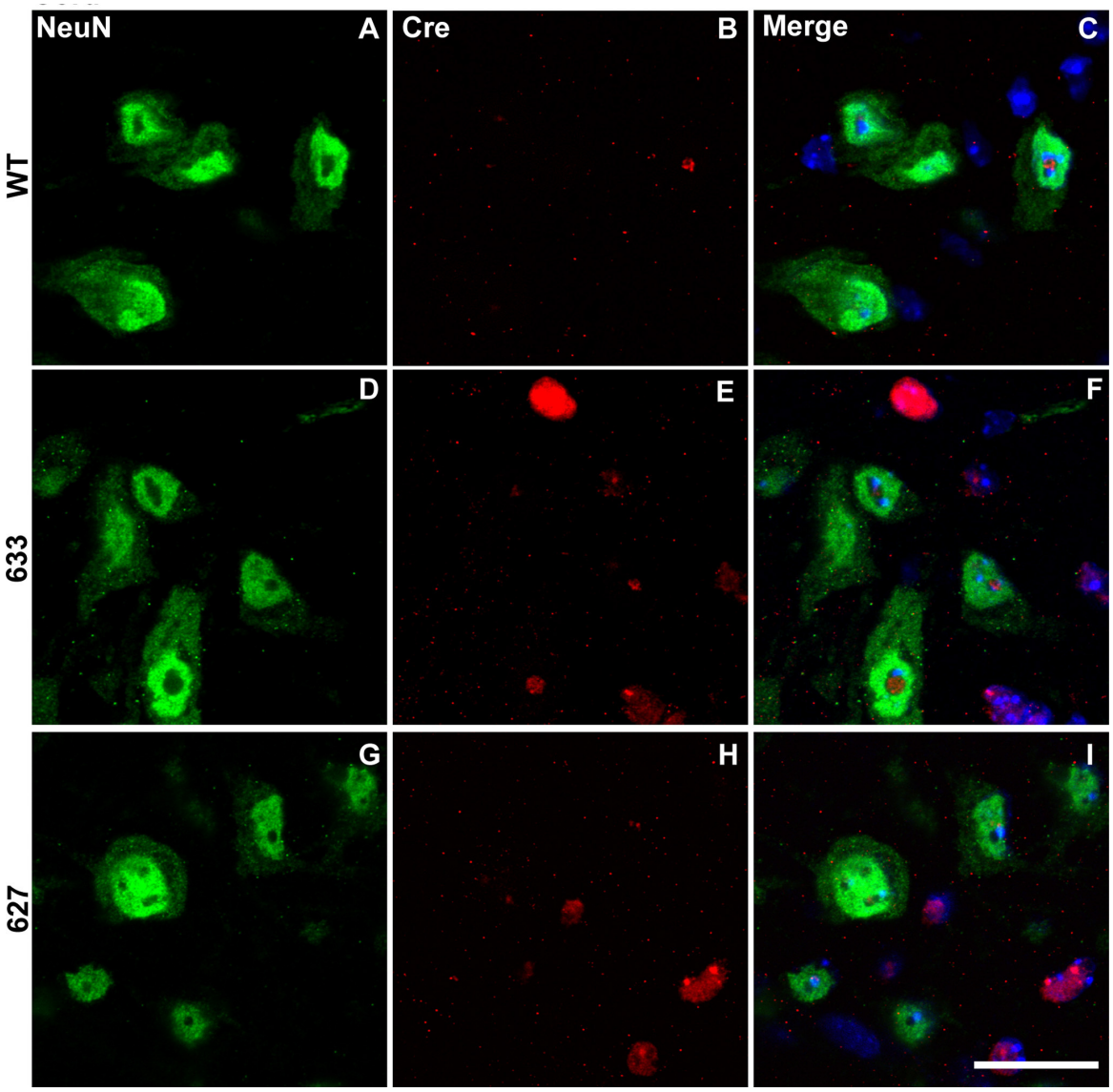

Figure S2.3. Cre-recombinase is not expressed in spinal cord neurons of P4 *Plp-Cre* mice. A-I. Ventral spinal cord sections were double-stained with antibodies specific to NeuN (green) as a marker for mature neurons, Cre (red), and counterstained with DAPI. Cre was not detected in WT sections (B). The low level puncti signal in the alpha motor neurons is background fluorescence. Sections from transgenic mice of both 633 (D-F) and 627 (G-I) lines exhibited a similar pattern of Cre expression. Cre-positive cells did not co-label with NeuN. Scale bar = 20 µm.

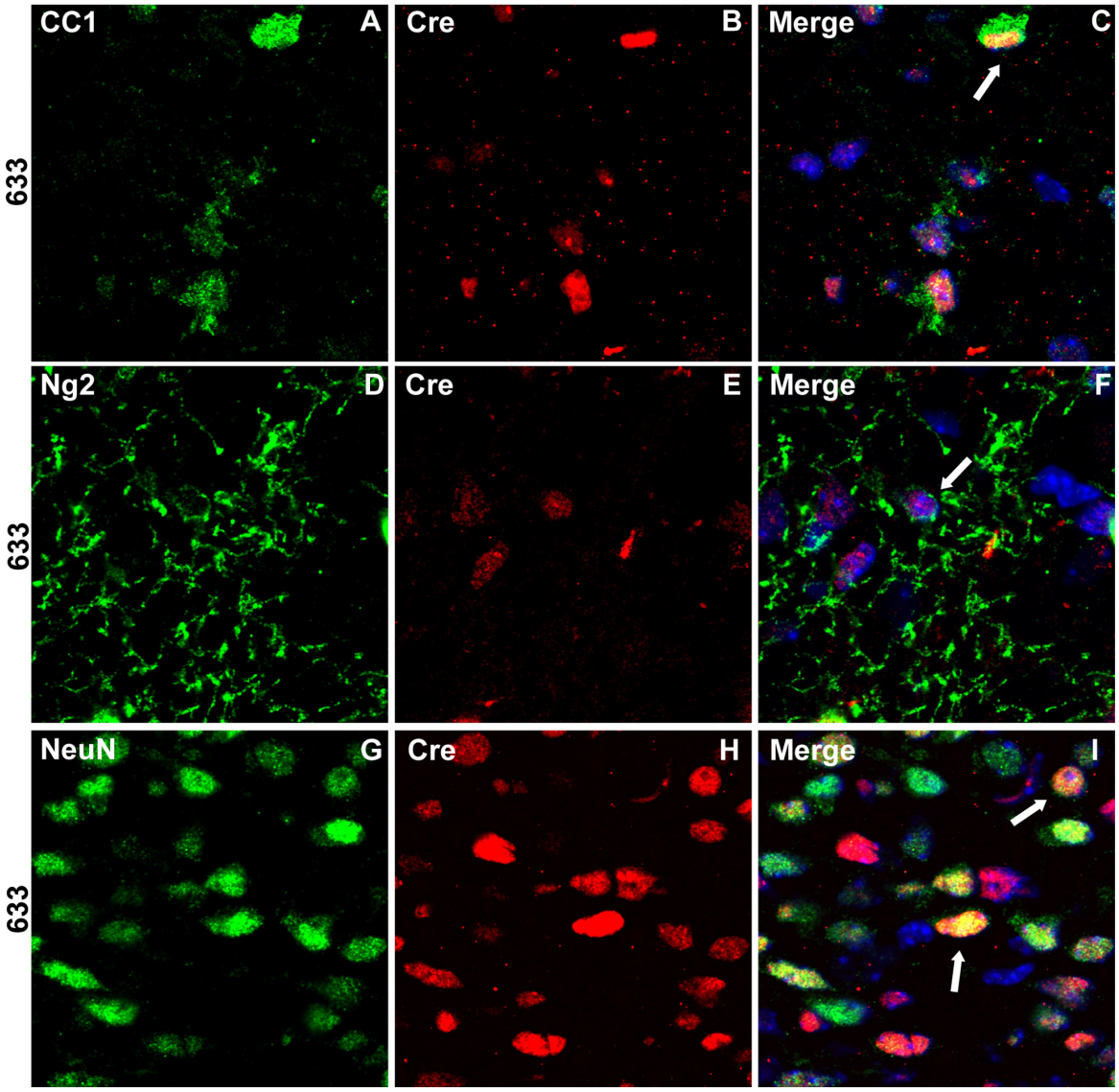

Figure S2.4. Cre-recombinase is expressed both in and outside of the oligodendrocyte lineage in the cerebellum of *Plp-Cre* mice from line 633. A-F. Deep cerebellar white matter regions from *Plp-Cre* line 633 mice were double-stained with antibodies specific to Cre (red) and either CC-1 (green) as a marker for mature oligodendrocytes (A-C), or Ng2 (green) as a marker for OPCs (D-F) and counterstained with DAPI. Similar to line 627, a large percentage of Cre-positive cells within the region co-stained for CC-1 and Ng2. **G-I.** Cerebellar sections of the developing granular layer from *Plp-Cre* line 633 mice were double-stained with antibodies specific to Cre (red), the

neuronal marker NeuN (green) and counterstained with DAPI. Similar to line 627, many Cre-positive cells co-stained for NeuN. Examples of Cre-positive cells co-labeling with neuronal or glial markers are denoted by arrows. Scale bar = 20 μm.

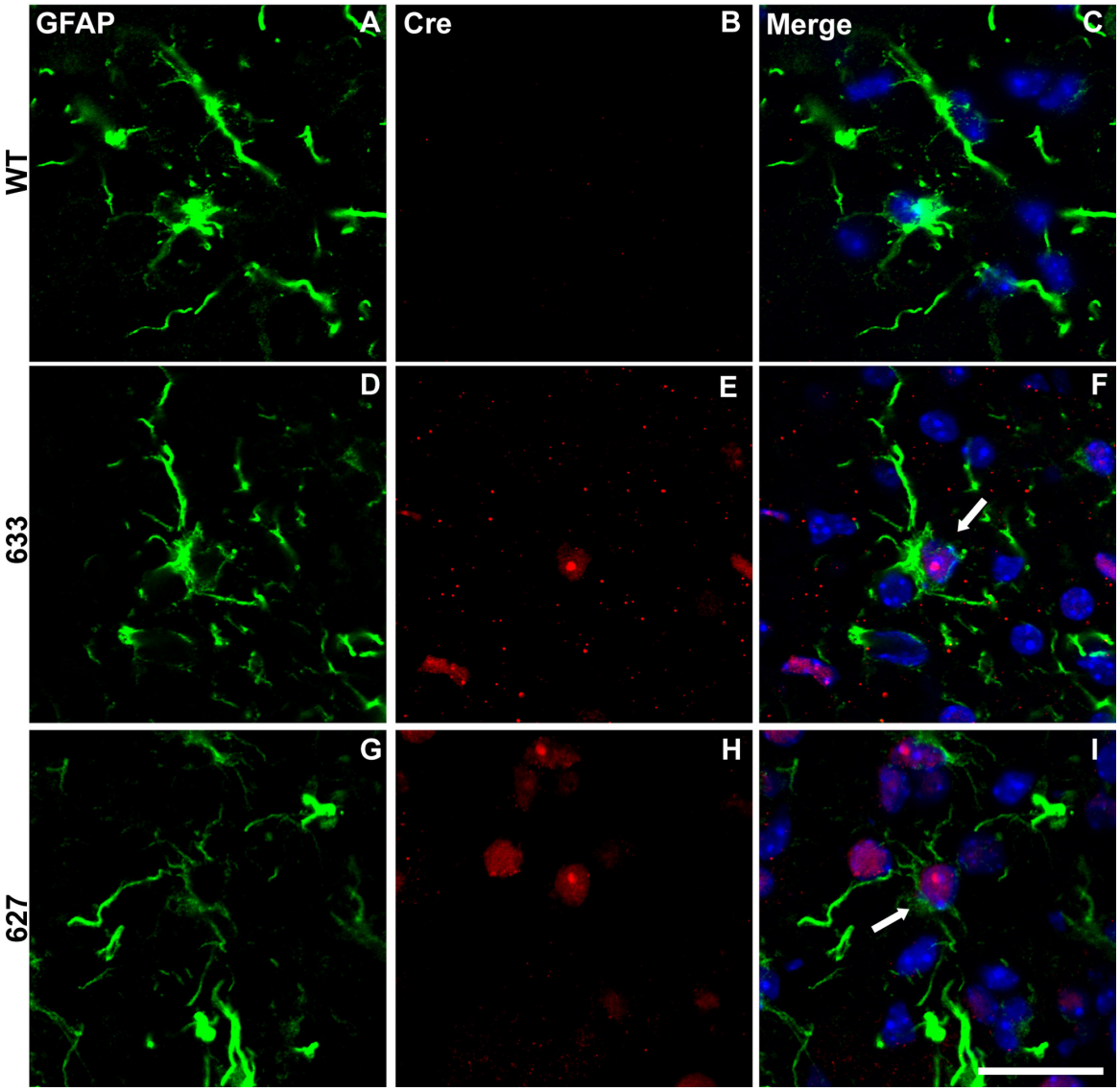

Figure S2.5. Cre-recombinase is expressed in cerebellar astrocytes of P4 *Plp-Cre* mice. A-I. Deep cerebellar white matter region sections were double-stained with antibodies specific to GFAP (green) as a marker for astrocytes, Cre (red), and counterstained with DAPI. Cre was not detected in WT sections (B). Sections from transgenic mice of both 633 (D-F) and 627 (G-I) lines exhibited a similar pattern of Cre expression. Only a small number of Cre-positive cells co-stained with GFAP. Examples of GFAP-positive cells co-labeling with Cre are denoted by arrows. Scale bar = 20 μm.

Chapter 3

Integrin-Linked Kinase Regulates Oligodendrocyte-Mediated Myelination of the CNS

Integrin-linked kinase regulates process extension in oligodendrocytes via control of actin cytoskeletal dynamics

Ryan W. O'Meara[1,*], John-Paul Michalski[1,*], Carrie Anderson[1], Kunal Bhanot[1], Peter Rippstein[2], and Rashmi Kothary[1,3,#]

[*]These authors contributed equally to this work

[1]Ottawa Hospital Research Institute, Ottawa, Ontario, Canada K1H 8L6; and Department of Cellular and Molecular Medicine, University of Ottawa, Ottawa, Ontario, Canada K1H 8M5;

[2]Lipoproteins and Atherosclerosis Group, University of Ottawa Heart Institute, Ottawa, Ontario, Canada K1Y 1V1;

[3]Department of Medicine, University of Ottawa, Ottawa, Ontario, Canada K1H 8M5

#Correspondence to: Rashmi Kothary

Published in *Journal of Neuroscience*, 2013 Jun 5, 33(23):9781-93.

Author Contributions

Conceived and designed the experiments: J-PM, RO, RK. Performed the experiments: J-PM (Figures 3.6, 3.7, 3.8, 3.9, 3.11), RO (Figures 3.1, 3.2, 3.3, 3.4, 3.5, 3.10). RO also helped construct Figure 3.9. KB generated an ILK-GFP construct. J-PM and RO analyzed the data. J-PM and RO wrote the paper and RK revised and edited the manuscript.

Abstract

Integrin-linked kinase (ILK) is a major structural adaptor protein governing signaling complex formation and cytoskeletal dynamics. Here, through the use of conditional knockout mice, we demonstrate a requirement for ILK in oligodendrocyte differentiation and axonal myelination *in vivo*. In conjunction, ILK deficient primary oligodendrocytes are defined by a failure in process extension and an inability to form myelin membrane upon axonal contact. Surprisingly, phosphorylation of the putative downstream targets Akt and GSK3β is unaffected following ILK loss. Rather, the defects are due in part to actin cytoskeleton dysregulation with a correspondent increase in active RhoA levels. Morphological rescue is possible following Rho kinase (ROCK) inhibition in an oligodendrocyte subset. Furthermore, phenotypic severity correlates with environmental complexity; oligodendrocytes are severely malformed *in vitro* (a relatively simple environment) but undergo phenotypic recovery in the context of the whole animal. Taken together, our work demonstrates ILK as necessary for normal oligodendrocyte development, reinforces its role as a bridge between the actin cytoskeleton and cell membrane, and highlights the overarching compensatory capacity of oligodendrocytes in response to cellular milieu.

Introduction

During development, oligodendrocyte precursor cells (OPCs) differentiate into oligodendrocytes (OLs) that extend processes to contact multiple axons of central nervous system (CNS) neurons. The process of myelination is controlled in part by cell extrinsic factors derived from the extracellular matrix (ECM). Laminin-2 (Ln-2) is an ECM component with high relevance to OL-mediated myelination of the CNS (O'Meara et al., 2011a). Ln-2 is deposited in developing axonal tracts (Colognato et al., 2002), providing a ligand for the α6β1 integrin receptor expressed by OLs. The β1 integrin subunit was previously shown to regulate OL process extension *in vitro* (Buttery and Ffrench-Constant, 1999; Relvas et al., 2001; Liang et al., 2004; Barros et al., 2009) and myelination *in vivo* (Relvas et al., 2001; Lee et al., 2006; Barros et al., 2009; Câmara et al., 2009). In light of these findings, precisely how β1 integrin transduces ECM cues via signaling intermediates, and the mechanism by which this translates to cellular responses need to be addressed.

Integrin-linked kinase (ILK), a focal adhesion protein, binds to the cytosolic C-terminus of β1 integrin (Hannigan et al., 1996), and mediates signaling between the ECM and the cellular interior. ILK is composed of three domains, an N-terminal ankryin domain, a pleckstrin homology domain and a putative kinase domain. ILK forms an obligate heterotrimeric complex with PINCH and parvin, which together lend stability to the actin cytoskeleton at focal adhesions (Brakebusch and Fässler, 2003). This function is likely mediated through additional signaling proteins, such as paxillin and PIX, ultimately impacting on actin modulator proteins via Rho GTPases (Rosenberger et al., 2003).

In this study, we sought to investigate the role of ILK in OL differentiation and myelination of the CNS. By ablating ILK from cultured OPCs, we show that it is

important for their molecular and morphological differentiation. Conditional ILK loss in post-natal mice results in amyelination of optic nerve axons, an effect that is compensated for at later time points. There is evidence of a bonafide kinase function for ILK (reviewed in Hannigan et al., 2011) however, we did not observe any changes in the phosphorylation status of its canonical targets GSK3β and Akt in ILK-depleted OLs. Rather, we observe an increase in active RhoA levels as a result of ILK loss, a phenomenon associated with actin cytoskeletal defects. Interestingly, pharmacological manipulation of the RhoA pathway is able to rescue aberrant morphology of a distinct population of ILK-deficient OLs. Our data indicate an important role for ILK in OL development and myelination of the CNS, which, in turn, is linked to regulation of the actin cytoskeleton. Understanding OL differentiation will be important for rectifying or circumventing myelinating diseases such as Multiple Sclerosis, where demyelinated lesions are characterized by stalled premyelinating OLs (Chang et al., 2002).

Materials and Methods

Transgenic and reporter mice: The mice used in this work were cared for according to Canadian Council on Animal Care (CCAC) guidelines. Ethical approval for experiments conducted was obtained from the University of Ottawa Animal Care Committee under protocol number OGH-119. *Ilk*$^{fl/fl}$ and *Plp-CreER*^{T} mice were provided by Dr. Rene St-Arnaud (Terpstra et al., 2003) and Dr. Brian Popko (Doerflinger et al., 2003), respectively. Two mouse strains were primarily employed for experiments, *Ilk*$^{fl/fl}$*;Plp-CreER*^{T}/+ mice (*Ilk cKO*), as well as *Ilk*$^{fl/fl}$;+/+ (WT) littermates controls. An injection of 0.375-0.5 mg of tamoxifen (7.5 or 10 µL of a 50 mg/mL solution, respectively) was administered to P4 pups to induce recombination. For the low dose tamoxifen experiments, P4 mice were given a single 10 µL injection from a 2 mg/mL tamoxifen solution to induce minimal recombination. *Ilk cKO* mice were crossed to a floxed stop tdTomato-EGFP (*mT/mG*) reporter line (Muzumdar et al., 2007) to generate *Ilk*$^{fl/fl}$*;Plp-CreER*^{T}*/+;mT/mG* (*Ilk cKO;mT/mG*) mice, which were bred to homozygosity for the reporter transgene. Mice of either sex were employed for all experiments.

Cell culture*:* OL cultures and OL/dorsal root ganglion neuron (DRGN) co-cultures were derived as previously described (O'Meara et al., 2011b). For ROCK inhibition, compound Y-27632 was added to each well at a final concentration of 10 µM daily, for 6 days. For control wells, an equal volume of water (vehicle) was added.

Immunohistochemistry: Cell culture coverslips were fixed with 100% methanol at -20^{o}C for 10 min or 3% paraformaldehyde (PFA) at room temperature for 15 min. Coverslips were then washed with phosphate buffered saline (PBS), permeabilized with 0.1% Triton-

X-100 solution, blocked with 10% goat serum (GS) and incubated with primary antibodies against myelin-associated glycoprotein (MAG; EMD Millipore), myelin basic protein (MBP; AbD Serotec), CC1 (Abcam), green fluorescent protein (GFP; Invitrogen), neurofilament-200 (NF-200; Sigma-Aldrich), cleaved caspase 3 (Cell Signaling [Asp175]), 5-bromo-2'-deoxyuridine (BrdU; BD Biosciences) and NG2 (EMD Millipore) in blocking solution at 4^{o}C overnight. Coverslips were then washed with PBS, and incubated with Alexa fluor conjugated secondary antibodies (Alexa-488, Alexa-555, Alexa-647; Invitrogen) and/or rhodamine phalloidin (Invitrogen). Samples were then counterstained with 4',6-diamidino-2-phenylindole (DAPI) and mounted in DAKO (Dako North America, Inc.) mounting medium.

For immunohistochemistry of murine tissue, mice were anesthetized with tribromoethanol (Avertin) and perfused transcardially with 4% PFA. Optic nerves were dissected in PBS and post-fixed overnight in 4% PFA at 4°C followed by overnight cryopreservation in 30% sucrose/PBS at 4°C and then embedded in a 1:1 mixture of 30% sucrose/OCT (Sakura, CA). Briefly, 10 μm sections were washed with PBS followed by a 10-30 min incubation in citrate buffer (10 mM citric acid, 26 mM NaOH, pH 6) for certain antibodies. Sections were blocked in either 10% GS with 1% BSA and 0.2% Triton-X-100 or TBLS (0.5 mM Tris-HCl pH 7.4, 0.0085% NaCl, 0.01% BSA, 0.009% L-lysine, and 10% sodium azide) with 20% GS and 0.3% Triton-X-100 for 1 hour. Primary antibodies were diluted in either 1% GS with 1% BSA and 0.2% Triton-X-100 or TBLS with 20% GS and 0.3% Triton-X-100 and placed on sections overnight at 4°C. Sections were then washed and incubated with Alexa fluor conjugated secondary antibodies (Invitrogen) in the same solution as primary antibodies. Sections were counterstained with DAPI and mounted in DAKO mounting medium.

***BrdU labeling**:* DIV2 OL cultures were pulsed with approximately 20 nM of BrdU for 4 hours, and subsequently fixed with 3% PFA at room temperature for 15 min. Coverslips were washed in PBS, permeabilized with 0.1% Triton-X-100 solution, and treated with 2 N HCl for 20 min on a rotary shaker. Samples were then topped up with an equal volume of 0.1 M Tris-HCl pH 9.5 and incubated on the rotary shaker for an additional 20 min. Samples were then stained with anti-BrdU antibody using the same method as described above.

Whole mount immunohistochemistry: Mice were anesthetized with Avertin and sacrificed at either P14 or P28. The optic nerve was immediately removed and placed in a 4% PFA solution for 1 hour at room temperature with gentle agitation. The nerve was then washed in PBS followed by a 30 minute incubation in 2% Triton-X-100 and blocked in a 4% BSA, 1% Triton-X-100 solution. The optic nerve was then incubated overnight with an antibody against GFP in blocking solution. The next day, an Alexa fluor conjugated secondary antibody was applied in blocking solution for 4 hours, followed by washes in PBS. The optic nerves were finally counterstained with DAPI, given final washes in 0.1% Triton-X-100 and mounted in DAKO mounting medium. Images were acquired and processed as Z-stacks through the whole mount preparation to visualize OLs and associated internodes in their entirety.

Electron microscopy: Mice were anesthetized with Avertin and perfused transcardially with Karnovsky's fixative (4% PFA, 5% glutaraldehyde, 0.08 M sodium cacodylate, pH 7.4). The optic nerve was then removed and post-fixed in Karnovsky's fixative at 4°C. Fixed optic nerves were cut into ultrathin sections, stained with uranyl acetate and lead

citrate, and analyzed by electron microscopy. Axon and myelin diameter was determined using the "analysis" tool in Image J set to a known scale. Number of myelinated fibers relative to total fibers was then determined and subdivided into groups by axon diameter. G-ratio was calculated by dividing the axon diameter by the axon plus myelin diameter.

Western blot: Mixed glial cultures were cooled on ice for 3 min, and washed with ice cold PBS. Cells were scraped off the dishes into protein lysis buffer (50 mM Tris-HCl, 150 mM NaCl, 1% NP-40 [IGEPAL]) containing protease inhibitor cocktail (0.01 mg/mL pepstatin, 0.01 mg/mL aprotinin, 0.01 mg/mL leupeptin, 5 mM Na_3VO_4, 1 mM PMSF) and centrifuged at high speed to remove insoluble material. For optic nerves, protein was extracted through tissue homogenization in a lysis buffer solution (50 mM Tris pH 7.4, 150 mM NaCl, 0.1% SDS, 0.5% sodium deoxycholate, and 1% Triton-X-100) containing protease inhibitor cocktail plus 50 mM NaF. Optic nerves from three mice were pooled for each protein sample. For western blotting of proteins obtained from OL cultures, vessels were briefly cooled on ice before cells were lysed in a commercial lysis buffer (Cytoskeleton Inc.). Lysate was then centrifuged at high speed to remove insoluble material. Western blot exposure films were scanned with EPSON Perfection 2450 PHOTO scanner and images were imported into Image J. A box of standard dimensions was placed over each band of a given blot, and the mean gray value was measured for each band. Levels of a given protein of interest were normalized to the GAPDH band intensity.

G-LISA RhoA activation assay*:* DIV3 vehicle and TAT-Cre treated primary OLs were scraped into RhoA G-LISA lysis buffer, and clarified lysates were flash frozen in liquid

nitrogen. The G-LISA assay was conducted on the lysates according to the manufacturer's instructions (Cytoskeleton Inc.). Raw luminescence values were normalized to total RhoA levels as measured by western blotting.

His-TAT-NLS-Cre recombinase (TAT-Cre) treatment*:* TAT-Cre (Excellgen) was added to mixed glial cultures at a concentration of approximately 2-5 μM for 1-4 hours. The following day, the efficiency of the recombination was qualitatively assessed by EGFP fluorescence. OPCs were extracted from the mixed glial cultures and seeded onto Ln-2 substrate 72 hours post TAT-Cre administration as previously described (O'Meara et al., 2011b).

Statistical analysis*:* All statistical analyses were performed using Prism 5/6 GraphPad software. Unless stated otherwise, two-tailed Student's t-tests were employed for statistical analyses, with significance set at $p < 0.05$.

Results

ILK is required for primary OL differentiation

ILK is well known for its role in focal adhesion stabilization (Legate et al., 2006), a function highly dependent on its binding partner α-parvin. Through α-parvin, ILK is connected to the actin cytoskeleton, thus linking cellular interior and ECM. Both ILK and α-parvin proteins were detected at all differentiation time points in cultured primary murine OLs (Figure 3.1A). Expression of 2',3'-cyclic-nucleotide 3'-phosphodiesterase (CNP) and MBP indicates the degree of OL differentiation in the cultures, as these are intermediate and late markers of OL differentiation, respectively (Figure 3.1A). To investigate the role of ILK in primary OL differentiation, we used a conditional knockout approach taking advantage of the $Ilk^{fl/fl}$ mutant mouse (Terpstra et al., 2003) (Figure 3.1B). In order to track which cells had undergone Cre-mediated recombination, $Ilk^{fl/fl}$ mice were crossed to the *mT/mG* reporter line (Muzumdar et al., 2007). Recombination was achieved in culture through the use of TAT-Cre (Peitz et al., 2002), resulting in cessation of tdTomato expression and induction of EGFP (Figure 3.1B, C) in conjunction with excision of the floxed region within the mouse *Ilk* gene (Figure 3.1D). Administration of TAT-Cre also significantly reduced ILK protein levels, and that of its obligate partner α-parvin in transgenic mixed glial cultures (Figure 3.1E, F). OPCs were then derived from these TAT-Cre treated mixed glial cultures (as described in O'Meara et al., 2011b) and seeded on Ln-2 substrates as a purified population for further study.

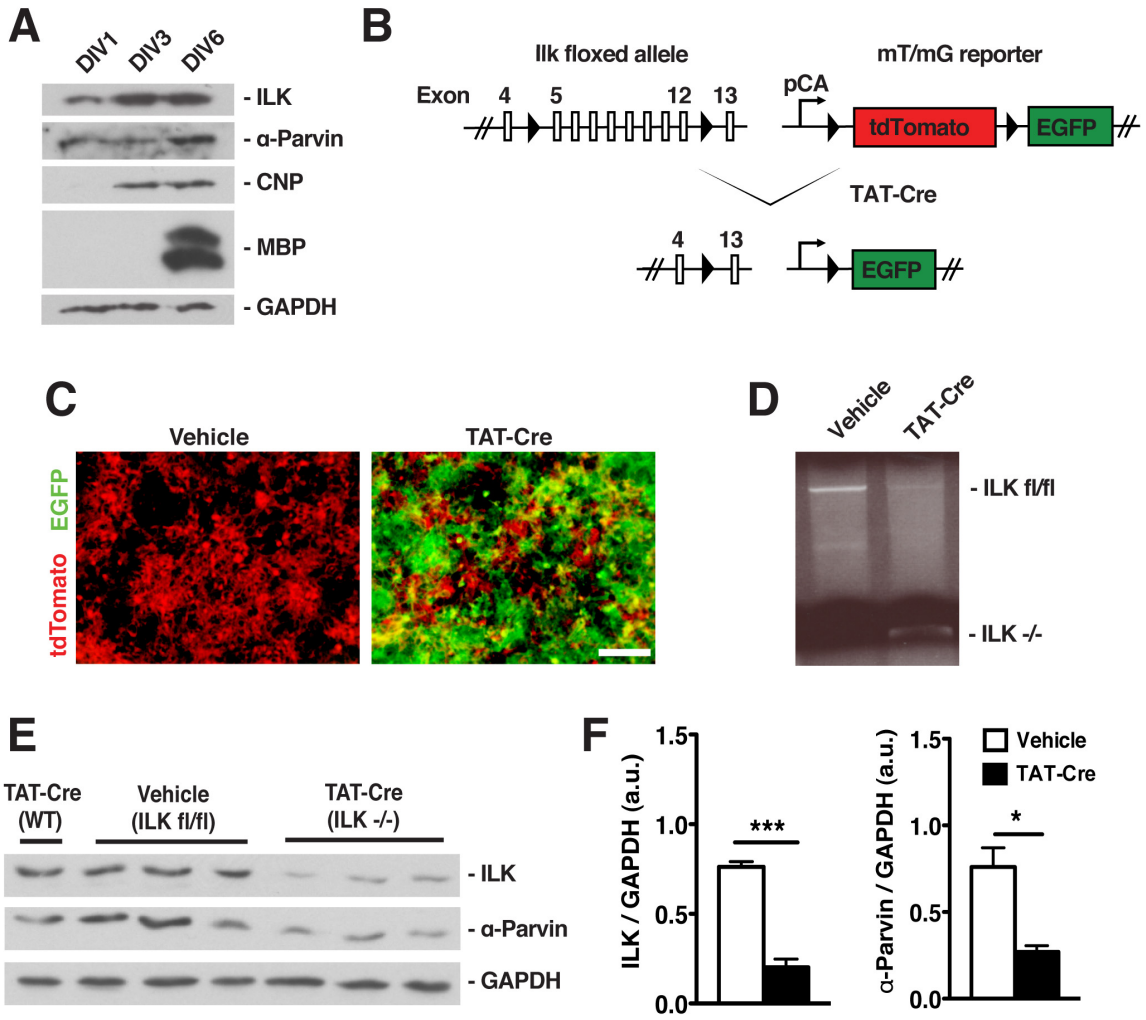

Figure 3.1. Genetic ablation of ILK from primary glial cells. A. Western blot analysis of ILK and α-parvin in primary murine OLs at 3 time points of differentiation (DIV1, DIV3, DIV6). CNP and MBP are intermediate and late maturation markers, respectively. **B.** Schematic showing the floxed *Ilk* allele, with loxP sites flanking the putative kinase domain (exons 5-12), and the *mT/mG* reporter allele. Cre recombination results in nullification of *Ilk*, concomitant with EGFP induction. **C.** Immunofluorescence micrographs of mixed glial cultures derived from $Ilk^{fl/fl}$;*mT/mG* mice treated with vehicle or TAT-Cre. **D.** PCR performed on DNA isolated from TAT-Cre or vehicle treated $Ilk^{fl/fl}$ mixed glial cultures. **E.** Western blot analysis for ILK and α-parvin in $Ilk^{fl/fl}$;*mT/mG*

mixed glial cultures treated with TAT-Cre or vehicle. Three independent samples of each are shown. TAT-Cre treated WT cells are shown as control for toxicity. **F.** Densitometry analysis of western blots in (E) for ILK and α-parvin between TAT-Cre and vehicle treated cultures. Data represents the mean ± SEM (n=3). *p < 0.05, ***p < 0.001; Student's *t* test. Scale bar: 100 μm.

OPC differentiation requires both molecular and morphological cellular alterations. Molecular differentiation coincides with decreased expression of NG2 concomitant with MAG and MBP expression. Upon loss of ILK (*Ilk*$^{-/-}$), a significant proportion of OPCs persisted as NG2^{+ve} precursors at DIV3 and DIV6 of the differentiation time course (Figure 3.2A, B). Accordingly, fewer *Ilk*$^{-/-}$ OLs expressed MAG or MBP as compared to wild type (*Ilk*$^{fl/fl}$) cells. However, a certain proportion of *Ilk*$^{-/-}$ OLs expressed MAG at DIV3 and DIV6, thus persistence of NG2^{+ve} precursors was not a completely penetrant phenotype in response to ILK loss. Furthermore, MBP protein levels (as measured by western blot) were decreased in TAT-Cre treated cultures at both DIV3 and 6 (Figure 3.2C).

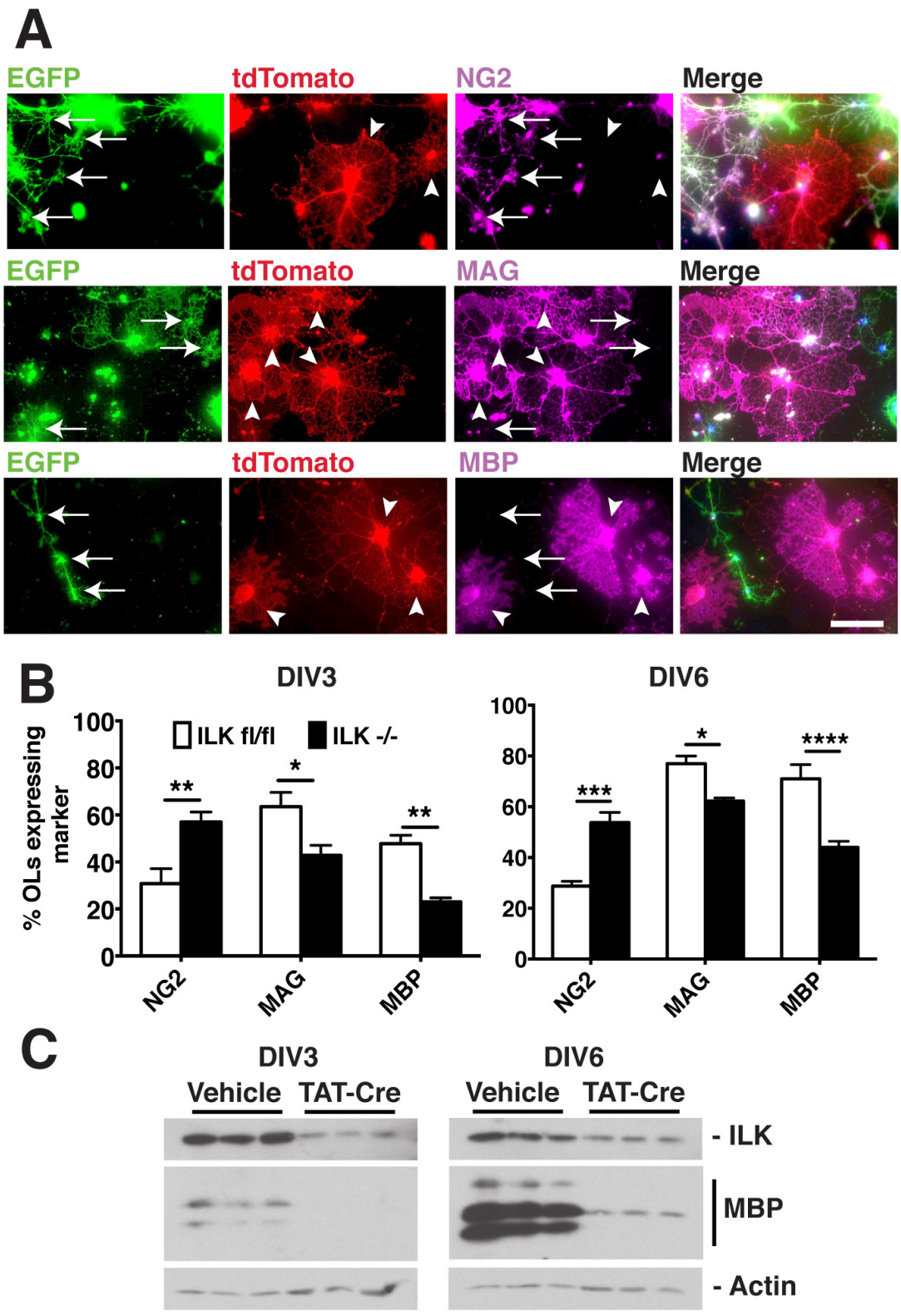

Figure 3.2. Loss of ILK impacts the expression of developmental stage-specific OL markers. **A.** Immunostaining of TAT-Cre treated DIV6 OL cultures for NG2, MAG and

MBP. Arrows and arrowheads indicate *Ilk*$^{-/-}$ and *Ilk*$^{fl/fl}$ OLs respectively. **B.** Quantification of percent of *Ilk*$^{-/-}$ versus *Ilk*$^{fl/fl}$ OLs expressing NG2, MAG or MBP at DIV3 and DIV6. **C.** Western blots of TAT-Cre and vehicle lysates probed for ILK and MBP, with actin serving as a loading control. Data represents the mean ± SEM (n=4). *p < 0.05, **p < 0.01, ***p < 0.001, ****p < 0.0001; two-way ANOVA followed by Bonferonni post-tests. Scale bar: 100 μm.

To investigate whether this apparent delay in lineage progression was an artifact of differential expansion/collapse of *Ilk*$^{-/-}$ or *Ilk*$^{fl/fl}$ OL populations, we conducted of series of cell death and proliferation assays. When total numbers of *Ilk*$^{-/-}$ and *Ilk*$^{fl/fl}$ OL-lineage cells were respectively considered as 100% at DIV1, there was no subsequent difference in cell counts between the genotypes at either DIV3 or DIV6 (Figure 3.3A). This suggests that loss of ILK does not translate to compromised survival of OL-lineage cells. In addition, there was no significant difference in the percentage of cleaved caspase 3^{+ve} OL-lineage cells at DIV1, DIV3 or DIV6 (Figure 3.3B). When this same cleaved caspase 3 data was parsed to segregate mature and immature OL-lineage cells, we still did not observe any significant difference in cleaved caspase 3 activity between *Ilk*$^{-/-}$ and *Ilk*$^{fl/fl}$ populations (Figure 3.3C). Finally, we investigated whether there were differences in the rate of proliferation between *Ilk*$^{-/-}$ and *Ilk*$^{fl/fl}$ OPCs. We did not observe any difference in BrdU incorporation after a 4-hour pulse at DIV2 (Figure 3.3D). Thus, our data strongly suggest a role for ILK in the initiation of a molecular differentiation program triggering MAG and MBP expression. Simply stated, upon loss of ILK, OPCs tend to persist as NG2^{+ve} precursors throughout the 6-day differentiation time course.

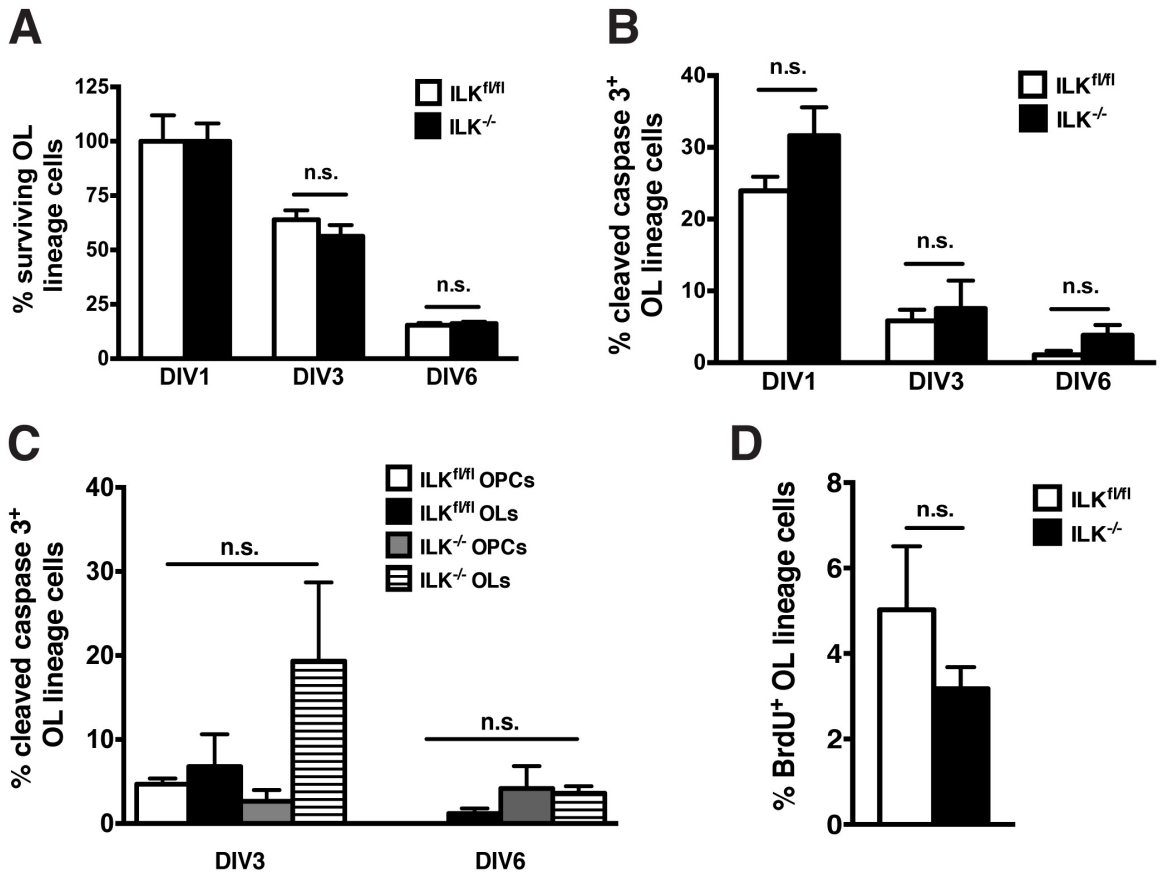

Figure 3.3. No significant difference in OL survival, cleaved caspase 3-mediated death or proliferation upon ILK depletion. A. Percentage of surviving OL-lineage cells over the 6 day differentiation time course when total numbers of *Ilk*$^{-/-}$ and *Ilk*$^{fl/fl}$ cells were respectively considered as 100% at DIV1. **B.** Percentage of cleaved caspase 3^{+ve} OL-lineage cells at DIV1, DIV3 and DIV6 for *Ilk*$^{-/-}$ and *Ilk*$^{fl/fl}$ populations. **C.** DIV3 and DIV6 cleaved caspase 3 data from panel [B] when immature OPCs and mature OLs are considered as distinct populations. **D.** Percentage of BrdU^{+ve} OLs after a 4-hour pulse on DIV2. Data represents the mean ± SEM (n=4 [A]; n=3 [B,C,D]); n.s. = no significant difference. Two-way ANOVA followed by Bonferonni post-tests (A,B,C); Student's *t* test (D).

Loss of ILK inhibits morphological maturation of OLs in primary culture

OL morphological differentiation is characterized by extension of multiple processes by OPCs, eventually generating myelin-like membranous structures. This morphological maturation coincides with the expression of MAG. At DIV3 of differentiation, MAG^{+ve} $Ilk^{fl/fl}$ OLs had developed a complex arbor network, and at DIV6, these OLs had further differentiated to form myelin-like membranes (Figure 3.4A top row). Interestingly, most MAG^{+ve} $Ilk^{-/-}$ OLs did not produce either an arbor network or myelin-like membranes (Figure 3.4A bottom row). Rather, they only extended a few primary arbors. To quantify this observation, a staging scheme was developed, from stage 1 to 4, where cells were binned based on their increasing morphological complexity (Figure 3.4B). At DIV3, MAG^{+ve} $Ilk^{-/-}$ OLs were predominantly stage 1, whereas MAG^{+ve} $Ilk^{fl/fl}$ OLs were largely stage 3 (Figure 3.4C). At DIV6, most MAG^{+ve} $Ilk^{fl/fl}$ OLs were of stage 4 morphology, but the majority of MAG^{+ve} $Ilk^{-/-}$ OLs persisted as stage 1 (Figure 3.4C). A subset of $Ilk^{-/-}$ OLs attained stage 4 morphology at DIV6, however, their cellular area was significantly reduced as compared to stage 4 MAG^{+ve} $Ilk^{fl/fl}$ OLs (Figure 3.4D, E). The observed morphological deficits resulting from ILK loss were not a consequence of EGFP induction, as Cre-recombined $Ilk^{+/+}$*;mT/mG* OLs displayed normal morphology (data not shown).

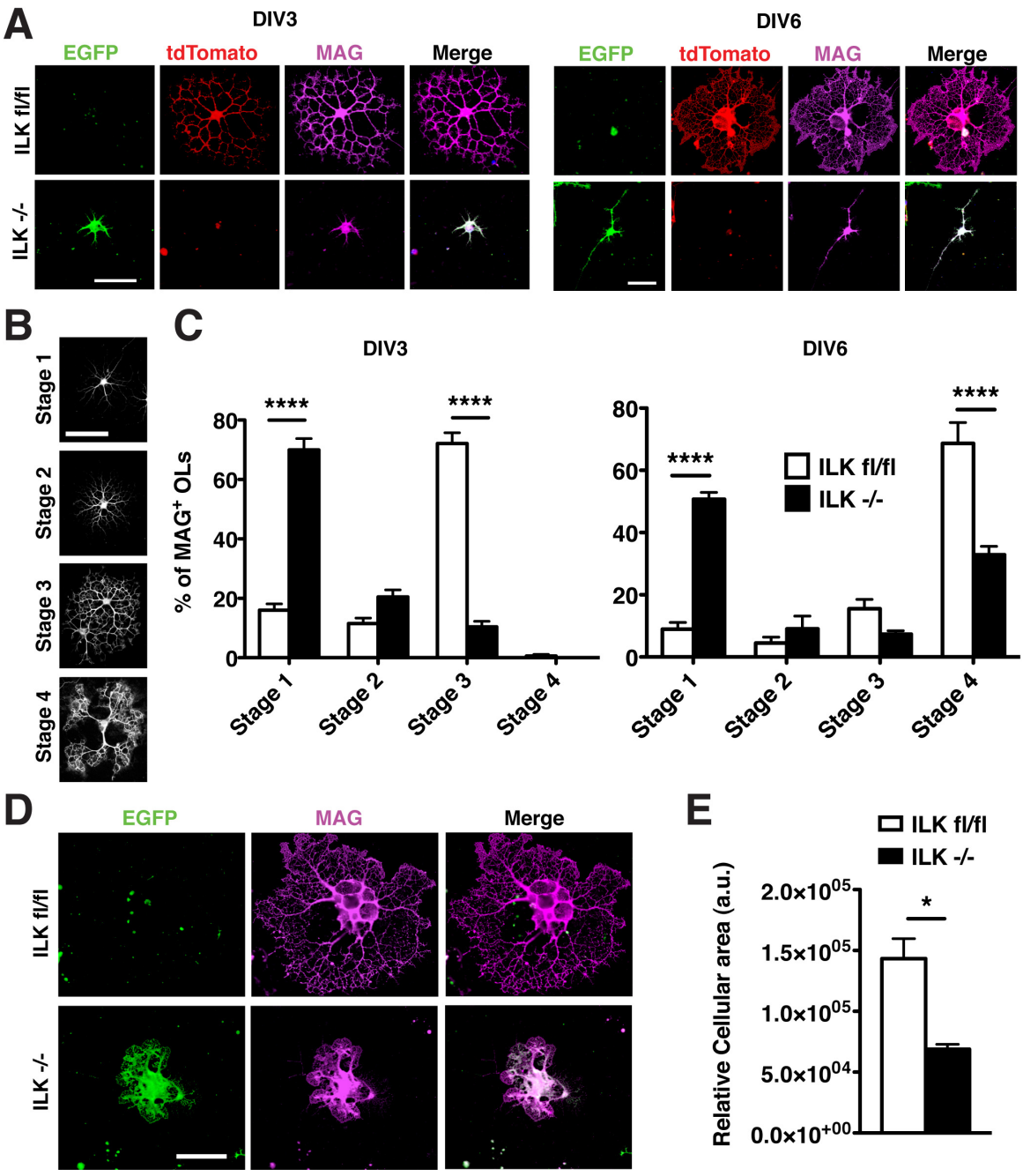

Figure 3.4. Loss of ILK perturbs morphological maturation of OLs. A. Immunofluorescence micrographs depicting morphology of MAG^{+ve} *Ilk*$^{-/-}$ and *Ilk*$^{fl/fl}$ at DIV3 and DIV6. **B.** Staging scheme used to categorize the morphological complexity of MAG^{+ve} OLs. **C.** Quantification of percent of *Ilk*$^{-/-}$ and *Ilk*$^{fl/fl}$ MAG^{+ve} OLs that fall into each of the 4 morphological stages at DIV3 and DIV6. **D.** Immunofluorescence

micrographs showing the extent of membrane extension of stage 4 *Ilk*$^{-/-}$ and *Ilk*$^{fl/fl}$ OLs. **E.** Quantification of the average cellular area of stage 4 *Ilk*$^{-/-}$ and *Ilk*$^{fl/fl}$ OLs. Data represents the mean ± SEM (n=4). *p < 0.05, ****p < 0.0001; Student's *t* test (E) or two-way ANOVA followed by Bonferonni post-tests (C). Scale bars: 50 μm.

Loss of ILK impacts in vitro myelinating capacity of OLs

Due to the morphological deficits observed when *Ilk*$^{-/-}$ OLs are cultured on Ln-2, we hypothesized that this would translate to compromised myelinating capacity in an *in vitro* myelination paradigm. To this end, we utilized DRGNs in co-culture with primary OLs (as described in O'Meara et al., 2011b). At DIV3 of co-culture, there was no significant difference in the capacity for *Ilk*$^{-/-}$ OLs to contact and enwrap DRGN neurites as compared to *Ilk*$^{fl/fl}$ OLs (Figure 3.5A-C). However, at DIV6, *Ilk*$^{-/-}$ OLs contacted fewer DRGN neurites and had a reduced capacity to enwrap neighboring neurites with MBP^{+ve} membrane (Figure 3.5A-C). The driving force underlying these deficits appeared to be an impaired ability of *Ilk*$^{-/-}$ OLs to form myelin leaflets (Figure 3.5D). These structures were observed solely when OLs were co-cultured with neurons, and may represent an *in vitro* version of early myelin sheaths. *Ilk*$^{-/-}$ OLs produced significantly fewer myelin leaflets per cell than *Ilk*$^{fl/fl}$ OLs (Figure 3.5E). These defects were not a result of ectopic EGFP expression, as *Ilk*$^{+/+}$*;mT/mG* OLs myelinated DRGN neurites normally, and produced expected numbers of myelin leaflets (data not shown). In addition, we confirmed that there were no differences in the density of DRGN neurite bed underlying myelinating OLs (data not shown), suggesting the OLs themselves were solely responsible for the myelination phenotypes in response to ILK loss.

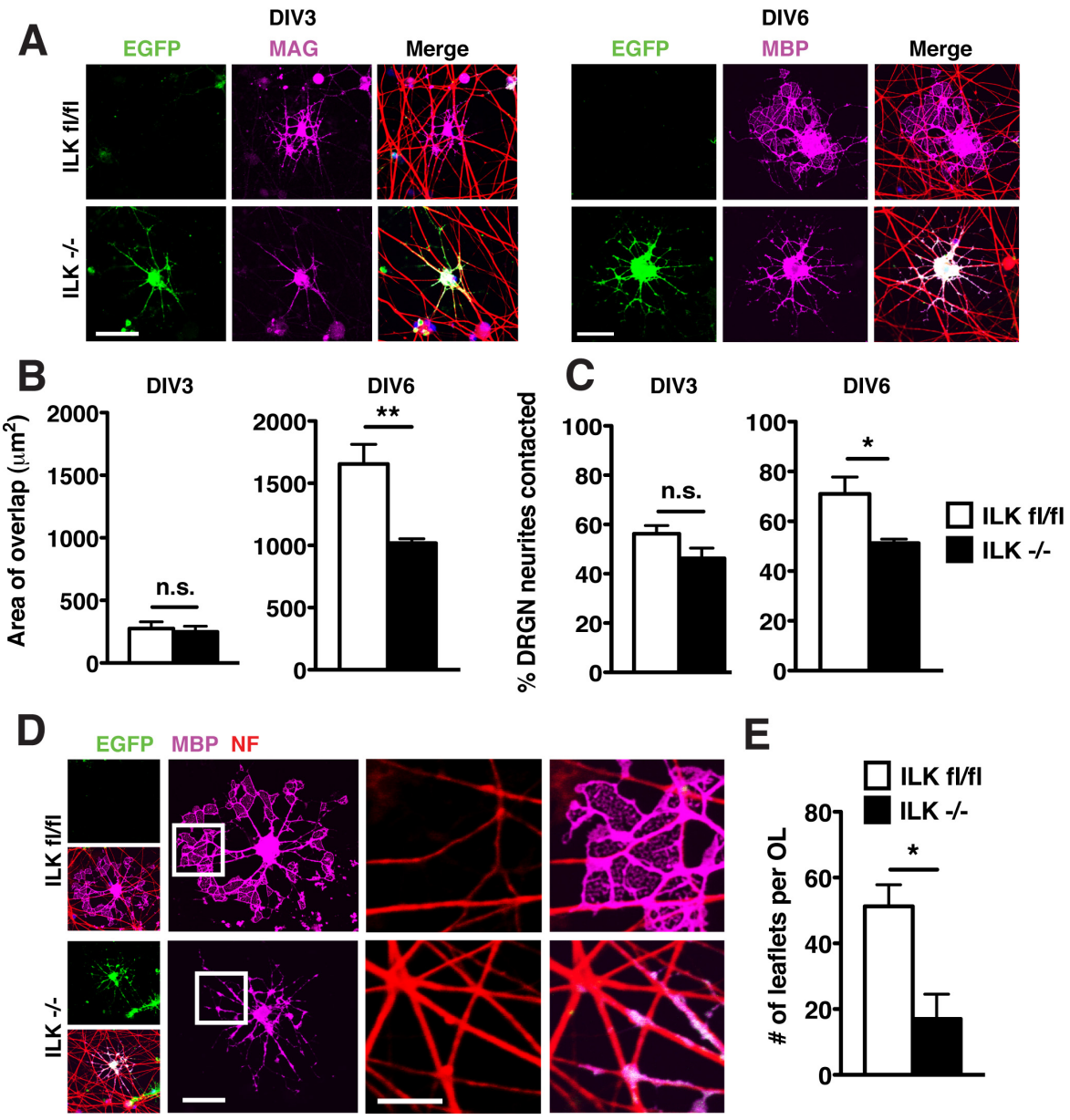

Figure 3.5. Loss of ILK disrupts ability of OLs to myelinate axons *in vitro*. A. Immunofluorescence micrographs of *Ilk*$^{-/-}$ and *Ilk*$^{fl/fl}$ OLs myelinating DRGN neurites at DIV3 and DIV6 of co-culture. **B.** Quantification of the area of overlap of myelin membrane with DRGN neurites by *Ilk*$^{-/-}$ and *Ilk*$^{fl/fl}$ OLs at DIV3 and DIV6. **C.** Quantification of the percentage of neighbouring DRGN neurites contacted by *Ilk*$^{-/-}$ and *Ilk*$^{fl/fl}$ OLs. **D.** Immunofluorescence micrographs depicting the structure of membrane extensions/leaflets for *Ilk*$^{-/-}$ and *Ilk*$^{fl/fl}$ OLs. **E.** Quantification of the number of membrane

extensions produced per cell for *Ilk*$^{-/-}$ and *Ilk*$^{fl/fl}$ OLs. Data represents the mean ± SEM (n=4). *p < 0.05, **p < 0.01; Student's *t* test. Scale bar: 50 μm.

Generation of ILK conditional knockout mice for in vivo study

To study the role of ILK in CNS myelination *in vivo* and avoid embryonic lethality associated with ILK deletion, we employed the Cre-loxP system. $Ilk^{fl/fl}$ mice were crossed to *Plp-CreER*^{T} mice to generate $Ilk^{fl/fl}$*;Plp-CreER*^{T} conditional knockout mice (hereafter referred to as *Ilk cKO* mice). The *Plp-CreER*^{T} line of mice allows for spatial and temporal control of floxed *Ilk* recombination; the Cre gene is placed under the control of the *proteolipid protein* (*Plp*) promoter, allowing for OL-specific expression (Doerflinger et al., 2003). As well, the Cre protein is fused to a mutated estrogen receptor, requiring tamoxifen administration for nuclear translocation (Figure 3.6A).

The optic nerve was chosen as a model system to study the impact of *Ilk* gene deletion on myelination, as it offers a relatively homogeneous population of cell types, with a large percentage of OLs, when compared to other CNS tissues. Since myelination of the optic nerve is initiated approximately 6 days post-natally (P6) (Thomson et al., 2005), *Ilk cKO* mice and WT littermates were administered tamoxifen at P4. Western blot analysis revealed a decrease in total ILK protein levels in the optic nerves of these mice following tamoxifen injection (Figure 3.6B). To verify specificity of the promoter to the OL lineage, *Ilk cKO* mice were crossed to the *mT/mG* reporter line (generating *Ilk cKO;mT/mG* mice). In these mice, EGFP is expressed predominantly in cells positive for the myelin markers MBP and MAG (Figure 3.6C), demonstrating the specificity of the *Plp* promoter to OLs.

Transient amyelination following ILK ablation in vivo

Initial analysis of *Ilk cKO* mice revealed no overt signs of shaking, ataxia, tremor, or head wobbling following tamoxifen injection at P4. Mice were sacrificed at two

developmental time points, P14 and P28, for ultrastructural analysis by electron microscopy. The optic nerves of P14 *Ilk cKO* mice displayed a significant reduction in total number of myelinated small caliber axons (0.3-0.8 μm) relative to WT littermate controls (Figure 3.6D, E). In contrast, there was no significant difference in number of myelinated large caliber axons (0.8 μm and above) at this time point (Figure 3.6D, E). That small rather than large caliber axons are affected is in concordance with previous work done on OL-specific knockout mice for other members of the integrin-signaling pathway (Chun et al., 2003; Câmara et al., 2009; Forrest et al., 2009). To determine whether myelin thickness was also affected by ILK loss, we assessed the G-ratio (axon diameter/axon and myelin diameter) of axons in two separate groups; those < 0.8 μm and those ≥ 0.8 μm in diameter (Figure 3.6F). There was no significant difference in the average G-ratio of axons either < 0.8 μm or those ≥ 0.8 μm. As well, no difference was observed in axonal distribution (by diameter) between WT and *Ilk cKO* littermates (Figure 3.6G), excluding a shift in axon caliber frequency as responsible for the observed decrease in total number of myelinated small caliber axons.

Interestingly, when *Ilk cKO* mice were analyzed at P28, there was no observable difference in total number of myelinated fibers (at any given diameter) relative to control mice (Figure 3.6H, I). In addition, there was no significant difference in the average G-ratio of axons with diameters either < 0.8 μm or ≥ 0.8 μm in P28 optic nerves (Figure 3.6J). Furthermore, no significant shift was observed between control and *Ilk cKO* mice in axonal distribution by diameter (Figure 3.6K), discounting the possibility of axonal loss as explanation for the resurgence of small myelinated fibers by P28. Rather, our results imply gradual myelination recovery of P14 amyelinated axonal populations in the ILK-depleted optic nerve.

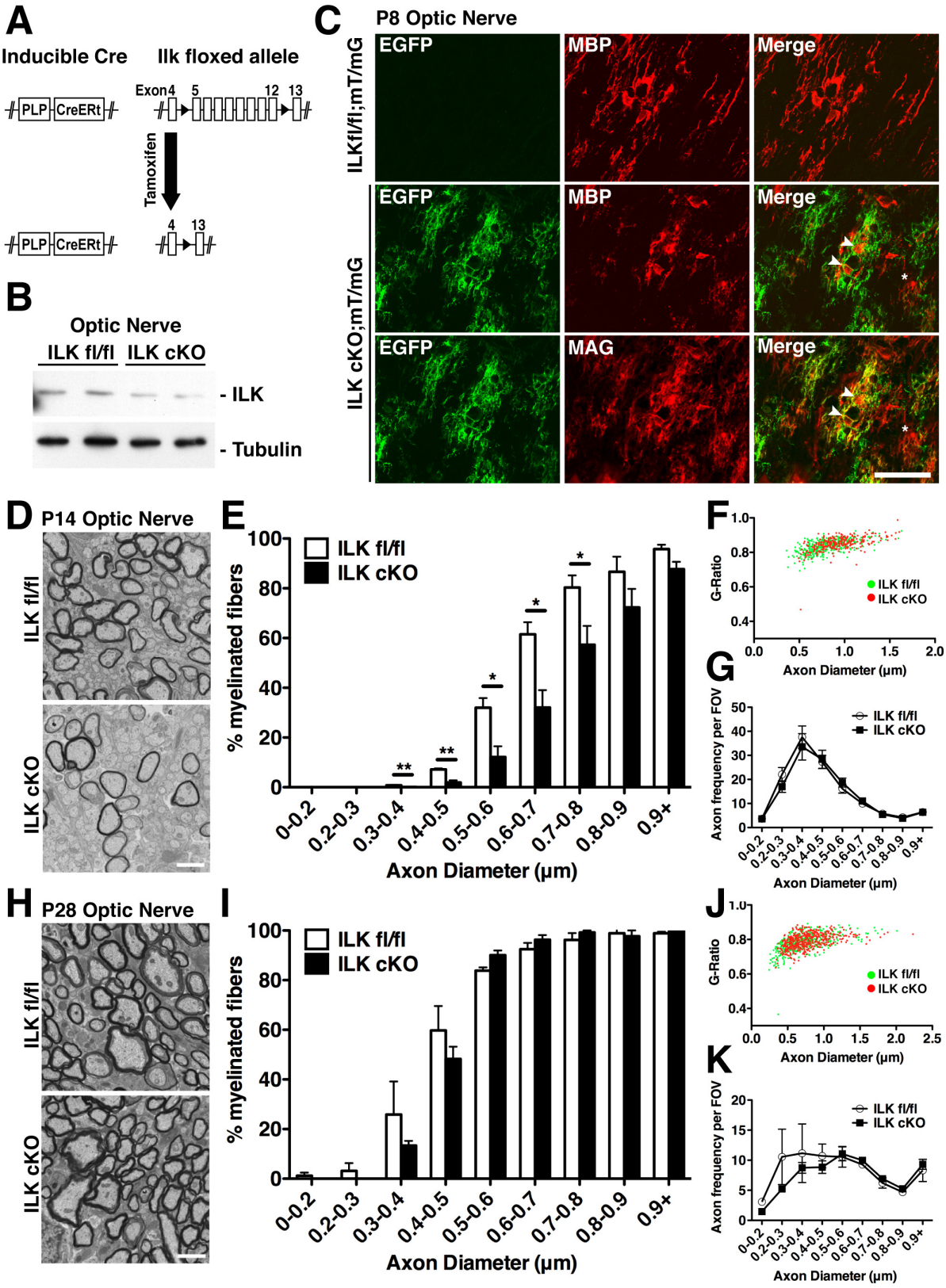

Figure 3.6. Number of myelinated axons is decreased in the optic nerves of tamoxifen treated *Ilk cKO* mice at P14 but not at P28. A. *Ilk cKO* mice were generated

by crossing *Plp-CreER*^{T} transgenic mice with *Ilk*$^{fl/fl}$ mice. Tamoxifen was administered to induce Cre translocation into the nucleus whereupon the *Ilk* gene was excised. **B.** Western blot analysis demonstrates reduction of ILK protein in the optic nerves of P4 tamoxifen injected *Ilk cKO* mice in comparison to WT controls. **C.** Optic nerves from control *Ilk*$^{fl/fl}$*;mT/mG* littermates at P8 contain MBP^{+ve} OLs but no EGFP signal. Optic nerves from P4 tamoxifen injected *Ilk cKO;mT/mG* mice sacrificed at P8 show co-localization of MBP/MAG^{+ve} OL cell bodies (both stains are on the same optic nerve section) with EGFP (arrowheads). There are also MBP/MAG^{+ve} cell bodies that do not express EGFP (asterisk). Scale bar: 50 μm. **D,H.** Electron micrographs of optic nerves from P14 and P28 *Ilk cKO* and control mice given tamoxifen at P4. **E,I.** Quantification for percentage myelinated axons at P14 and P28, further subdivided by axon caliber. **F,J.** Representative scatter plot of G-ratio versus axon diameter at P14 and P28. **G,K.** Frequency histogram for axons of varying diameter per field of view (FOV) (3000x magnification) at P14 and P28. Data represents the mean ± SEM (n=3-4). *$p < 0.05$, **$p < 0.01$; Student's *t* test (E,I), two-way ANOVA with Bonferroni post-tests (G,K). Scale bars: 1.5 μm.

The transient defects observed are due neither to a loss or a gain in total number of OLs as measured by NG2^{+ve} OPCs and CC1^{+ve} mature OLs at P14 or P28 (Figure 3.7A, B). To assess the possibility of OL turnover, we measured the number of cleaved caspase 3^{+ve} cells in the optic nerves of P14 *Ilk cKO* and WT mice. No significant increase in the number of apoptotic cells was observed in ILK-depleted optic nerves (Figure 3.7C). Furthermore, qualitative analysis for the abundance of recombined (EGFP^{+ve}) *Ilk*$^{-/-}$ OLs in the optic nerves of *Ilk cKO;mT/mG* mice demonstrated a persistent EGFP^{+ve} cell population capable of forming MBP^{+ve} myelin tracts across multiple time points (data not shown). If *Ilk*$^{-/-}$ OLs were indeed being turned over, we would expect a progressive loss in EGFP signal as *Ilk*$^{-/-}$ cells were replaced by WT precursors.

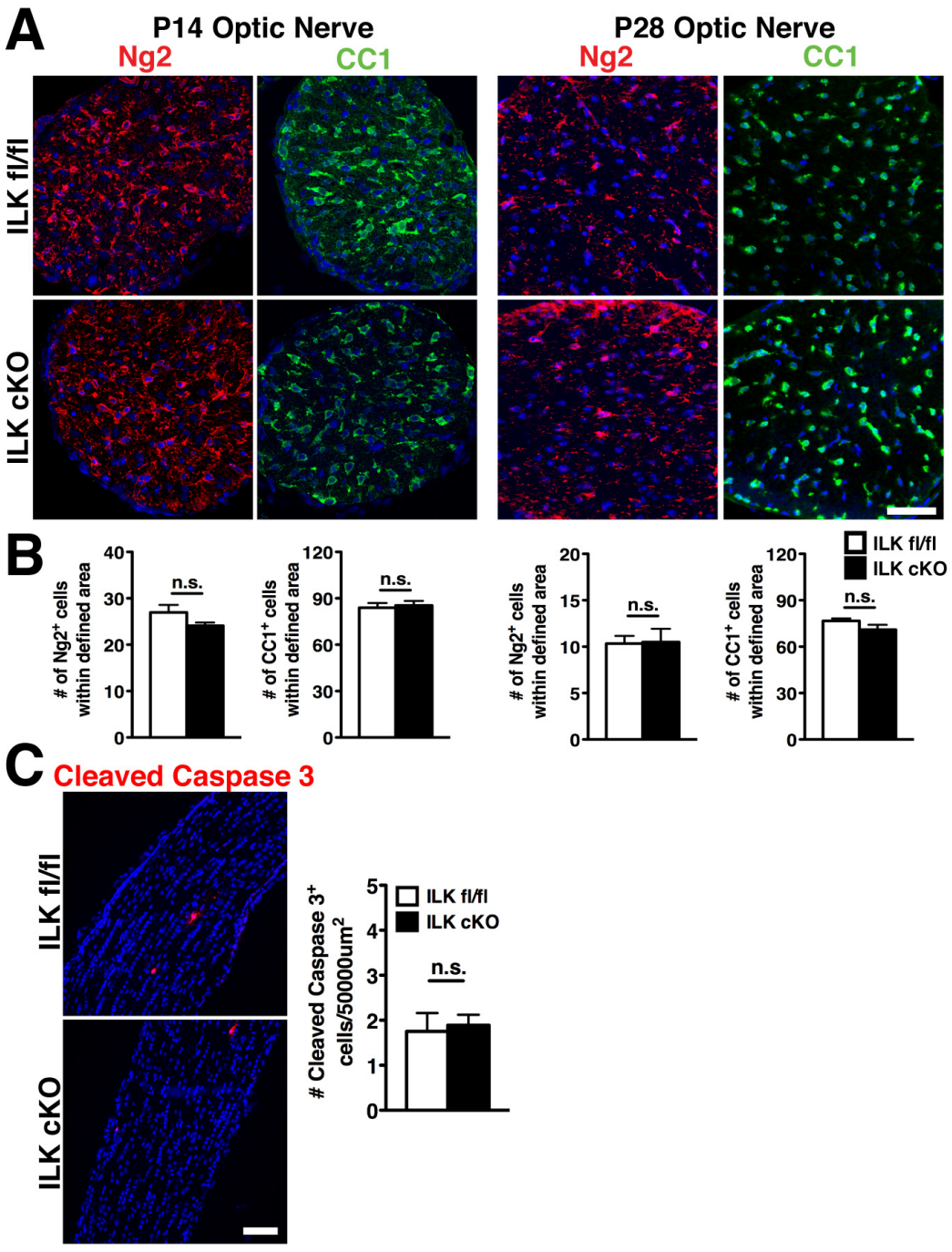

Figure 3.7. Number of precursor and mature OLs is unchanged in optic nerves of *Ilk cKO* mice. **A.** Immunofluorescence micrographs of NG2^{+ve} OPCs (red) and CC1^{+ve} mature OLs (green) counterstained with DAPI in the optic nerves of *Ilk cKO* and WT mice at P14 or P28. **B.** Quantification of NG2^{+ve} OPCs and CC1^{+ve} mature OLs at P14 and P28. Respective cells were counted within a defined area of the optic nerve. **C.**

Immunofluorescence micrographs of cleaved-caspase 3^{+ve} cells counterstained with DAPI along the length of an optic nerve in P14 *Ilk cKO* and WT mice. Quantification for total number of cleaved-caspase 3^{+ve} cells within 50000 μm^2 of the P14 optic nerve. Data represents the mean ± SEM (n=3), Student's *t* test. Scale bars: 50 μm.

In an effort to draw parallels between defects observed *in vitro* (morphological aberrations) and *in vivo* (loss of myelination), we employed a low dose tamoxifen regimen in our *Ilk cKO;mT/mG* and *PLPCreER^T;mT/mG* control animals. Reducing tamoxifen levels allowed for spatial resolution of individual recombined OLs and associated myelin processes. Following administration of the drug, mice were sacrificed at P14 and the optic nerves were removed for whole mount preparations. A series of Z-stack images were taken so as to capture recombined OLs in their entirety. Strikingly, at a strictly qualitative level, many of the ILK-depleted OLs displayed fully formed myelin internodes similar to controls (Figure 3.8A). However, the average internode-length was less than that measured for reporter controls (Figure 3.8A, B), corroborating our *in vitro* data for a subset of mature ILK-depleted OLs which form smaller amounts of membrane. As well, loss in internode-length implies a defect in the growth of the process responsible, as the distance it is able to travel around the axon will determine length of the myelin segment. In conjunction we measured internode diameter to account for possible bias as a result of axon diameter (larger axons having longer myelin internodes and vice versa). No significant difference was observed between ILK-depleted and control OLs (Figure 3.8B) eliminating the variable as potential confounder. We did, however, observe ILK-depleted OLs whose processes failed to form myelin internodes (Figure 3.8C). While occasionally present in controls, the defect was more prevalent in the optic nerves of *Ilk cKO;mT/mG* mice, suggesting a role for ILK in directing myelin formation following axonal contact and/or process extension *in vivo*, defects observed in both purified and co-cultured OLs *in vitro*. Taken together, our data, both *in vitro* and *in vivo*, points to a role for ILK in the initial steps of myelination, and suggests that the observed amyelination is not due to a loss of OLs but rather to a defect in OL branching and membrane formation.

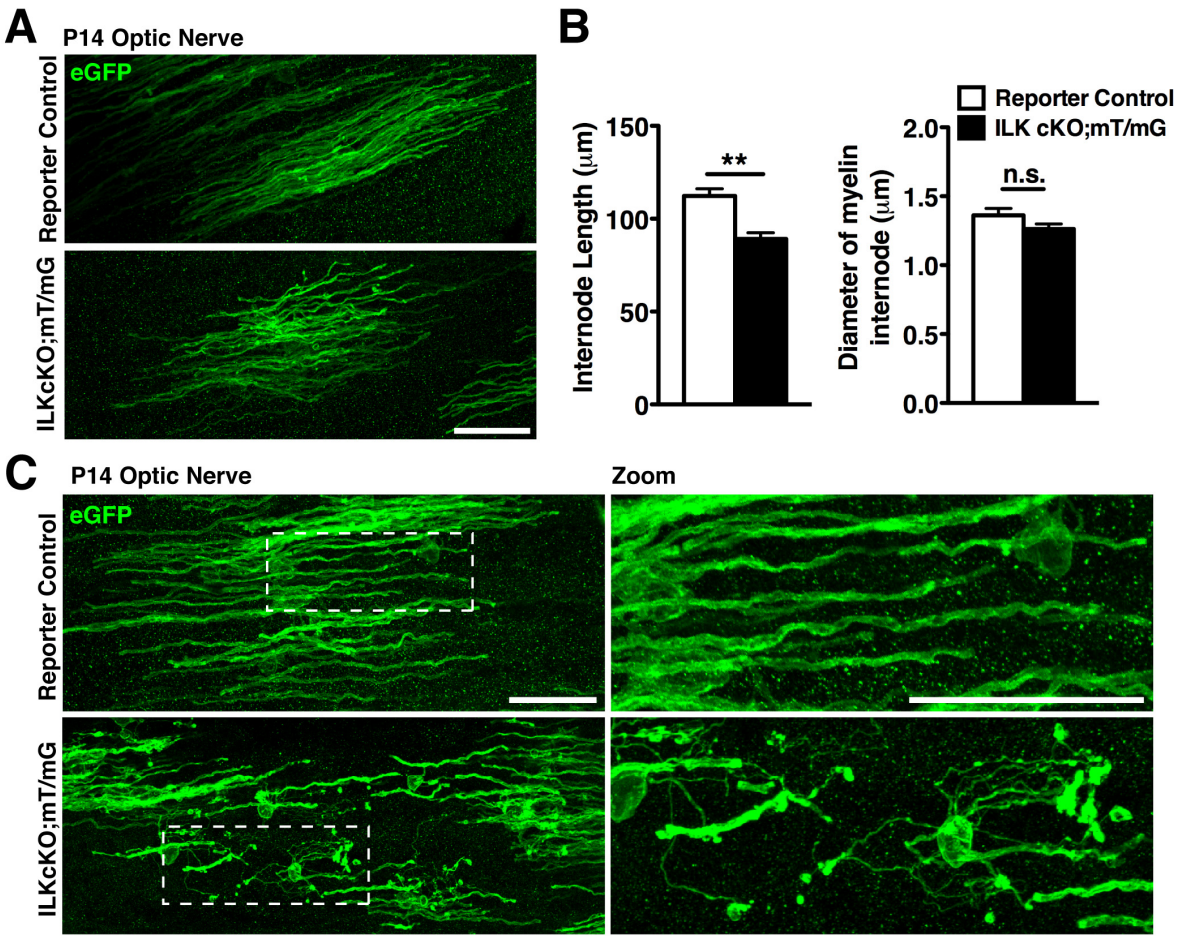

Figure 3.8. ILK regulates internode length and triggers internode formation *in vivo*.

A. Compressed stack of immunofluorescence micrographs from the optic nerves of P14 *PLPCreER^{T};mT/mG* control and *ILK cKO;mT/mG* mice. EGFP (green) denotes a recombination event and allows for tracing of reporter only (top panel) or ILK-depleted internodes (bottom panel). **B.** Quantification of internode length and diameter between control and ILK-depleted mice. **C.** Compressed stack of immunofluorescence micrographs from the optic nerves of P14 *PLPCreER^{T};mT/mG* control and *ILK cKO;mT/mG* mice depicting abnormal morphology observed in a subset of ILK-depleted OLs. Data represents the mean ± SEM (n=4). **p < 0.01; Student's *t* test. Scale Bar: 50 μm.

Morphological deficits of Ilk-deficient OLs are associated with abnormal actin accumulation, and are partially rescued through Rho kinase inhibition

In our search for a mechanistic explanation for the aforementioned OL defects, we first explored the phosphorylation state of ILK's canonical downstream effectors Akt and GSK3β. To our surprise, no apparent change in Akt (Ser 473) or GSK3β (Ser 9) phosphorylation was observed in ILK-depleted OL cultures at DIV3 or 6 (Figure 3.9A, B). We thus sought to investigate other possible mechanisms that could account for the observed morphological aberrations. ILK has previously been shown to co-localize with β1 integrin and paxillin in OL focal adhesions (Chun et al., 2003). We further demonstrate ILK localization to the filamentous-actin (F-actin) rich leading edge or distal tips of outgrowing processes in the immortalized OL cell line OLi-neu (data not shown). When ILK is lost from primary OLs, there is an abnormal accumulation of F-actin in the cell body and sub-cortically in the developing process (Figure 3.9C, D). A well-known regulator of neural cell actin organization is the small RhoGTPase RhoA (Govek et al., 2005), and perturbation of RhoA results in morphologically aberrant OLs (Rajasekharan et al., 2009, 2010). As ILK is required for RhoA-dependent actin cytoskeleton reorganization (Graness et al., 2006), we hypothesized that the morphological deficits and actin accumulation in *Ilk*$^{-/-}$ OLs are caused by upregulation of the RhoA signaling pathway. Indeed, when we probed for active RhoA levels, an increase in GTP bound RhoA was detected in our TAT-Cre treated DIV3 OL cultures (Figure 3.9E).

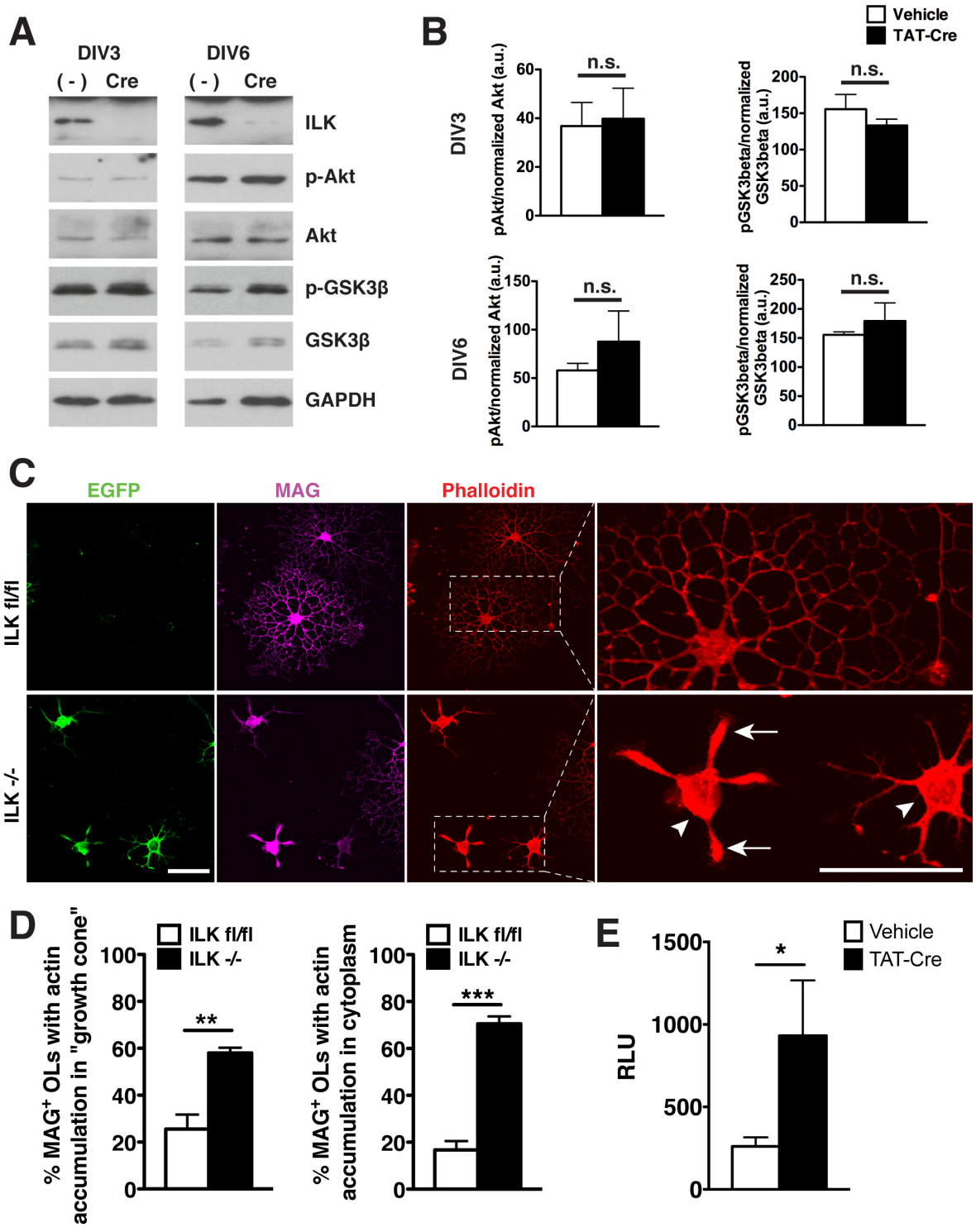

Figure 3.9. Abnormal actin accumulation is linked with *Ilk*$^{-/-}$ OL morphology. A. Western blots performed on DIV3 and DIV6 vehicle (-) or TAT-Cre (Cre) treated primary OL lysates. Membranes were probed for ILK, Akt (p-Ser 473 and total), GSK3β (p-Ser 9 and total) and GAPDH as a loading control. **B.** Densitometry analysis of relative

band intensity for western blots depicted in panel (A). **C.** Immunofluorescence micrographs of *Ilk*$^{-/-}$ and *Ilk*$^{fl/fl}$ OLs showing actin localization with rhodamine-phalloidin staining. **Arrowhead denotes F-actin accumulation in OL cytoplasm, and arrows F-actin accumulation in the process/growth cone. D.** Quantification of the percent of MAG^{+ve} *Ilk*$^{-/-}$ and *Ilk*$^{fl/fl}$ OLs with actin accumulation in the cytoplasm and/or in growth cone-like structures. **E.** Results from a RhoA G-LISA activation assay measuring the relative amount of active (GTP-bound) RhoA between vehicle and TAT-Cre treated DIV3 OL cultures. Data represent the mean ± SEM (n=3-4). *$p < 0.05$, **$p < 0.01$, ***$p < 0.001$; Student's *t* test (B,D); one-tailed Mann Whitney U-test (E). Scale bars: 50 μm.

Stimulation of the RhoA pathway involves activation of ROCK, an event that is associated with destabilization of actin. The ROCK inhibitor Y-27632 is often used to rectify the effects of overactive RhoA signaling. We tested whether Y-27632 treatment would improve the morphological deficits of *Ilk*$^{-/-}$ OLs. Interestingly, this did not rescue the morphological deficits of MAG^{+ve} *Ilk*$^{-/-}$ OLs (data not shown). Rather, Y-27632 had a specific impact on the morphology of immature (MAG^{-ve}) *Ilk*$^{-/-}$ OLs (Figure 3.10A). Under normal conditions, MAG^{-ve} *Ilk*$^{-/-}$ OLs mostly displayed primary (1^{o}) branched morphology, whereas MAG^{-ve} *Ilk*$^{fl/fl}$ OLs tended to have equal numbers of 1^{o} and secondary/tertiary (2^{o}/3^{o}) branched cells (Figure 3.10B). Upon administration of Y-27632, quantification revealed a restoration of the proportion of 2^{o}/3^{o} branched MAG^{-ve} *Ilk*$^{-/-}$ OLs to wild-type levels at DIV6 of culture (Figure 3.10B). It was unlikely that this phenomenon was a non-specific event independent of ILK loss, since application of Y-27632 to *Ilk*$^{fl/fl}$ OLs did not enhance MAG^{-ve} OL morphology as compared to *Ilk*$^{fl/fl}$ vehicle treated cells.

We were apparently enhancing the morphology of an immature (*i.e.* MAG^{-ve}) population of *Ilk*$^{-/-}$ OL-lineage cells by inhibiting ROCK. We next sought to investigate whether these morphologically-rescued MAG^{-ve} cells were in fact NG2^{+ve} OPCs. To this end, we characterized the morphology of DIV6 NG2^{+ve} *Ilk*$^{-/-}$ and *Ilk*$^{fl/fl}$ cells treated with either Y-27632 or vehicle. *Ilk*$^{-/-}$ NG2^{+ve} OPCs responded in a similar fashion as did the MAG^{-ve} OLs described above (Figure 3.10C). Y-27632 administration resulted in an increase from mainly NG2^{+ve} 1^{o} branched OPCs to predominantly 2^{o}/3^{o} branched cells (Figure 3.10D). Interestingly, in contrast to the above-described MAG^{-ve} population, Y-27632 also enhanced the morphology of the NG2^{+ve} *Ilk*$^{fl/fl}$ population. However, even when considering this apparent indirect (*i.e.* ILK independent) impact of Y-27632 on

NG2^{+ve} OPC morphology, ROCK inhibition enhanced the morphology of *Ilk*$^{-/-}$ NG2^{+ve} OPCs to a greater extent than *Ilk*$^{fl/fl}$ OPCs (Figure 3.10E). Thus, RhoA regulation seems to be ILK-dependent during distinct phases of OL development. Specifically, ILK appears to depend on RhoA signaling at the point of differentiation when OPCs are transitioning from NG2^{+ve} precursors to MAG^{-ve} immature OLs.

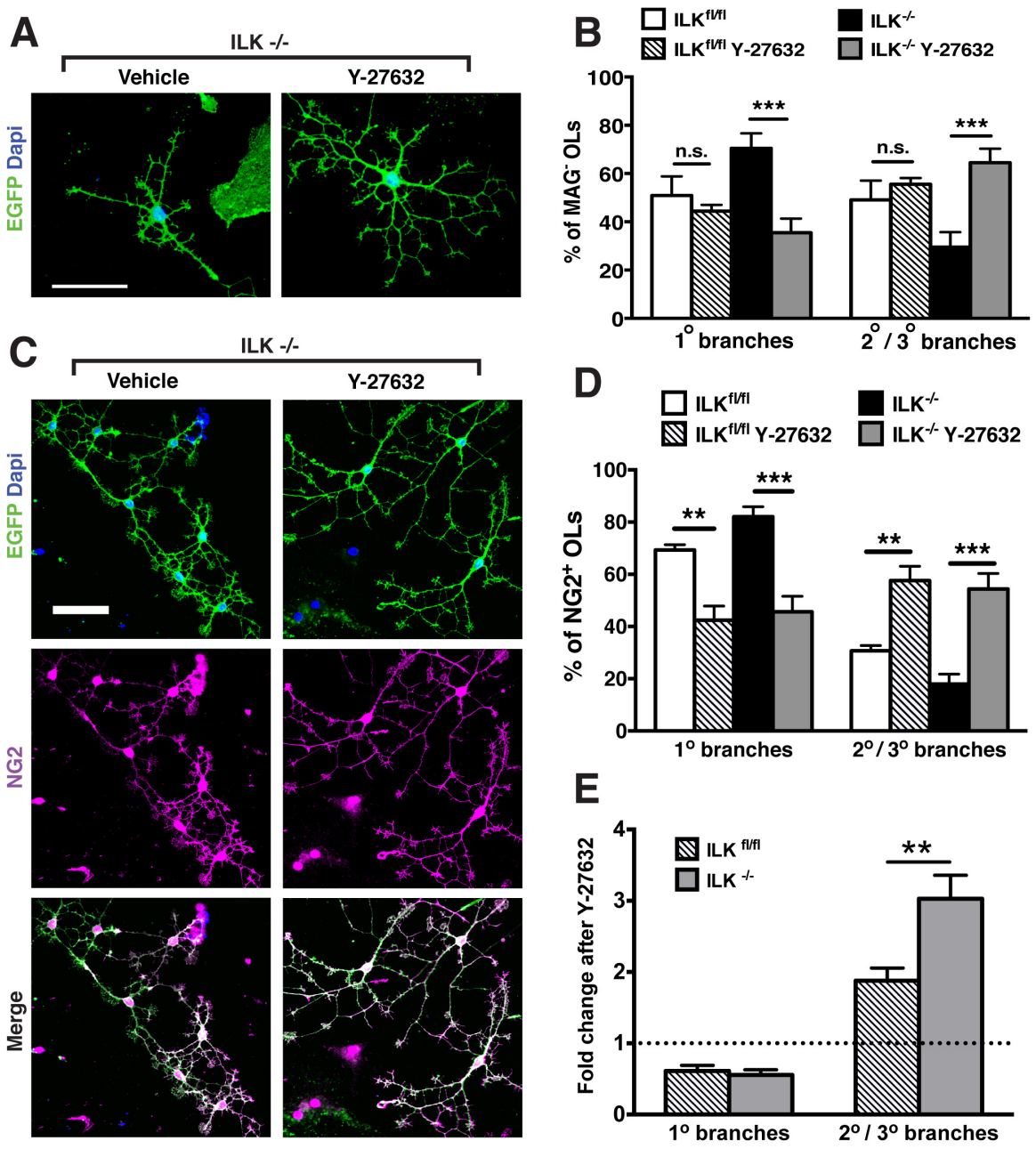

Figure 3.10. Administration of ROCK inhibitor Y-27632 rescues the morphology of a distinct *Ilk*$^{-/-}$ population of OL-lineage cells. **A.** Confocal micrographs depicting the morphology of DIV6 MAG^{-ve} *Ilk*$^{-/-}$ OLs treated with Y-27632 or vehicle control. **B.** Morphological quantification of MAG^{-ve} *Ilk*$^{-/-}$ and *Ilk*$^{fl/fl}$ OLs treated with either vehicle or Y-27632. A morphological staging scheme adapted from the one depicted in Figure 3.4B was used for this experiment. **C.** Confocal micrographs depicting the morphology of

DIV6 NG2^{+ve} *Ilk*$^{-/-}$ OLs treated with ROCK inhibitor Y-27632 or vehicle. **D.** Morphological quantification of NG2^{+ve} *Ilk*$^{-/-}$ and *Ilk*$^{fl/fl}$ OLs treated with either vehicle or Y-27632. **E.** Fold change in proportion of 1^{o} and 2^{o}/3^{o} branched NG2^{+ve} OPCs upon administration of Y-27632 to *Ilk*$^{fl/fl}$ and *Ilk*$^{-/-}$ populations. Data represent the mean ± SEM (n=4). n.s. = no significant difference; **p < 0.01, ***p < 0.001; two-way ANOVA with Bonferroni post-tests. Scale bar: 50 μm.

Discussion

ILK regulates OL development

Following ILK loss in enriched primary OL cultures, two phenotypes were observed: (1) the persistence of $NG2^{+ve}$ OPCs coupled with a decrease in mature (MAG^{+ve}) cells, and (2) an inability of the MAG^{+ve} population to form arborizations or myelin-like membranes (Figure 3.11). At first glance, it is plausible to suspect a general delay in Ln-2 mediated differentiation as cause. While, to a degree, we believe this true, several observations suggest this interpretation as overly simplistic. First, the persistence of $NG2^{+ve}$ precursors in the $Ilk^{-/-}$ population remains static from DIV3 to 6, implying this OL subpopulation requires ILK signaling for both morphological and molecular differentiation. Second, there is the discord between morphology and maturation markers observed in a separate OL subpopulation; those capable of MAG expression upon ILK loss. Together, this suggests a functional OL heterogeneity exists with regard to ILK. Some cells necessitate ILK to initiate the entire differentiation gamut, while others require ILK for morphological maturation only. Alternatively, ILK's role could be linked to the exact maturation stage of the precursor cell at the time of its deletion. In either case, we would assume functional differences are an outcome of signaling alteration downstream of ILK, most likely through a shift in ILK complex composition at the β1 integrin cytoplasmic tail. Elucidation of the mechanistic switch that defines the observed OL subgroups will be important as we move towards a fuller understanding of OL development.

Initial characterization of P14 *Ilk cKO* optic nerves revealed a decrease in total number of myelinated small caliber axons. Extrapolating from our *in vitro* (aberrant morphological differentiation) and *in vivo* (low dose tamoxifen) data, we suggest a dual

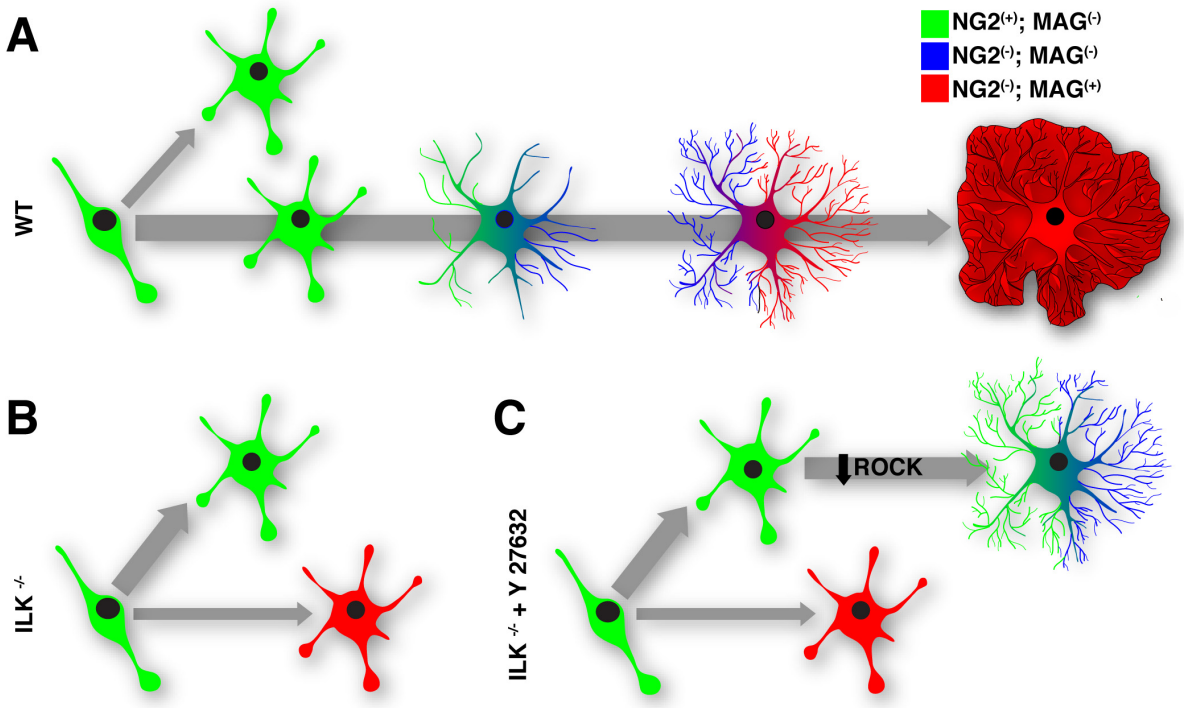

Figure 3.11. ILK differentially regulates both morphology and molecular marker activation in at least two OL subgroups. A. During normal OL development, OPCs give rise to two general populations when presented with a Ln-2 substrate; a smaller pool of $NG2^{+ve}$ cells which remain in a precursor state, and a second, larger group, which progresses through the various stages of morphological maturation with concomitant expression of molecular markers of differentiation (MAG). **B.** Following ILK loss, an increased percentage of OPCs fail to commit to the maturing population, remaining as $NG2^{+ve}$ precursors. Simultaneously, a second pool of ILK-depleted OLs express MAG but remain morphologically stunted. This pool correlates with defects observed *in vivo*. **C.** ROCK inhibition rescues a select group of immature OLs, restoring secondary and tertiary branching to normal levels. However, cells expressing MAG do not display a similar increase in morphological maturity, suggesting differential regulation of the Rho/ROCK pathway by ILK between varying OL subgroups.

explanation for the small axon phenotype; that *Ilk*$^{-/-}$ OLs suffer both from an inability to generate and extend the requisite network of processes as well as a deficiency in their capacity to initiate myelination following axonal contact. In regards to the former, OL morphological complexity is negatively correlated with the diameter of the axon(s) it myelinates. Individual OLs will either myelinate a large number of small axons or a small number of large axons (Butt and Berry, 2000; Almeida et al., 2011). Thus, following ILK loss, we would expect exacerbation of small axon amyelination as a result of the OLs inability to generate a high number of processes. The second mechanism, failure to initiate myelination following axonal contact, was first proposed by Câmara and colleagues in a dominant-negative model of β1 integrin (Câmara et al., 2009). The idea is as follows; once axonal contact is established, the OL process requires an axonal ligand "threshold" be broken to trigger a myelinating event. Larger axons are unaffected in this paradigm, as they provide excess surface ligand. Smaller axons, however, necessitate integrin-mediated signal amplification and, as such, are preferentially affected.

In contrast to our own model, Câmara et al. (2009) initially propose and then reject the possibility of morphological abnormalities as cause for small axon amyelination. We believe our *in vitro* data, together with the low dose tamoxifen experiments, imply morphological defects following ILK loss *in vivo*. However, our two models do not preclude one from the other. Rather, they highlight possible differences in functional outcome between receptor and effector disruption. Our findings are also congruent with work published by others (Benninger et al., 2006), which controversially concluded no essential role for β1 integrin in CNS myelination. Here, the authors focused primarily on G-ratio as readout for myelination, which, similar to our own model, was unaffected. As well, the study was conducted primarily in older mice (2 months and

above), by which time, full phenotypic recovery had occurred in our model. Coupled with our work, these findings strongly suggest the β1 integrin signaling pathway is critical for myelination during a small developmental window, with compensation occurring thereafter.

As alluded, our *in vivo* model demonstrates the capacity for compensation. When considering the transient nature of the amyelination phenotype, we are presented with two general possibilities, that death of $Ilk^{-/-}$ OLs permits WT cells to compensate, or that $Ilk^{-/-}$ OLs are developmentally delayed, requiring more time for myelination to proceed. We have eliminated the former, as there was no change in total OL number or an increase in apoptosis between the optic nerves of *Ilk cKO* and WT mice. The second scenario, a delay in morphological maturation, therefore seems the most likely explanation; that upon ILK loss compensation occurs through up-regulation of other integrin adhesion complexes such as those containing Fyn or FAK. Alternatively, compensation could arise through a switch in Ln-2 directed signaling from integrin to dystroglycan, another Ln-2 receptor expressed by OLs (Colognato et al., 2007).

However, given the nature of our *in vivo* model (a single tamoxifen injection), we must also consider a paradigm wherein non-recombined OLs outcompete $Ilk^{-/-}$ cells for bare axons. Two qualities lend credence to this theory. First, the myelination potential of any single OL is dependent on its ability to compete with neighboring OLs for axonal space (Chong et al., 2012). Second, OLs are plastic, able to form myelin beyond what a permissive environment would normally allow (Almeida et al., 2011; Chong et al., 2012). It is therefore reasonable to postulate compensation as occurring through endogenous "WT" OLs, an intriguing possibility when considering future development of demyelinating disease therapies.

We must also consider the nature of the *Plp* promoter, as it defines two separate $NG2^{+ve}$ OPC populations; one that expresses PLP, and one that does not (Mallon et al., 2002). While it is unknown whether these two subpopulations differ functionally, we cannot exclude the possibility that ILK has a distinct role within each (recall, we observe phenotypic disparity between $Ilk^{-/-}$ OLs *in vitro*). As our $PLPCreER^{T}$ model would target one subpopulation ($NG2^{+ve}$/PLP^{+ve}) to the exclusion of the other, the question of whether we could exacerbate (or not) the amyelination phenotype by targeting all $NG2^{+ve}$ cells remains. If answered, it would provide some of the first insight into functional continuity, or lack thereof, for a member of the β1 integrin signaling pathway between OL subgroups *in vivo*.

ILK regulates OL actin cytoskeleton dynamics in part through RhoA

To our surprise, the phosphorylation status of the downstream effectors Akt and GSK3β were unchanged following ILK loss, prompting us to instead explore the actin cytoskeleton. ILK is known to provide a bridge between environmental cues and intracellular machinery, linking the ECM and integrins to the actin cytoskeleton across a multitude of cell types and species (McDonald et al., 2008). In the OL, dynamic remodeling of the actin cytoskeleton is necessary for filopodia and lamellipodia formation, the engines driving arborization (Kim et al., 2006; Bacon et al., 2007). We therefore propose the morphological defects following ILK loss result from a breakdown in the connection between the ECM and actin cytoskeleton, ultimately leading to F-actin accumulation/disorganization and subsequent process outgrowth failure.

As ILK regulates actin dynamics indirectly through recruitment of focal adhesion complexes (Legate et al., 2006), the observed perturbation in F-actin is most likely an

outcome of ILK complex dissolution. Under normal conditions, ILK-assembled complexes are capable of both direct F-actin binding and indirect actin remodeling, the latter an event largely regulated by the small Rho GTPase family (Wickström et al., 2010b). With relevance to our work, ILK-directed focal adhesions act as checkpoints for RhoA and its effector ROCK, with loss of ILK or α-parvin leading to increased pathway activity and subsequent F-actin disorganization (Kogata et al., 2009; Montanez et al., 2009; Pereira et al., 2009). Up-regulation of RhoA signaling in neurons manifests as cortical actin accumulation with concomitant inhibition of neurite extension (Yamaguchi et al., 2001), and in OLs as reduction in process outgrowth and branching (Liang et al., 2004; Rajasekharan et al., 2009, 2010; Wang et al., 2012). We observed an increase in active RhoA levels following ILK depletion in our OL cultures. When treated with the ROCK inhibitor Y-27632, MAG^{+ve} $Ilk^{-/-}$ OLs did not respond as expected, with no increase in morphological complexity. Instead, $NG2^{+ve}/MAG^{-ve}$ $Ilk^{-/-}$ OLs displayed a surge in arbor sprouting. The results suggest ILK regulation of the RhoA/ROCK pathway is limited to a distinct OL subpopulation, specifically, that which is transitioning from a precursor to immature OL state.

It was surprising to note no change in morphological complexity of MAG^{+ve} $Ilk^{-/-}$ OLs upon ROCK inhibition. The controlled manipulation of the actin cytoskeleton by ILK within this cell population must occur through pathways independent of Rho/ROCK signaling. One possibility is de-activation of the ILK regulated N-WASP/Arp2/3 complex (mediators of actin polymerization), as N-WASP disruption negatively impacts OL process outgrowth (Bacon et al., 2007). In addition, ILK is required for α-parvin/β-parvin stabilization and paxillin localization, both of which bind F-actin directly (Attwell et al., 2003; Legate et al., 2006). Therefore, loss of ILK could lead to F-actin/integrin/ECM

uncoupling, which may explain the observed OL morphological defects. Additionally, *Ilk*$^{-/-}$ OLs are characterized by an inability to extend myelin-like membranes. While this is possibly due to cytoskeletal defects, our results following ROCK inhibition (improved branching but not membrane formation) suggest other pathways are at play, implying ILK's governance of OL process outgrowth and myelin membrane formation occur through separate mechanisms.

Through our work, we have begun to dissect ILK-directed signaling pathways overseeing unique aspects of OL development. Precisely which downstream targets potentiate ILK's role in cytoskeletal reorganization, and how their actions differ at varying stages of OL differentiation remains an intriguing question for the future.

Acknowledgements

The authors declare no competing financial interests. We thank Andrew Ferrier and Dr. Lyndsay Murray for comments on the manuscript and the rest of the Kothary laboratory for helpful discussions. We also thank Dr. Brian Popko, Dr. Rene St-Arnaud and Dr. Steffany Bennett for generous donation of transgenic mice. This work was supported by a grant from the Multiple Sclerosis Society of Canada. JPM and RWO are recipients of Frederick Banting and Charles Best Canadian Institutes of Health Research Doctoral Research Awards, and RK is a recipient of a University Health Research Chair from the University of Ottawa.

Chapter 4

Integrin-Linked Kinase Regulates Oligodendrocyte Cytoskeleton, Growth Cone, and Adhesion Dynamics

Integrin-linked kinase regulates oligodendrocyte cytoskeleton, growth cone, and adhesion dynamics

John-Paul Michalski[1], Sarah E. Cummings[1], Ryan W. O'Meara[1], and Rashmi Kothary[1,2,3,#]

[1]Ottawa Hospital Research Institute, Ottawa, Ontario, Canada K1H 8L6 and Department of Cellular and Molecular Medicine, University of Ottawa, Ottawa, Ontario, Canada K1H 8M5;

[2]Department of Medicine, University of Ottawa, Ottawa, Ontario, Canada K1H 8M5

[3]University of Ottawa Centre for Neuromuscular Disease, Ottawa, Ontario, Canada K1H 8M5

#Correspondence to: Rashmi Kothary

Submitting to journal *Glia*

Author Contributions

Conceived and designed the experiments: J-PM, RK. Performed the experiments: J-PM all Figures, SC helped with Figure 4.1. J-PM and SC analyzed the data. J-PM wrote the paper and RK revised and edited the manuscript.

Abstract

Integrin-linked kinase (ILK), a focal adhesion protein, brokers the link between cytoskeleton, cell membrane and extracellular environment. Here, we demonstrate a role for ILK in laminin-2 mediated adhesion in primary murine oligodendrocytes (OLs), with partial recovery on a non-integrin activating substrate poly-L-lysine. Intriguingly, ILK loss on the neutral poly-L-lysine substrate led to swelling at the tips of OL processes, which we identified as enlarged growth cones. Employing the bloated ILK-depleted structures as template, we demonstrate the appearance of distinct cytoskeletal domains within OL growth cones bearing classic neuronal growth cone architecture. Further, microtubule organization is severely perturbed following ILK loss, with centripetal microtubule looping and failure to bundle occurring in a laminin-2 independent manner. Together, our work highlights differences in specific aspects of OL biology as driven by laminin-2-dependent or independent ILK governed mechanisms. We reinforce the idea of OLs as growth cone bearing cells, describing the neuronal-like cytoskeleton therein. Finally, we demonstrate a role for ILK in OL growth cone maturation through microtubule regulation, the loss of which translates to decreased process length and myelin production capacity.

Introduction

The intricate relationship between extracellular environment and oligodendrocyte (OL) affects all aspects of OL development, from migration and proliferation to growth and differentiation. Signals relayed from the extracellular milieu trigger integrin clustering/activation, driving widespread cytoskeletal change. The change is orchestrated through adaptive protein recruitment to β1 integrin's cytoplasmic tail. At the heart of the recruitment is integrin-linked kinase (ILK). Along with obligate binding partners PINCH and parvin (the canonical IPP complex), ILK forms structural platforms. Through interactions with a variety of cytoskeletal linker proteins, the platform bridges the extracellular environment and underlying cellular actin network (Ghatak et al., 2013). ILK also guides microtubule stability and polarization through partnership with microtubule binding proteins, linking and anchoring actin/microtubules at the cell membrane (Wickström et al., 2010a; Akhtar and Streuli, 2013; Ghatak et al., 2013).

We previously reported a role for ILK in regulating OL actin cytoskeleton and morphogenesis (O'Meara et al., 2013). *In vivo*, ILK-depleted OLs give rise to temporal defects in myelination capacity, with full recovery in the aged animal. This thread – a remarkable ability to compensate following early amyelination – appears common to knockouts of the integrin pathway (Câmara et al., 2009; Forrest et al., 2009; O'Meara et al., 2013). At the time, we questioned whether recovery was due to an intrinsic ability of ILK-depleted OLs to 'catch-up', or rather, compensation by a small subpopulation of wild type (WT) OLs. We felt the answer lay in the nature of the cellular environment – the rich milieu *in vivo* providing substrates unavailable to the *in vitro* matrix, in our case, the mono-substrate laminin-2 (Ln-2). This was made clear by discrepancies in phenotypic

severity from *in vitro* (severe) to *in vivo* (mild phenotype, recovery) models of ILK loss (O'Meara et al., 2013).

To test whether a simple change in matrix could ameliorate phenotype following ILK loss, we grew primary ILK-depleted OLs on either Ln-2 or poly-L-lysine (PLL), a "neutral", non-integrin activating substrate (Machesky and Hall, 1997). We noted an immediate phenotypic change; increased complexity and membrane formation on the neutral substrate. More striking still, however, were the bloated lamellae on the growing ends of ILK-depleted OLs. When stained for tubulin and filamentous-actin (F-actin), a unique cytoskeletal architecture emerged; that of a growth cone. We are not the first to propose the OL as growth cone bearing (Fox et al., 2006). However, we now describe the structure as having cytoskeletal domains similar to a neuronal growth cone's. We also characterize myelin membrane cytoskeleton, with both F-actin and microtubules seemingly removed from the maturing membrane. Finally, we demonstrate Ln-2-independent perturbations in the OLs microtubule network following ILK loss. Taken together, our work showcases the OL's ability, given a non-integrin binding substrate, to maintain relative normalcy in branching and membrane formation in the absence of ILK. We also fill a surprising knowledge gap with regards to OL growth cone cytoskeleton, and ascribe a novel role for ILK, independent of Ln-2-based integrin signaling, in OL growth cone dynamics.

Materials and Methods

***Transgenic mice*:** Mice used in this study were cared for under the Canadian Council on Animal Care guidelines. Ethical approval for experiments was obtained under the University of Ottawa Animal Care Committee protocol OGH-131. *Ilk*$^{fl/fl}$ mice were a generous gift from Dr. René St-Arnaud, McGill University, Montreal, Canada (Terpstra et al., 2003). These mice were crossed to a floxed stop tdTomato-EGFP (*mT/mG*) reporter line (Muzumdar et al., 2007) and bred to homozygosity for both transgenes. Mice of either sex were employed in all experiments.

***Cell culture**:* OL primary cultures were generated as described previously (O'Meara et al., 2011b). Briefly, the cortex was removed from P0-P2 pups, dissociated, and a mixed glial culture formed over 10-12 days. TAT-Cre (Excellgen) or vehicle-control (where applicable) was added to the culture for 1-2 hours in two separate 48-72 hour applications prior to shaking and seeding of pure primary OLs. Pure OL cultures were grown on coverslips coated with either human placental merosin (laminin-2 (Ln-2); Millipore) or poly-L-lysine ((PLL); Sigma-Aldrich).

Immunohistochemistry: Cells were fixed for observation at 1, 3 and 6 days *in vitro* (DIV) as previously described (O'Meara et al., 2013). Briefly, OLs were fixed with 3% paraformaldehyde (PFA) for 15 min, permeabilized with 0.1% Triton-X-100 and blocked with 10% goat serum. All primary antibodies were placed in blocking solution and incubated overnight. They include: myelin-associated glycoprotein (MAG; EMD Millipore), myelin basic protein (MBP, AbD Serotec) and α-tubulin (EMD Millipore). Alexa secondary antibodies (Invitrogen) and/or rhodamine/488 phalloidin (Invitrogen)

were then applied. Samples were counterstained with 4',6'-diamidino-2-phenylindole (DAPI) and mounted in Dako mounting media. Images were captured either on an Axio Imager M1 microscope or a Zeiss LSM 510 Meta DuoScan confocal microscope. Image analysis was conducted using ImageJ 1.48r software.

Process length and membrane area determination: Concentric rings were placed around MAG^+ OLs at 50 pixel intervals (see Figure 4.1D). The OL was then subdivided into four equal quadrants. A single length was recorded for each quadrant demarking the furthest distance travelled by any given process within. Four values/OL (as there were four quadrants) were then averaged to give a single impression of general maximal length attained by any given OL. A minimum 20 OLs were recorded per group ($Ilk^{fl/fl}$ vs. $Ilk^{-/-}$) per experiment.

Membrane area of MBP^+ OLs was traced and recorded. We removed the two smallest and largest membranes from both WT and $Ilk^{-/-}$ OLs for each experiment performed. This was done to minimize the impact of a small population of OLs that express EGFP but are in fact still WT (they still express ILK) and vice versa. This was especially important for $Ilk^{-/-}$ OLs on Ln-2, as the pool of myelin producing cells is relatively small, and, as such, even a few extremely large WT OLs can introduce huge data variability.

Live imaging: Primary cultures were derived as described above and plated onto specialized 8 well chamber slides (Bd Falcon, 0877426) coated with PLL. OLs were initially grown in a cell culture incubator and then moved to a Zeiss live imaging system at DIV1. Phase contrast images were captured with an inverted Axiovert 200M

microscope. Image contrast was adjusted so as to best define contour of the OL growth cone. A single experiment was performed and a minimum 3 fields of view (FOV) taken per condition (TAT-Cre vs. vehicle). For growth cone size a minimum of 18 growth cones from 11 OLs were counted per condition. Images were captured every 20 seconds. For process length, a minimum 11 growth cones from 6 OLs were counted per condition. Images were captured every 5 minutes and length was recorded at 20-minute intervals over 320 minutes total. N value in all experiments equates the number of individual growth cones counted. All analysis was performed using ImageJ 1.48r software.

***Western blot*:** Primary cultures were lysed in RIPA buffer (Cell Signaling) with 1 mM PMSF added prior to use. SDS-PAGE gels were run with 3 samples for each group (TAT-Cre or vehicle treated). Gels were transferred to a PVDF membrane and then blocked in 5% milk. Primary antibodies against ILK (Cell Signaling), α-parvin (Cell Signaling) and GAPDH (Abcam) were used. Following secondary HRP-conjugated antibody administration, membranes were washed and then treated with enhanced chemiluminescent substrate (Thermo Scientific). Western blot film was scanned with an EPSON Perfection 2450 scanner.

***Statistical analysis**:* All statistical analysis was performed using Prism 6 GraphPad software. Unless otherwise stated, a minimum of three independent experiments were performed for all data collected (see Live imaging section). Two-tailed Student's *t* tests were used for statistical analysis unless otherwise stated. Significance was set at $p < 0.05$.

Results

Substrate dependence and ILK's role in OL differentiation

We tested the ability of ILK-depleted cells to grow on an "inert" adhesive substrate, poly-L-lysine (PLL). It provides an adhesive surface for cellular growth through charge interaction with cellular membranes and not through integrin receptor binding. Primary OLs were grown on either Ln-2 or PLL over three days. Cells were derived from *Ilk$^{fl/fl}$;mT/mG* mice as previously described (O'Meara et al., 2013). Briefly, *Ilk$^{fl/fl}$;mT/mG* transgenic mice carry both a floxed *Ilk* (*Ilk$^{fl/fl}$*) allele and a *tdTomato/EGFP* reporter gene (*mT/mG*). The fluorophore is membrane bound and allows visualization of cellular morphology. The addition of a Tat-Cre fusion recombinase (TAT-Cre) simultaneously depletes ILK (dubbed *Ilk$^{-/-}$*) (Figure S4.1) and triggers EGFP expression (*tdTomato* is switched off), effectively turning ILK null cells from red to green (Figure 4.1A). For simplicity, we will refer to ILK-depleted OLs as *Ilk$^{-/-}$* and *Ilk$^{fl/fl}$;mT/mG* (non-recombined) as WT or simply *Ilk$^{fl/fl}$*. Further, when grown on Ln-2, we will refer to OLs as Ln-2 WT or Ln-2 *Ilk$^{-/-}$*, and when on PLL as PLL WT or PLL *Ilk$^{-/-}$*.

As previously reported, ILK-depleted cells expressing the differentiation marker MAG, when grown on Ln-2, form stunted processes and fail to branch over 3 days in culture (Figure 4.1A). When binned by morphological maturity, the majority are stage 1 (Figure 4.1B, C). F-actin accumulates both within the cell soma and in processes of Ln-2 *Ilk$^{-/-}$* OLs (Figure 4.1A). In stark contrast, PLL *Ilk$^{-/-}$* cells advance to stage 3 – having highly branched processes – and when binned solely for morphological complexity, are no different from WT on either Ln-2 or PLL. Strikingly, they are not characterized by somal F-actin accumulation as seen on Ln-2 (Figure 4.1A).

We further quantified process length, an indication of the cell's ability to (i) myelinate at a distance and (ii) the volume of membrane produced. MAG^+ OLs were subdivided into four quadrants and the furthest distance travelled by a process within each was measured (see Figure 4.1D). Unsurprisingly, Ln-2 *Ilk*$^{-/-}$ OLs formed the shortest processes (Figure 4.1E), followed by PLL *Ilk*$^{-/-}$ cells (Figure 4.1E). Unlike general complexity (Figure 4.1C), processes from PLL *Ilk*$^{-/-}$ OLs failed to reach overall WT length on either substrate (with Ln-2 WT forming the longest) (Figure 4.1E). A graph depicting general distribution between WT and *Ilk*$^{-/-}$ OLs on each substrate was generated, demonstrating general trends (Figure 4.1F). *Ilk*$^{-/-}$ OLs are therefore capable of maintaining complexity, but not length, barring Ln-2 mediated integrin activation. Translated *in vivo*, our findings suggest an intrinsic ability of OLs to function in the absence of ILK to a much greater degree than seen *in vitro* (on a Ln-2 substrate).

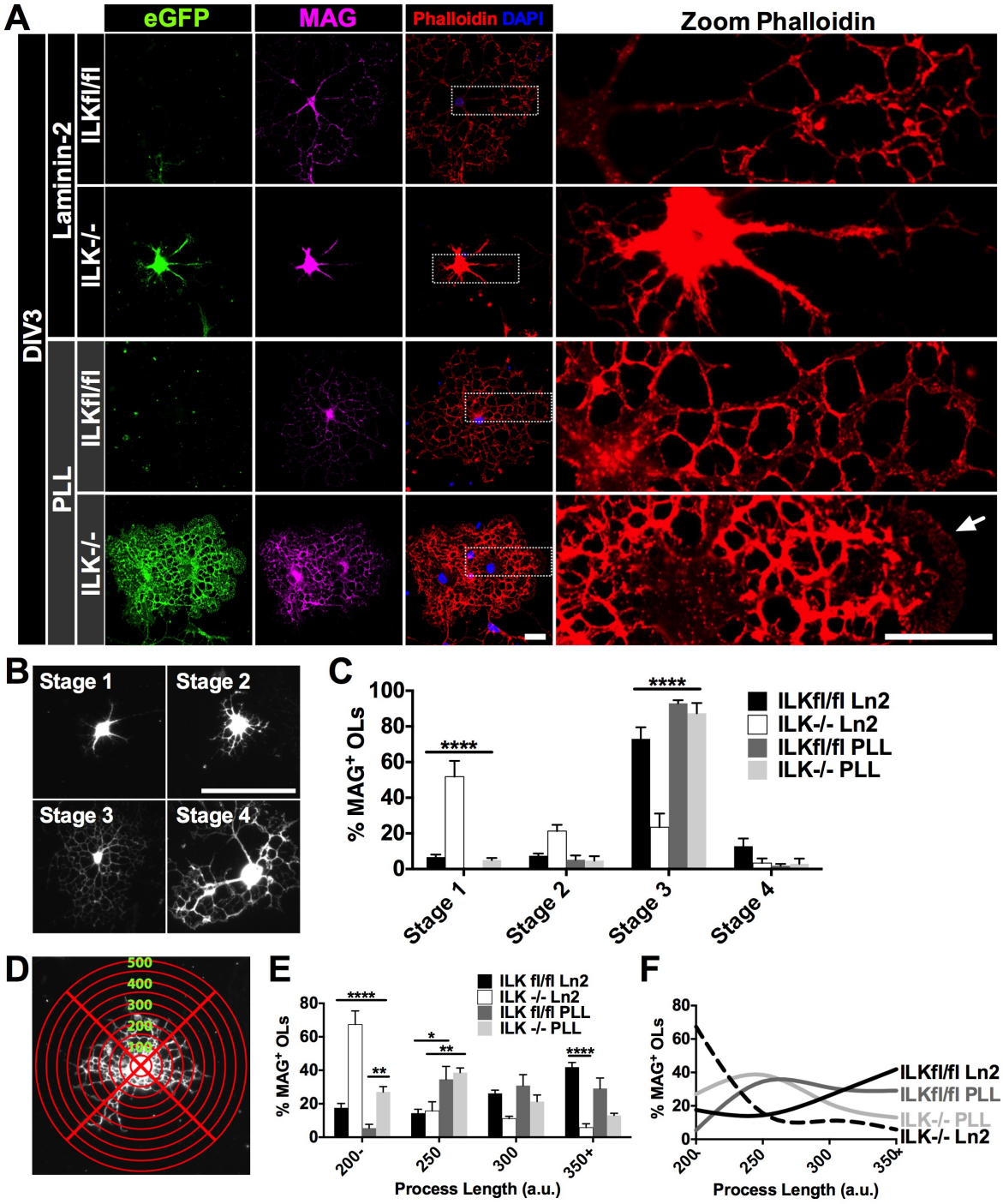

Figure 4.1. ILK loss impacts OL complexity and process length in a substrate dependent manner. A. Immunostaining of TAT-Cre treated OLs at DIV3 for MAG (purple), phalloidin (red) and DAPI (blue) on either Ln-2 or PLL. EGFP expression denotes recombined ILK-depleted OLs. Far right panels are zoomed in from the

demarcated region. Arrow depicts a swollen growth cone **B.** Example of morphological stages used in the binning process. **C.** Quantification of percentage MAG^+ cells falling within each stage between ILK-depleted and WT groups on either Ln-2 or PLL. **D.** Example of concentric rings and quadrants employed to measure maximal process length of MAG^+ OLs. **E.** Quantification of percentage MAG^+ cells with given maximal process length between ILK-depleted and WT groups on either Ln-2 or PLL. **F.** Curve generated from (E) depicting overall patterning of process length between OL groups. Data represent the mean ±SEM (n=3). $*p < 0.05$, $**p < 0.01$, $****p < 0.0001$ (two-way ANOVA test). Scale bars: (A) 20 μm (B) 100 μm.

The OL growth cone and cytoskeleton

While branching is maintained following ILK loss on PLL, there is a clear deficit in process length. To elongate, the OL process must grow outwards, which requires a growing tip. However, we, like others, would suggest the tips are growth cone-like, and, as such, would label them as OL growth cones (Jarjour and Kennedy, 2004; Fox et al., 2006; Haber et al., 2009; Rajasekharan et al., 2009). That is not to say they are identical to neuronal counterparts, but rather to acknowledge the presence of a highly motile and guidance responsive structure bearing classic neuronal growth cone morphology (Fox et al., 2006). The distinction is also important when considering the peculiar nature of OL growth cones following ILK depletion on PLL. As depicted in Figure 4.1A (arrow), PLL *Ilk*$^{-/-}$ OLs protrude a bulbous growth cone, many times larger than WT (on either substrate) and/or Ln-2 *Ilk*$^{-/-}$ OLs. Neuronal growth cone morphology is dependent on cytoskeletal architecture, and is defined by three distinct cytoskeletal zones; peripheral (P), central (C) and transitional (T) (Figure 4.2A) (for a review see Vitriol & Zheng, 2012). Little work has been done to qualify whether the OL growth cone can be similarly described. To establish a baseline, DIV1 WT OLs were grown on either Ln-2 or PLL and then stained for F-actin and tubulin (Figure 4.2B, C). As previously described (Fox et al., 2006), OL growth cones shrink in size as the cell increases in complexity (matures) (Figure 4.2B). Whether this is an outcome of programmed contraction over time, the result of the larger initial cone splitting cytoplasm during bifurcation, or the growth cone halting and projecting consecutively smaller "daughter" processes remains to be determined.

Our focus was on the larger cones, as they provide maximal resolution. Similar to a neuronal growth cone, there was a clear P zone, defined by radial bundles of F-actin

containing filopodia that extrude the most distal edge of the lamellipodium (Figure 4.2B, C). Tubulin, originating from the process, invades the cone centrally, in a region relatively devoid of F-actin. Its bulk stays well behind the leading P zone, sending individual 'pioneering' microtubules that extend and colocalize along F-actin rich filopodia (Figure 4.2C arrow). This tubulin patterning (in general terms) also defines the central microtubule core, the C zone, of a neuronal growth cone. Interestingly, in immature OLs on PLL, F-actin accumulates centrally, just behind the P region (this is rarely seen in Ln-2 WT OLs) (Figure 4.2C asterisk). Here, it overlaps with the distal microtubule tip. While distinct, it draws parallels to the neuronal growth cone's T zone. The transition (T) zone is defined by an F-actin arc separating the P and C regions. In neurons, this junction provides an interface for microtubule and F-actin interaction and can only be seen in high resolution. It is also here that contractile structures are formed and F-actin is turned over (Medeiros et al., 2006; Burnette et al., 2008; Vitriol and Zheng, 2012). As the OL matures, and the cone shrinks, zones become much more difficult to define, often appearing as extended filopodia (Figure 4.2B). As researchers tend to study the mature OL, it is unsurprising these structures have received so little attention.

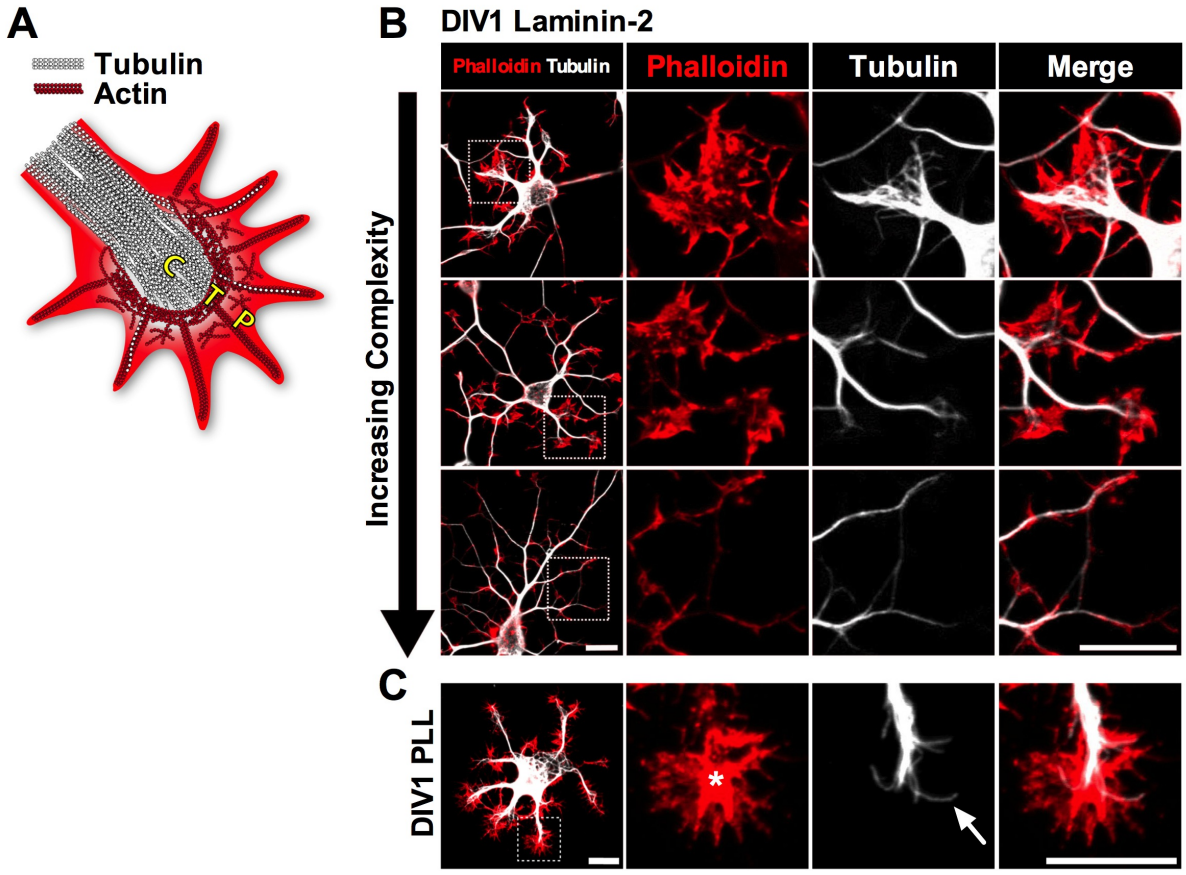

Figure 4.2. OLs share cytoskeletal architecture with neuronal growth cones. A. Schematic representation of a neuronal growth cone. Organization of the cytoskeleton gives rise to unique domains: central (C), transitional (T) and peripheral (P). Tubulin is depicted in white and F-actin in red. **B.** Immunostaining of WT OLs at DIV1 on Ln-2 for phalloidin (red) and tubulin (white). From top to bottom, increased morphological complexity correlates with decreased growth cone size. All panels to the right are zoomed in on demarcated region in left image. **C.** Immunostaining of WT OLs at DIV1 on PLL for phalloidin (red) and tubulin (white). All panels to the right are zoomed in on demarcated region in left image. Asterisk depicts putative T zone with F-actin accumulation separating microtubules from F-actin rich filopodial P zone. Arrow depicts "pioneering" microtubules, which pass into the P zone and travel along actin filaments. Scale bar: 10 μm.

At DIV3, MAG^{+} PLL *Ilk*$^{-/-}$ growth cones are twice the size of any other group and yet morphological complexity is maintained (Figure 4.3A, C). The result defies expectations – growth cones should shrink as the OL develops. When stained for tubulin and F-actin, PLL *Ilk*$^{-/-}$ growth cones appear primordial. The largest exhibit cytoskeletal organization distinctly similar in structure to the neuron's P, C and T regions (Figure 4.3A, B). Here, the regions are hyper-defined, often with clear arcing F-actin (again, reminiscent of the neuron's T zone) delineating P and C regions (see Figure 4.3A). Whether F-actin distribution within the "T zone" is similar to early PLL WT OLs (see Figure 4.2C), simply on a larger scale (and therefore affording higher resolution) is unclear. F-actin does, however, appear denser than PLL WT counterparts. Possible explanations include abnormal F-actin accumulation and/or an inability to clear F-actin in the region.

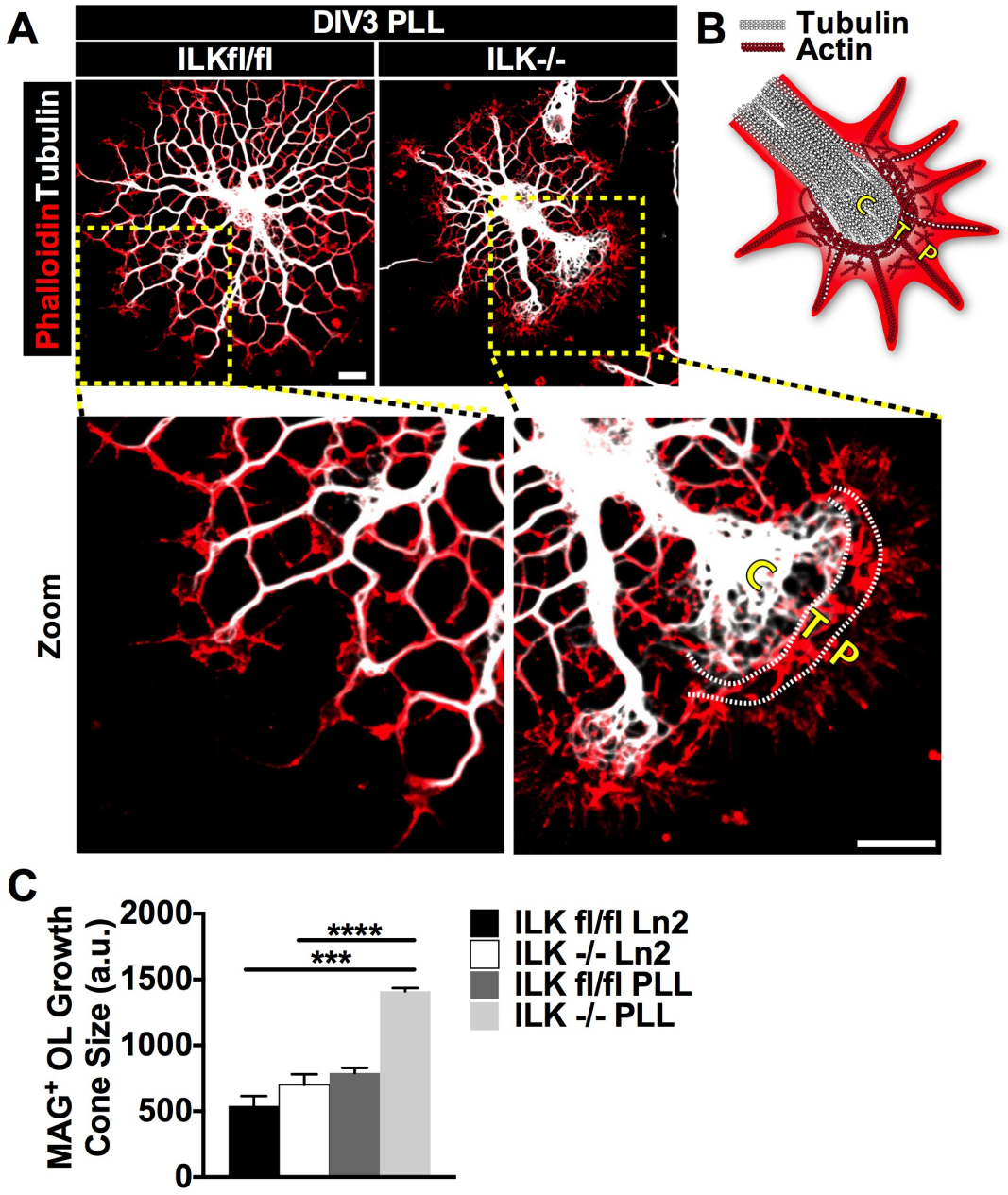

Figure 4.3. ILK-depleted growth cones on PLL are bloated and allow for high-resolution view of the cytoskeleton. **A.** Immunostaining of DIV3 WT and *Ilk*$^{-/-}$ OLs on PLL for phalloidin (red) and tubulin (white). Cytoskeletal zones are superimposed. **B.** Schematic representation of a neuronal growth cone. Organization of the cytoskeleton gives rise to unique domains: central (C), transitional (T) and peripheral (P). Tubulin is depicted in white and actin in red. **C.** Quantification of MAG^{+} growth cone size. Data

represent the mean ±SEM (n=3). ***$p < 0.001$, ****$p < 0.0001$ (one-way ANOVA test). Scale bar: 10 μm.

ILK regulates OL growth cone dynamics

PLL *Ilk*$^{-/-}$ OLs suffer an inability to fully extend processes, but maintain complexity. As ILK loss leads to morphological growth cone defects, we sought to gauge whether the cone's growth dynamics were also affected. WT (vehicle treated) and ILK-depleted (TAT-Cre treated) OLs were grown on PLL and followed with a live imaging system at DIV1, a time when WT growth cones are still relatively large. Images were first captured every 20 seconds to access growth cone mutability. Initial assessment demonstrated highly dynamic cones extending and retracting multiple filopodia in both WT and *Ilk*$^{-/-}$ OLs (Figure 4.4A). This was further demonstrated when growth cones from Figure 4.4A were overlaid (Figure 4.4B). We next measured total change in growth cone size over time. The readout is presented as percent change in growth cone size from one frame to the next. Percent change is employed to control for size discrepancy between WT (smaller) and *Ilk*$^{-/-}$ growth cones. Both shrinking and expanding events over a 2-minute period were recorded and summed to highlight whole growth cone dynamism. There was a slight, but significant, decrease in the percentage change for *Ilk*$^{-/-}$ cones relative to WT (Figure 4.4C), suggesting the cone's size becomes increasingly static following ILK loss. WT growth cones also tended to have more shrinking events than *Ilk*$^{-/-}$ counterparts (Figure 4.4D). Both findings correlate with fixed *Ilk*$^{-/-}$ OLs at DIV3 maintaining overly large primordial growth cones.

We next tested primary process growth by live recording WT and *Ilk*$^{-/-}$ OLs on PLL at DIV1 (Figure 4.4E). Distance travelled was measured every 20 minutes over a 320 minute time period. Surprisingly, total outwards growth, as measured by the difference in length between time 0 and time 320 (from the OL cell body to the growth cone's center), was no different between *Ilk*$^{-/-}$ and WT cones (Figure 4.4F). However,

when both cone growth (outwards movement) and retraction (inwards movement) were summed, there was a clear and significant decrease in total distance travelled following ILK depletion (Figure 4.4G). Therefore, within the observed time frame, ILK loss does not affect net distance travelled outwards, but rather, the overall dynamic range assessable to the process through continued growth and retraction.

Next, the live imaging model was used to better understand how PLL *Ilk*$^{-/-}$ OLs maintained morphological complexity. Upon investigation, multiple mechanisms were at play and all seemed to revolve around growth cone filopodia. At this juncture, we must emphasize that OL growth cones, on either Ln-2 or PLL, continue to form F-actin filopodia following ILK loss. When these actin rich structures contacted adjacent growth cones and/or processes a bridge formed (Figure 4.4H asterisk). From there, the growth cone either dissociated from the newly formed branch (Figure 4.4H arrow head) or itself contracted and formed multiple interconnecting branches seeded from the initial filopodia (Figure 4.4H, arrow). Due to the enlarged growth cone, contact between filopodia and other structures is a regular occurrence on PLL. This strongly suggests, independent of Ln-2 based adhesion, ILK is dispensable for interconnecting branch formation. Also, that the molecular mechanisms governing growth cone dynamics shift when the cone comes into contact with itself (and also other OLs), as we see rapid change in growth cone size leading to branch formation.

Unfortunately, we could not consistently grow Ln-2 *Ilk*$^{-/-}$ OLs for comparison (within the live imaging system). These cells, when fixed, have smaller growth cones and, unlike PLL, form almost no interconnecting branches (see Figure 4.1A and 4.5A). We know Ln-2 alone is sufficient to drive highly complex branching in WT OLs (see Figure 4.1A and 4.5A). It therefore follows – the interaction between OL and the ECM

component Ln-2 (through integrin receptor binding), leading to focal adhesion formation, requires ILK. If integrins are bypassed and adhesion secured (by plating the OLs on PLL), then ILK appears dispensable for OL branch complexity but not normal growth cone behavior. Future work should therefore focus on understanding and identifying which molecular players are responsible for the apparent switch and compensation.

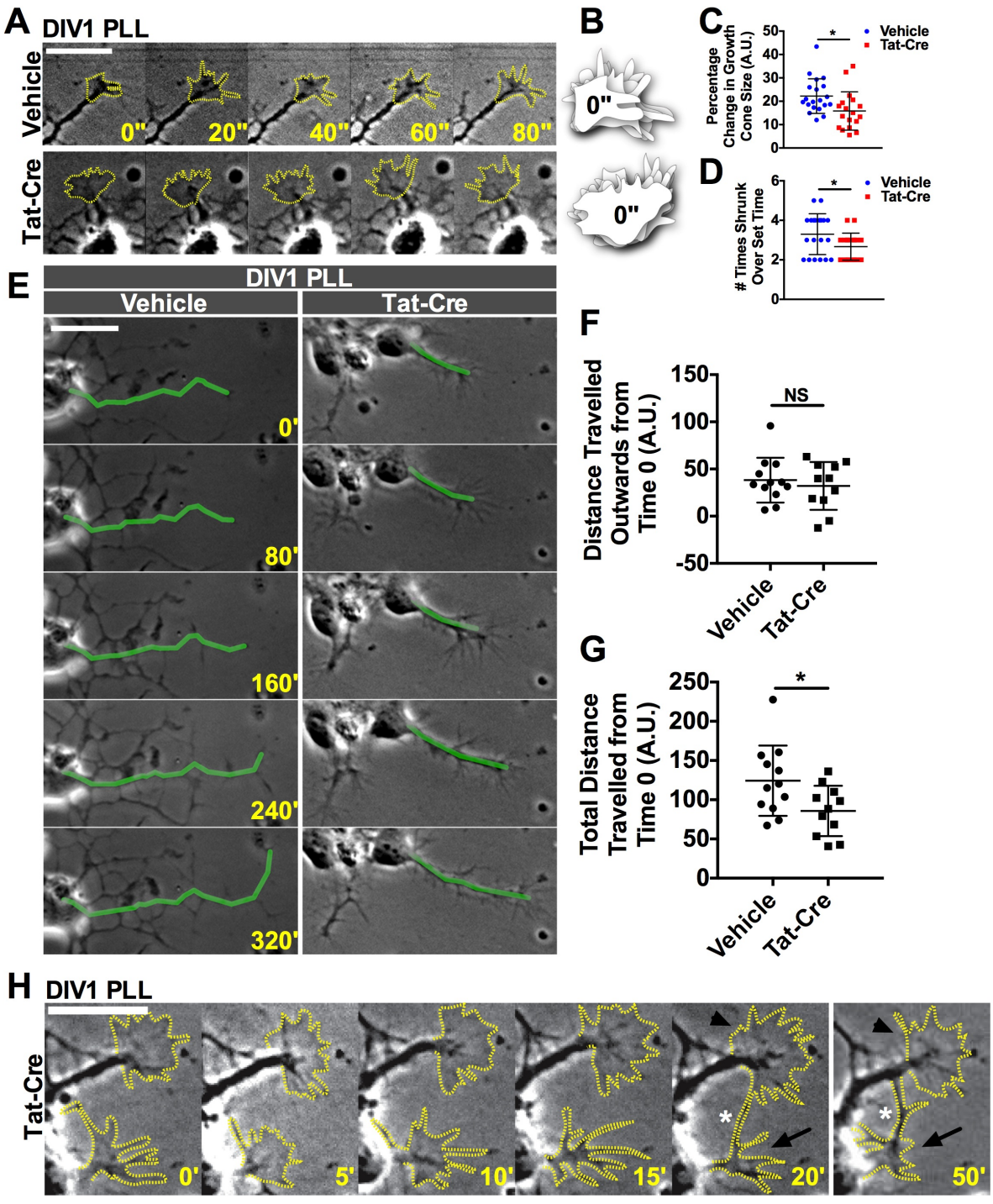

Figure 4.4. ILK-depleted growth cones on PLL are less dynamic. A. Phase contrast images of vehicle and TAT-Cre treated cultures at DIV1 on PLL. Growth cones are highlighted in yellow. Images were taken every 20 seconds (a total of 80 seconds is depicted). **B.** Overlay of growth cones from (A). Each overlay represents 20 seconds, and 80 seconds total is depicted. **C.** Quantification of percent change in growth cone size over

120 seconds at 20-second intervals. **D.** Quantification of times growth cone shrank over 120 seconds at 20-second intervals. **E.** Phase contrast images of vehicle and TAT-Cre treated OLs on PLL at DIV1. Each image represents an 80-minute interval (pictures were taken every 5 minutes). 320 minutes total is depicted here. **F.** Quantification of distance travelled outwards from time zero. Calculations were based on measurements every 20 minutes over 320 minutes total. **G.** Quantification of total distance travelled, both forwards and backwards. Calculations were based on measurement every 20 minutes over 320 minutes total. **H.** Phase contrast images at DIV1 of TAT-Cre treated OLs on PLL. Images were taken every 5 minutes for a total of 20 minutes depicted here. A final shot of the same cell at 50 minutes is also shown. The asterisk depicts a branch between growth cones forming, the arrowhead a growth cone dissociating from the branch, and the arrow a growth cone which itself is splitting into multiple branches. Data represent the mean ±SD (C,D; vehicle n=20 TAT-Cre n=18 – F,G; vehicle n=12 TAT-Cre n=11). NS = not significant, *$p < 0.05$, (Student's *t* test). Scale bar: 20 μm.

ILK loss and growth cone enlargement is associated with microtubule disorganization

We previously ascribed a role for ILK in regulating OL F-actin networks in mature cells (O'Meara et al., 2013). There, Ln-2 *Ilk*$^{-/-}$ OLs were defined by F-actin accumulation in the process and cell body (recapitulated in Figure 4.1A). Here, we further demonstrate F-actin accumulation in enlarged PLL *Ilk*$^{-/-}$ growth cones, though, importantly, not in the cell soma (see Figure 4.2A). In light of our growth cone focus, we sought to establish the impact of ILK loss on the cone's second cytoskeletal component, microtubules. WT and *Ilk*$^{-/-}$ OLs were plated on either Ln-2 or PLL and differentiated over 3 days. Similar to WT, microtubules in Ln-2 *Ilk*$^{-/-}$ MAG^{+} (maturing) OLs localized to the central (C zone) growth cone base (Figure 4.5A). However, in approximately 30% of *Ilk*$^{-/-}$ OLs (relative to ~2.5% in Ln-2 WT), we observed microtubule accumulation, often seen as a ballooning upon cone entry (Figure 4.5A arrow, B). On PLL, the effect was exacerbated. Tubulin was replete throughout the entirety of the cone's base and central regions (Figure 4.5A). Microtubules accumulated in large looping formations, rather than appearing compact, narrow and in line with the cone's growth direction (as seen in mature WT OLs) (Figure 4.5A, B). The only comparable "loose" patterning in WT occurs in the largest, most immature WT cones (see Figure 4.2A). We were unable to ascertain whether looping also occurred in Ln-2 *Ilk*$^{-/-}$ OLs, due to the increased microtubule density. It is important to note, that while lower than Ln-2 *Ilk*$^{-/-}$ OLs, ~15% of PLL WT OLs did have bulbous microtubule accumulation. As the phenotype is almost non-existent in Ln-2 WT OLs, it suggests a shift in OL microtubule behavior, further compounded with ILK loss, when differentiating in the absence of active integrin signaling.

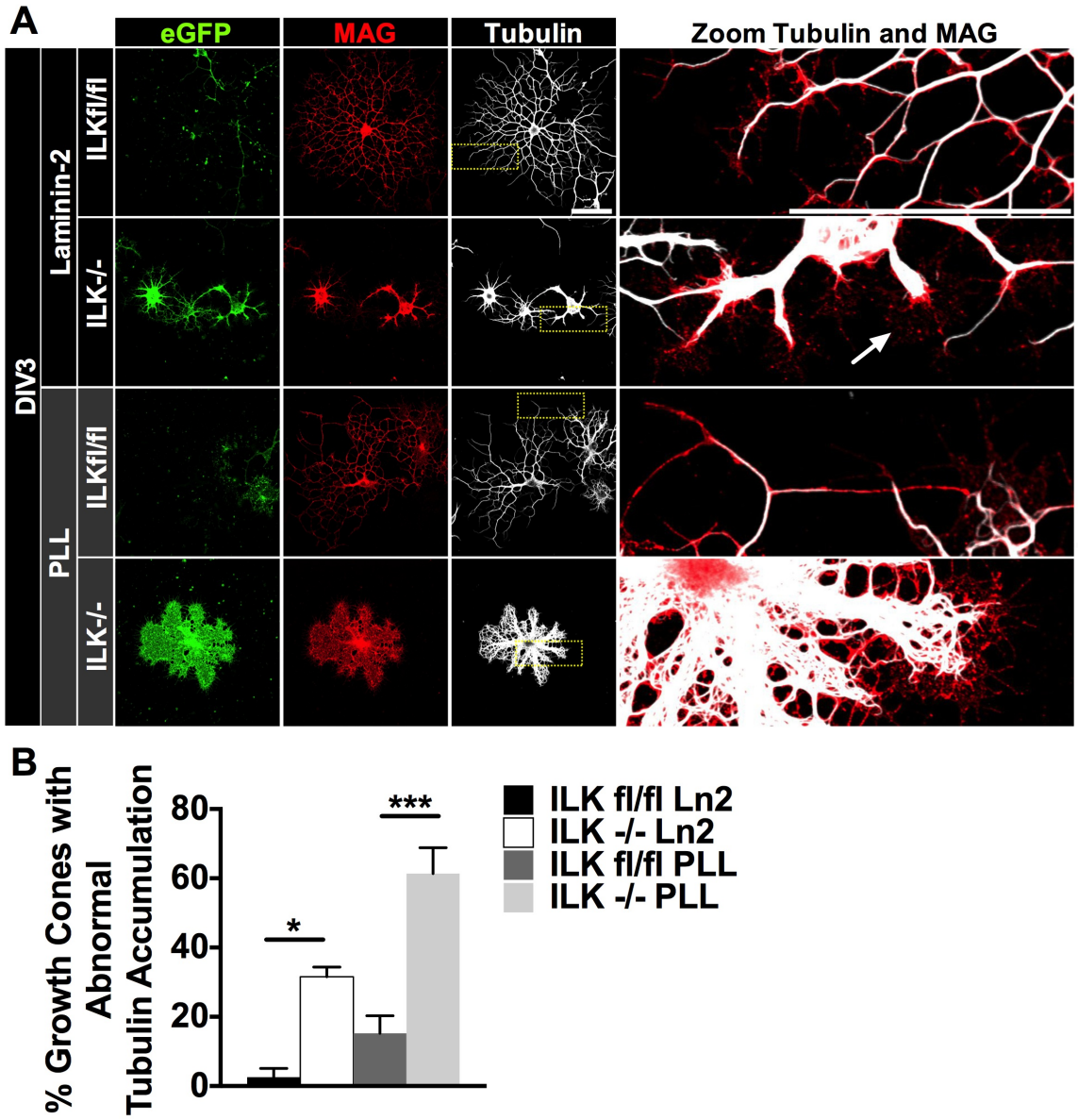

Figure 4.5. Abnormal tubulin organization following ILK loss. A. Immunostaining of TAT-Cre treated OLs at DIV3 stained for MAG (red) and tubulin (white). EGFP is shown in green. OLs were grown on either Ln-2 or PLL. Panels to the far right represent the demarcated zoomed-in regions. Arrow indicates abnormal bulge in tubulin following entry into growth cone. **B.** Quantification for percentage MAG^+ OLs with abnormal tubulin accumulation. Data represent the mean ±SEM (n=3). *$p < 0.05$, ***$p < 0.001$, (one-way Anova test). Scale bar: 50 µm.

Membrane cytoskeleton in cultured oligodendrocytes

We have so far focused on OLs in the early and middle phases of differentiation. We now turn to myelin membrane formation. As ILK played a role in pre-myelin cytoskeletal dynamics, we thought it prudent to establish a baseline for membrane cytoskeleton in our culture system. Primary OLs were seeded on Ln-2 and differentiated over 6 days. All cells were stained for myelin basic protein (MBP), a late stage myelin marker. Functionally, MBP is required for membrane compaction – it draws opposing membrane surfaces together. Areas of compaction can also be determined through tdTomato red localization (fluorescent signal is lost), expressed by all *mT/mG* derived OLs. When co-labelled with phalloidin, a clear pattern emerges; tdTomato red containing membrane co-locates with F-actin and the two segregate from MBP. Simply, as MBP puncta accumulate in discrete pocketed zones, membrane is compacted, tdTomato red is expelled, and F-actin staining is lost (Figure 4.6). We have classified OL membrane maturity with respect to F-actin in three stages; early (Figure 4.6A), mid (Figure 4.6B) and late (Figure 4.6C). The earliest membrane is composed of contiguous tdTomato$^+$ myelin with F-actin replete throughout. Small compacting pockets form, and here, MBP$^+$ puncta cluster and define the pockets edge (Figure 4.6A). As the membrane matures, pockets widen and fill with MBP$^+$ puncta. Now, clear and striking delineation between uncompacted tdTomato/F-actin$^+$ and MBP$^+$ compacted domains occur (Figure 4.6B). In the final stage, F-actin is relegated to the OLs distal edge and appears sporadically within uncompacted channels proximal to the soma (Figure 4.6C). Microtubules are found throughout mature myelin, the network clearly defining compacted (MBP$^+$) regions (Figure 4.6D, Figure S4.2 Late). In membrane with little to no MBP accumulation (early membrane), microtubules can become quite thick and tangled, often forming the

beginnings of small circular pockets (Figure S4.2 Early). As the cell matures, these pockets fill with MBP^+ puncta (which often seed alongside microtubules at the pocket's inner edge), the membrane compresses, and microtubules seem to disentangle, expanding along with the compaction zones border (Figure S4.2 Late). At the F-actin heavy distal edge, however, microtubules form a quasi border between themselves and the $tdTomato^+$/microfilament rich membrane (perhaps similar to the inner and outer loops which contain cytoplasm and define the outer edge of the myelin sheath *in vivo*). This clear transition from microtubule to microfilament suggests a relatively dynamic uncompacted membrane running along the OLs outer rim. Together, the data speaks to a system whereby microfilaments, a highly dynamic component in constant flux, are removed from compacted MBP^+ myelin membrane, while stability providing microtubules define compressed membrane domains. These two cytoskeletal components, in opposition, achieve the static equilibrium myelin necessitates. Our results are in agreement with work done previously, where MBP clustering and OL maturity correlates with decreased cytoskeletal staining (Dyer and Benjamins, 1989a, 1989b; Boggs and Wang, 2001, 2004; Bauer et al., 2009).

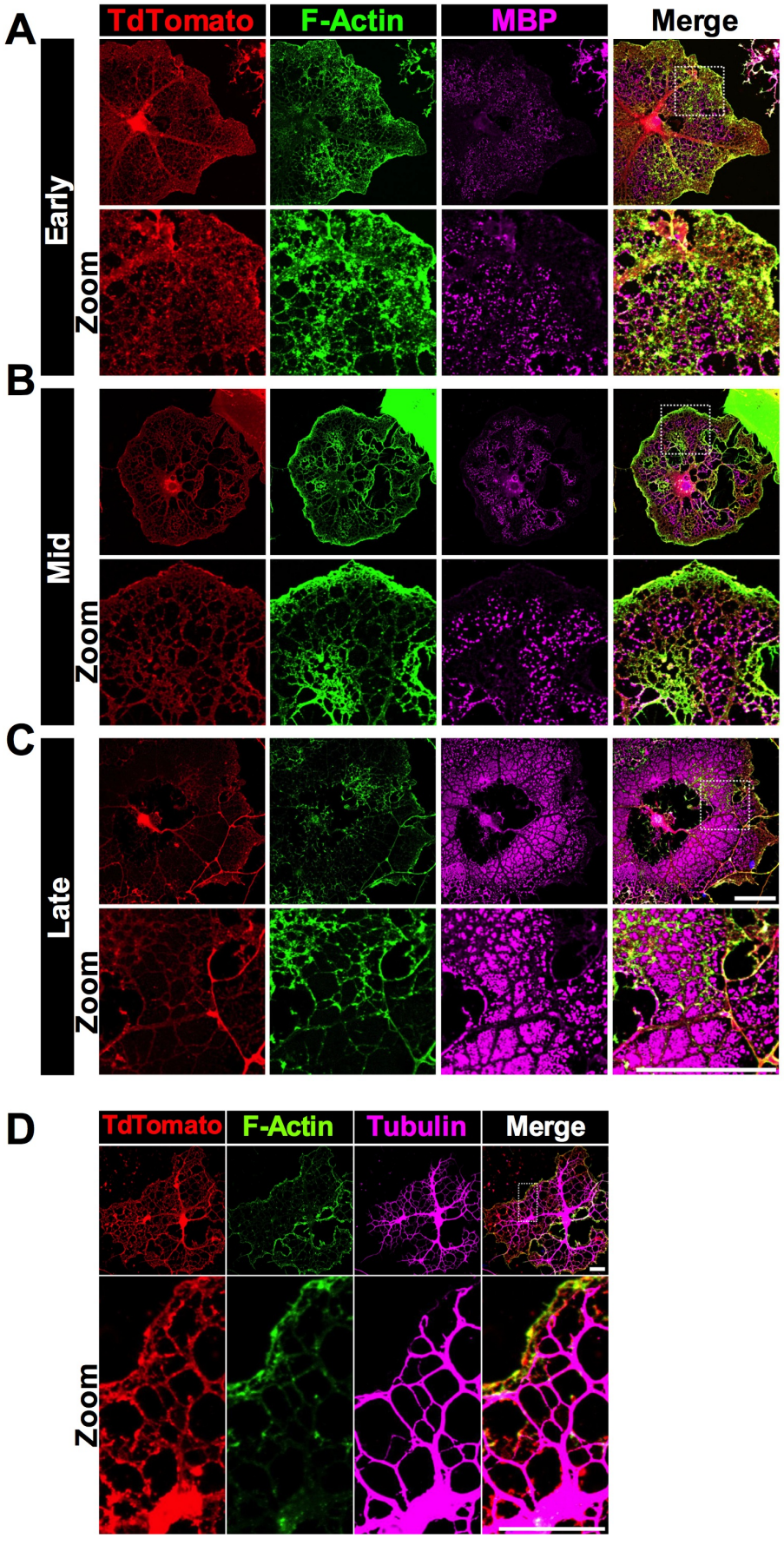
A
TdTomato
F-Actin
MBP
Merge
Early
Zoom
B
Mid
Zoom
C
Late
Zoom
D
TdTomato
F-Actin
Tubulin
Merge
Zoom

Figure 4.6. Cytoskeletal distribution linked to myelin compaction and MBP expression. A. Immunostaining of early stage Ln-2 WT OL at DIV6 for F-actin (green, phalloidin) and MBP (purple). tdTomato is in red. Panels below represent demarcated zoomed-in region. Note wide F-actin distribution and large amount of uncompacted tdTomato-positive membrane. Small pockets of clustered MBP have begun to form, distinct from F-actin/tdTomato. **B.** Immunostaining of mid stage Ln-2 WT OL at DIV6 for F-actin (green, phalloidin) and MBP (purple). tdTomato is in red. Panels below represent demarcated zoomed-in region. Note clear delineation of F-actin rich tdTomato regions from MBP pockets. **C.** Immunostaining of late stage Ln-2 WT OL at DIV6 for F-actin (green, phalloidin) and MBP (purple). tdTomato is in red. Panels below represent demarcated zoomed-in region. Note a general absence of F-actin/tdTomato and presence of large MBP clusters. **D.** Immunostaining of Ln-2 WT OL at DIV6 for F-actin (green, phalloidin) and tubulin (purple). tdTomato is in red. Panels below represent demarcated zoomed-in region. Scale bars: (A-C) 50 μm, (D) 25 μm.

ILK regulates OL membrane formation and cytoskeleton in a substrate specific manner

We set out to determine the outcome for ILK-depleted OLs if adhesion were maintained in the absence of Ln-2 induced signaling. Ln-2 *Ilk*$^{-/-}$ OLs grown 6 days lag behind WT counterparts on both Ln-2 and PLL in their ability to form membrane (Figure 4.7A, B) and in the area of membrane formed (Figure 4.7A, C). When the same cells are grown on PLL, the percent cells with membrane is no different than WT (Figure 4.7A, B) and membrane area formed is only slightly less than WT OLs on PLL (Figure 4.7A, C, E). For full effect, if membrane area of *Ilk*$^{-/-}$ OLs on Ln-2 and PLL are directly compared, a clear and significant difference emerges (Figure 4.7D). As expected, membrane distribution across all groups (Figure 4.7C) mirrors the pattern for process length at DIV6 (see Figure 4.1E and F) – with Ln-2 WT the longest and Ln-2 *Ilk*$^{-/-}$ the shortest, and PLL WT followed by PLL *Ilk*$^{-/-}$ in between. It implies process extension and growth cone do not limit the ability of OLs to form membrane, rather, they limit the volume of membrane formed in a Ln-2-independent manner.

Similar to DIV3 (see Figure 4.1A), F-actin accumulated behind the membrane in Ln-2 *Ilk*$^{-/-}$ MBP^{+} OLs at DIV6 (Figure 4.7A zoom). F-actin predominantly accumulated behind the membrane in PLL *Ilk*$^{-/-}$ OLs as well (Figure 4.7A zoom). At first, we thought this a by-product of large growth cones merging, followed by an inability to turn over accumulated excess F-actin (see Figure 4.3A). However, the same phenotype presents in PLL WT OLs (Figure 4.7A zoom). In light of our work describing baseline cytoskeleton in Ln-2 WT OLs, we suggest the data supports a shift in actin handling at the uncompacted membrane base when integrin signaling is not engaged, though ILK loss may exacerbate the phenotype in conjunction with substrate presented.

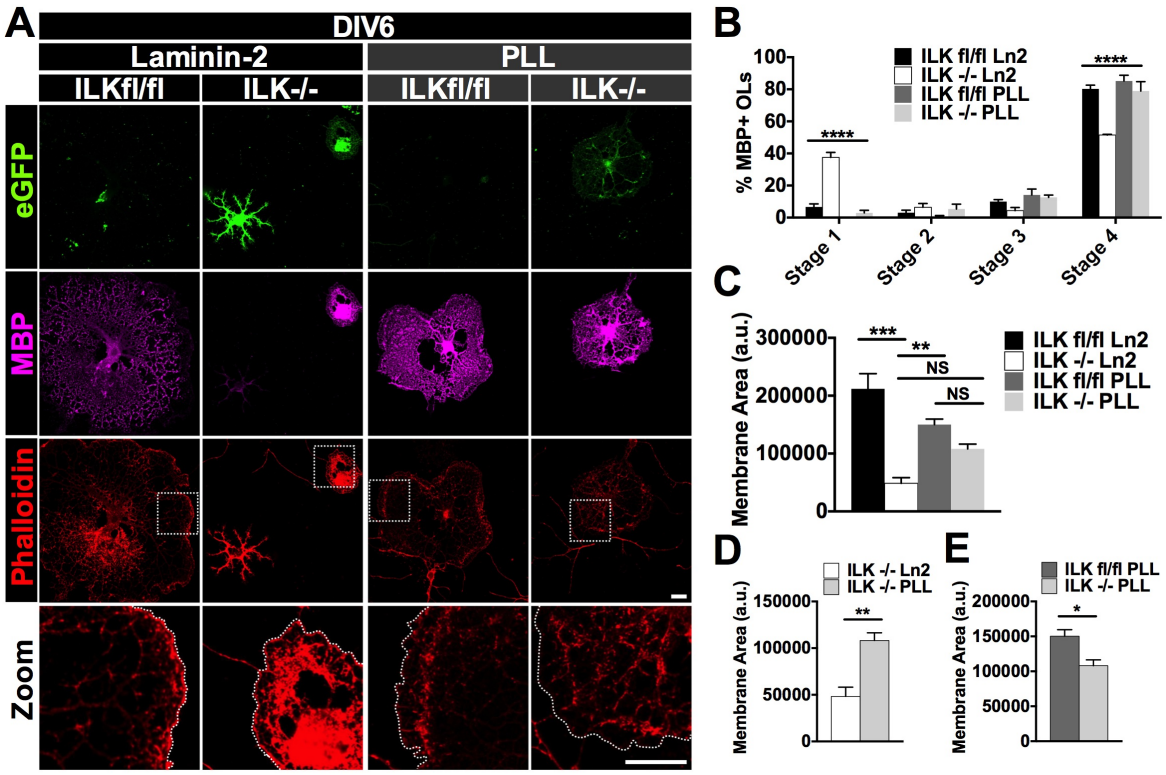

Figure 4.7. Effect of ILK loss on myelin membrane production partially rescued by neutral substrate. A. Immunostaining of TAT-Cre treated OLs at DIV6 for phalloidin (red) and MBP (purple). EGFP, denoting recombination and *Ilk*$^{-/-}$ OLs, is in green. Zoomed in images are shown in the bottom row. White dotted line denotes membrane edge. Note F-actin at leading edge in Ln-2 WT but behind in all others. **B.** Quantification of percent MBP^{+} OLs binned by stage. **C.** Quantification of MBP^{+} membrane area between all groups. **D.** Quantification of MBP^{+} membrane area between *Ilk*$^{-/-}$ on Ln-2 or PLL. **E.** Quantification of MBP^{+} membrane area between PLL WT and PLL *Ilk*$^{-/-}$. Data represent the mean ±SEM (n=3). NS = not significant, *$p < 0.05$, **$p < 0.01$, *** $p < 0.001$, ****$p < 0.0001$ (B; two-way ANOVA test – C; one-way ANOVA test – D,E; Student's *t* test). Scale bar: 20 μm.

We noted thick blunt microtubules in Ln-2 *Ilk*$^{-/-}$ MBP^{+} OLs. These structures terminated well behind the membrane edge (Figure 4.8A arrowhead). On PLL, *Ilk*$^{-/-}$ OLs still contained a relatively dense microtubule network (Figure 4.8A), most likely a throwback to the density observed at DIV3 (see Figure 4.3A and 4.5A). In both PLL WT and PLL *Ilk*$^{-/-}$ OLs, microtubules would sit well behind areas of membrane protrusion (Figure 4.8A arrowhead). When quantified, all OLs had increased propensity for this select phenotype relative to Ln-2 WT (Figure 4.8B). Coupled with the observed F-actin accumulation (see Figure 4.7A) it would suggest a decoupling of the cytoskeleton from the myelin's leading edge following integrin abrogation, either through substrate presented or ILK loss.

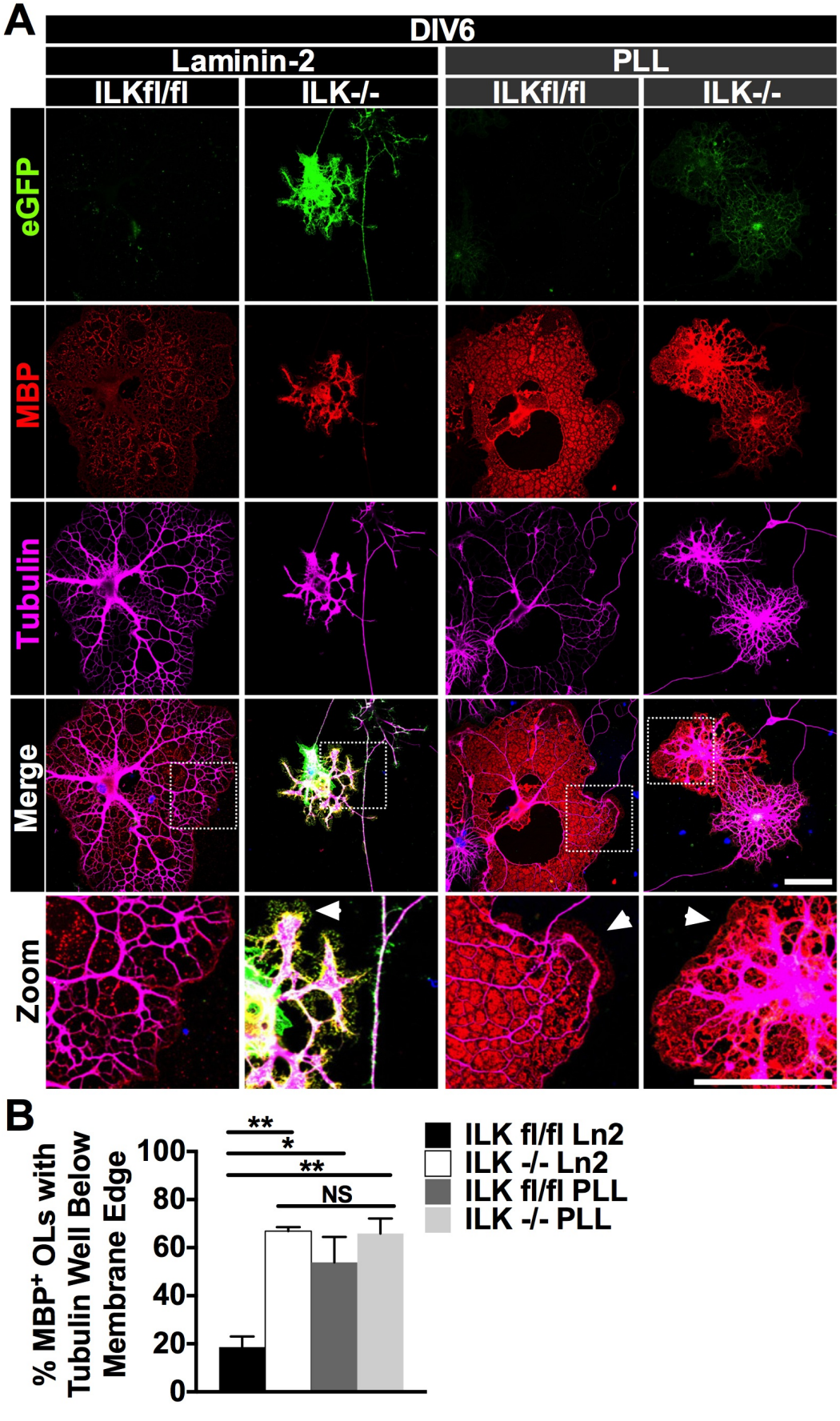
A
DIV6
Laminin-2
PLL
ILKfl/fl
ILK-/-
ILKfl/fl
ILK-/-
eGFP
MBP
Tubulin
Merge
Zoom
B
% MBP+ OLs with Tubulin Well Below Membrane Edge
100
80
60
40
20
0
**
*
**
NS
ILK fl/fl Ln2
ILK -/- Ln2
ILK fl/fl PLL
ILK -/- PLL

Figure 4.8. Abnormal microtubule localization in ILK-depleted OLs at DIV6. A. Immunostaining of TAT-Cre treated OLs at DIV6 for MBP (red) and tubulin (purple). EGFP denotes recombination and *Ilk*$^{-/-}$ OLs. Zoomed in images are shown in the bottom row. Arrowhead denotes microtubules well behind the membrane. **B.** Quantification of percent MBP^{+} OLs with tubulin staining well behind the leading edge. Data represent the mean ±SEM (n=3). NS = not significant, *$p < 0.05$, **$p < 0.01$, (one-way ANOVA test). Scale bar: 50 μm.

Discussion

When we consider the role played by members of the integrin signaling pathway, from the receptor to downstream effectors such as ILK or focal adhesion kinase (FAK), a common thread appears – phenotypic recovery *in vivo* (Câmara et al., 2009; Forrest et al., 2009; O'Meara et al., 2013). This is in clear juxtaposition to our findings *in vitro*, where ILK loss leads to severe defects in almost all aspects of OL development (O'Meara et al., 2013). How can we reconcile this disparity? A major difference from *in vitro* to *in vivo* is matrix complexity – by presenting only Ln-2 *in vitro*, we force reliance on a single substrate for adhesion/force generation and pathway activation. We therefore introduced a neutral substrate (PLL), allowing adhesion to occur in a non-Ln-2 manner. *Ilk*$^{-/-}$ OLs on PLL kept pace with WT counterparts in ability to both generate complex morphology and transition to myelin producing cells. Although not directly corollary to an *in vivo* scenario, that ILK-depleted OLs on PLL outdo those on Ln-2 demonstrates the effect substrate shift has on phenotypic severity.

ILK in oligodendrocyte adhesion and actin dynamics

Normally, when integrin-specific substrates are present, ILK binds the underlying cytoskeleton through actin binding partners, such as α-parvin (as an obligate partner, it is reduced following ILK loss, see Figure S4.1) (Legate et al., 2006; Ghatak et al., 2013). Integrins, in turn, link the F-actin/ILK complex to the external matrix, allowing internal force transmission from cell to bound surface, a process driving multiple aspects of cell behavior, such as migration and morphogenesis (Ghatak et al., 2013). Phenotypic differences between MAG^{+} *Ilk*$^{-/-}$ OLs on Ln-2 and PLL are, therefore, likely a result of

decreased adhesion, an issue PLL avoids as it functions through membrane charge differential (Machesky and Hall, 1997).

Previously, we described an increase in active GTP bound RhoA following ILK loss in primary OLs cultured on Ln-2 (O'Meara et al., 2013). At the time, ROCK inhibition (a RhoA downstream effector), failed to rescue either morphological or myelin production defects in mature cells (although increased sprouting was observed in a subpopulation of immature *Ilk*$^{-/-}$ OLs). A requirement for ILK in Ln-2-mediated cell adhesion would explain ROCK inhibition failure. Even if the observed F-actin disorganization (see Figure 4.1A) was RhoA dependent, if the link between F-actin and extracellular matrix was severed, relieving excess contractile elements generated through RhoA would be insufficient to overcome adhesion loss. *In vivo*, one can imagine compensation through activation of similar adhesion complex members such as Fyn and/or FAK or other Ln-2 binding receptors, such as dystroglycan (Colognato et al., 2007; Forrest et al., 2009; Eyermann et al., 2012).

Oligodendrocytes and growth cones

There remain however striking differences between *Ilk*$^{-/-}$ and WT OLs on PLL. We were most surprised by the bulging "tips" observed in ILK-depleted cells. Staining for cytoskeletal components revealed architecture similar to a neuronal growth cone's. It made us stop and reevaluate, searching for a similar structure in WT OLs. While we did not find quite the same level of detail (the largest *Ilk*$^{-/-}$ cones provided unrivalled resolution), we did find similar organizational patterns. That OLs possess neuron-like growth cones is not a new idea (Fox et al., 2006). In support of our work, other laboratories have demonstrated long F-actin bundles, which penetrate from the peripheral

region centrally (a unique feature of growth cones), and shrinking cones in the maturing OL (Fox et al., 2006). OL growth cones have also been shown capable of turning in response to repulsive extracellular cues (Fox et al., 2006). We now provide evidence that suggests OL cytoskeletal architecture can be further subdivided into classic neuronal growth cone regions – a P, C and T domain with pioneering microtubules that extend peripherally. We do not suggest the two (neuron and oligodendrocyte) are identical, as growth cone governance can vary widely even among neuronal subtypes. Rather, that we acknowledge its existence, and allow insight, where appropriate, from one to the other. Such insight could prove critical when making mechanistic determinations, especially when cytoskeletal regulators are involved.

ILK in oligodendrocyte growth cone maturation and cytoskeletal organization

The most striking feature following ILK ablation on PLL was the enormous growth cones formed. We and others have shown these structures to shrink as the cell matures (Fox et al., 2006). It would appear, even as the *Ilk*$^{-/-}$ OL undergoes differentiation (through increased complexity and expression of myelin markers), the growth cone remains in a primordial state. Unfortunately, as there is little data regarding enlarged OL growth cones (or process tip/end), we looked to neurons instead for mechanistic insight.

Neuronal growth cone morphogenesis is the end result of coordinated cytoskeletal reorganization. There is evidence for the Ln-2/integrin pathway, and therefore ILK as transducer, in pushing neuronal growth towards a "mature" state, through growth cone contraction and increased outward movement, an event characterized by microtubule bundling to fit the smaller architecture (Tang and Goldberg, 2000). Rather than bundling, PLL *Ilk*$^{-/-}$ OLs are characterized by looping microtubules and dense F-actin arcs within the

cone (see Figure 4.3A). *Ilk*$^{-/-}$ growth cones also appear sluggish when viewed live (see Figure 4.4). In neurons, microtubule deregulation seems a common culprit for irregular growth cone expansion (Lucas et al., 1998; Goold et al., 1999; Purro et al., 2008; Marcos et al., 2009). Microtubule "looping", disequilibrium in microtubule dynamics (stable versus unstable), and growth cone stalling often accompany the increased size. ILK is known to have a role in microtubule stability through binding and localization of the adaptor protein IQGAP1 (Wickström et al., 2010a). IQGAP1, along with mDia1, anchors microtubules at the cell cortex (Wickström et al., 2010a). With ILK lost, IQGAP1 re-localizes, leaving behind peripheral F-actin networks and precipitating microtubule withdrawal. As microtubules retreat, a shift in global equilibrium, from stable (acetylated) to unstable (deacetylated) microtubules, occurs. In OLs, tubulin acetylation status correlates with OL maturity - deacetylation results in delayed differentiation (Li et al., 2007). We can speculate a similar fluctuation in microtubule stability for *Ilk*$^{-/-}$ OLs. If we view microtubules as taut cables anchored by ILK complexes at F-actin heavy sites, if and when the connection is broken the cable springs back, 'looping' centripetally. The result is a sluggish growth cone and loss of process outgrowth (which we see).

Another possibility is inability of the OL to decouple microtubules from actin flow. IQGAP1 interacts with APC, a microtubule plus-end-binding protein whose neuronal accumulation is ILK-dependent (Watanabe et al., 2004; Zhou et al., 2004). APC knockdown results in looped microtubules and increased stalling and size of neuronal growth cones (Purro et al., 2008). As APC is required for microtubule/F-actin disengagement, the following mechanism was purported – microtubules, unable to disengage from rear flowing F-actin, are dragged (looped) back into the neuron's C domain (Lowery and Van Vactor, 2009). The described mechanism fits the dense F-actin

arcs seen just above, or coinciding with microtubule loops following ILK loss on PLL. They may represent F-actin backflow (perhaps increased) from the peripheral region awaiting turnover. Further, while growth cones were not analyzed, APC deficient OLs, similar to *Ilk*$^{-/-}$ OLs, have decreased process length (Lang et al., 2013). How either, stability or failure to uncouple leads to growth cone swelling in OLs remains to be seen, although we can assume looping microtubules fill a much larger volume than bundled.

When comparing microtubules from *Ilk*$^{-/-}$ OLs on Ln-2 to PLL, commonalities exist. While we believe ILK plays a role in actin/microtubule anchoring independent of Ln-2 engagement, *Ilk*$^{-/-}$ OLs on Ln-2 do show microtubule accumulation, though not to the same extent as seen on PLL. This may be due to loss of adhesion partially masking other underlying issues on Ln-2. Further, at DIV6, Ln2 *Ilk*$^{-/-}$ OLs share oddities in their cytoskeletal character with both WT and *Ilk*$^{-/-}$ OLs on PLL, in particular, F-actin and microtubule membrane dissociation (see Figure 4.7A, 4.8A for examples). All told, our work demonstrates roles for ILK in regulating Ln-2 mediated adhesion and Ln-2-independent growth cone size/activity in OLs. It suggests a model whereby compensation, to a degree, allows *Ilk*$^{-/-}$ OLs to play catch-up, giving rise to a transient phenotype *in vivo*. We also provide further evidence demonstrating shared cytoskeletal architecture between neuronal and OL growth cones, strongly suggesting one can inform the other.

Acknowledgments

We declare no competing financial interests. This work was supported by a grant from the Multiple Sclerosis Society of Canada. John-Paul Michalski and Ryan W. O'Meara are both recipients of the Frederick Banting and Charles Best Canadian Institutes of Health Research Doctoral Award. Rashmi Kothary is a recipient of a University of Ottawa University Health Research Chair. We thank the rest of the Kothary laboratory for helpful discussion. We also thank Dr. René St-Arnaud and Dr. Steffany Bennett for donating transgenic mice.

Supporting Information

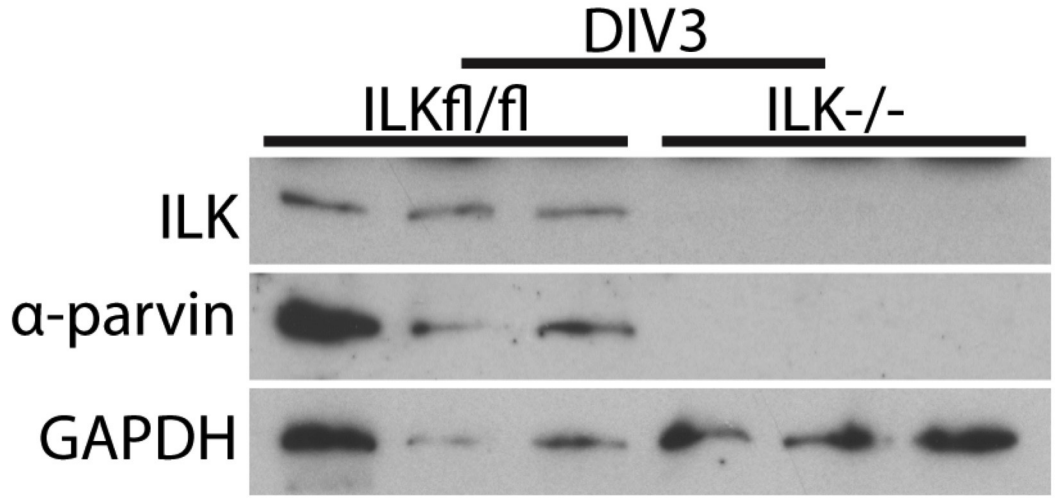

Figure S4.1. ILK and α-parvin depletion following TAT-Cre administration. Western blot of TAT-Cre and vehicle treated primary OLs at DIV3. The membrane was probed for ILK, α-parvin and GAPDH as loading control.

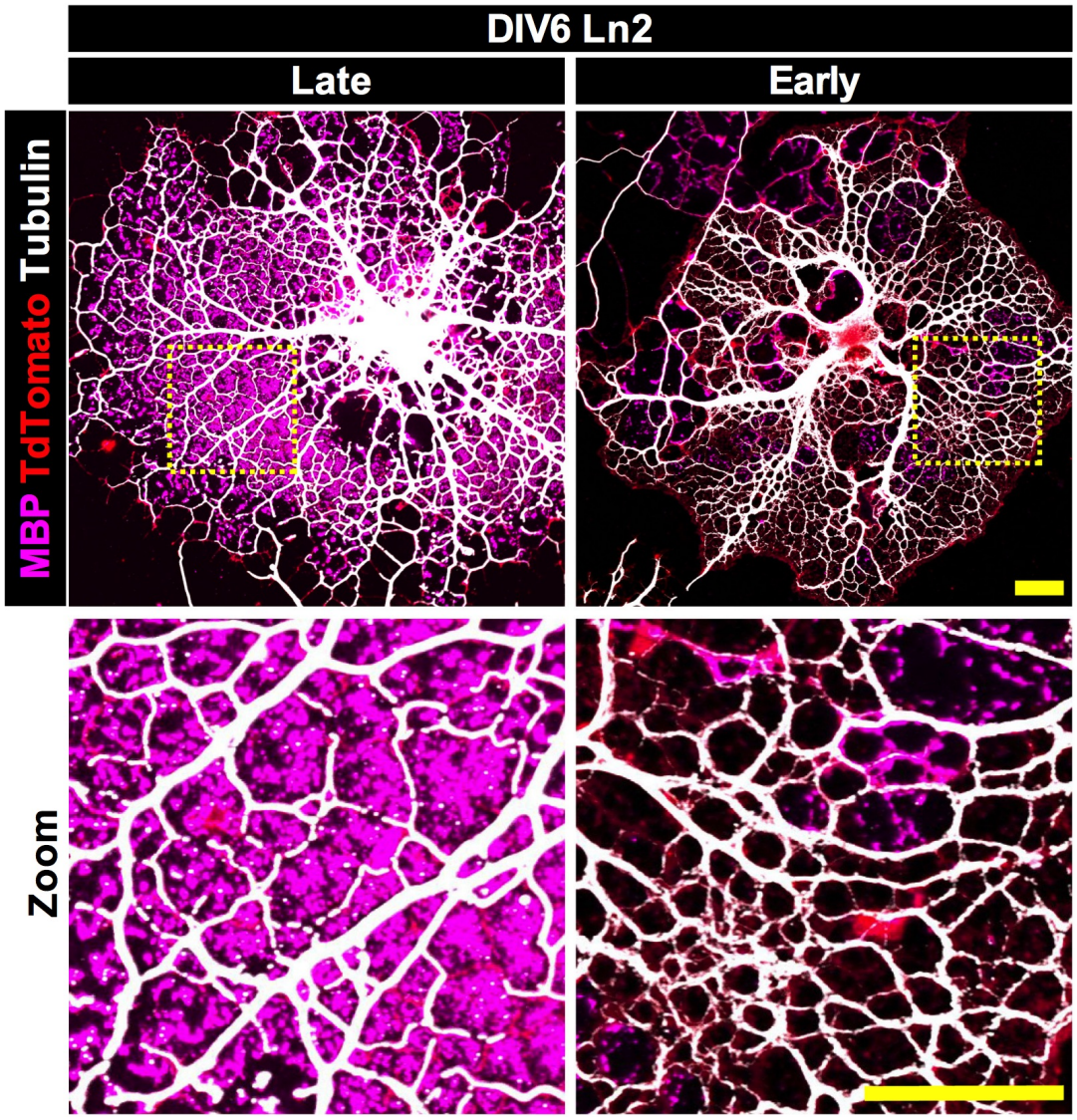

Figure S4.2. Tubulin in the oligodendrocyte membrane. Immunostaining of Ln-2 WT OLs at DIV6 for tubulin (white) and MBP (purple). tdTomato is in red. Note the difference in tubulin density between early and late OL maturity. Scale bar: 20 μm.

Chapter 5
General Discussion

The Plp promoter as tool for oligendrocyte study

The use of lineage-restricted promoters is an incredibly powerful tool in targeted transgenic study, allowing manipulation of select cell-types *in vivo*. For knockouts (in our case, Cre-loxP mediated), a lineage specific promoter mitigates off target effects (gene recombination outside the desired cell-type), effects that would be present if a system wide approach were taken. When the ILK project first began, we generated a line of *Plp* promoter driven mice to maximize ILK excision in the OL lineage. However, when crossed to a floxed *Ilk* line, the eventual homozygotes never came to term. This led to the generation of numerous reporter lines in an attempt to better understand the promoter.

In Chapter 2, we demonstrated clear promiscuity of the *Plp* promoter early in development. We were struck by the extent – a seemingly unrestricted profile across multiple CNS tissues (see Figure 2.8, Chapter 2). We concluded the promoter, if used as an OL-specific driver, should have restrictions in place to limit its activity to postnatal stages, as OL selectivity increased with age. Its use in Cre-loxP knockouts (or any system where *Plp* drives an irreversible change) therefore demands a form of temporal control, an on/off switch (in our case, tamoxifen inducible). We do not, however, suggest the *Plp* promoter, without temporal control, be avoided all together. Rather, that care is taken when deciding whether the promoter is suited to the experimental question being asked.

For example, a *Plp* driven reporter is extremely useful when high quality resolution of cellular processes and myelin internodes is required. Also, due to the reporters transient nature (versus our own floxed reporter, where fluorophore signal cannot be turned off), researchers can track the ebb and flow of *Plp* activity through time.

This point is highlighted by a recent paper from Wendy Macklin's laboratory (Harlow et al., 2014). Here, the authors employ a *Plp-EGFP* line to chart *Plp* promoter activity in the murine spinal cord (SC). During early development (E12.5), the promoter drove EGFP expression across multiple cell-lineages within the ventricular (VZ) and subventricular zones (SVZ) of the SC's central canal. These included multipotent progenitors, as well as neuronal and glial precursors, findings in line with our own work describing early unrestricted *Plp* promoter patterning. EGFP positive cells migrated laterally as the animal aged, and, again, similar to our own work, the promoter's activity was progressively OL restricted in the maturing animal. Intriguingly, *Plp*'s activity in the OL-lineage was wave-like; extremely active in the most primordial OPCs (located in the VZ/SVZ), and then rapidly downregulated as the same OPCs migrated toward future white matter tracts, followed again by upregulation at time of myelination. The authors posit the findings as possible explanation for previous reports describing two distinct OPC populations *in vivo*; one with *Plp* promoter activity, and one without (Spassky et al., 1998, 2000; Harlow et al., 2014). They suggest, rather, a single population with early promoter activity – the split populations an illusion created through progressive promoter diminishment concomitant with migration. Perhaps, in the future, researchers will craft a *Plp* promoter tailored to the OL-lineage, but until such a time, those focused on OL research should be aware of the promoter's breadth of activity during embryonic development.

ILK regulates oligodendrocyte morphological maturity and myelination

The CNS places a high demand on the OL; it must branch to contact tens of axons, then produce hundreds of times its own volume in myelin membrane. The process, from first sheath to last, is accomplished in just a few short hours (~5 hours in the zebrafish) (Czopka et al., 2013). However, the precise molecular underpinnings governing process outgrowth and transition to myelin membrane remain elusive. One candidate – integrin signaling – has come under intense scrutiny as it links the OL and ECM, a necessary step in fine tuning the response between OL and environment (Buttery and Ffrench-Constant, 1999; Lee et al., 2006; Câmara et al., 2009; Laursen et al., 2009; O'Meara et al., 2011a; Baron et al., 2014). We set out to study where and how the adaptor and cytoskeletal-linker protein ILK, bound to β1 integrin's cytoplasmic tail, regulated CNS myelination, both through, and independent of, active integrin signaling.

Our studies *in vitro*, showcase ILK's role in governing morphological differentiation and myelination capacity of the OL, although absolute necessity differs with substrate presented and OL maturity. First, ILK is required for proper adhesion through the Ln-2 substrate, as many of the observed defects following ILK loss (such as stunted process outgrowth, branching, and membrane formation) were mitigated when OLs were grown on an inert adhesion guaranteeing substrate (PLL). ILK-depleted OLs were also characterized by general F-actin disorganization/accumulation, which, again, was more pronounced on Ln-2. With this in mind, we suggest ILK loss severs the link between ECM and F-actin network, limiting the OLs ability to undergo morphogenesis and grow. Further, ILK appears to have a role in microtubule organization and localization (both in the growth cone and myelin membrane), a cytoskeletal component we know is critical to process outgrowth and myelin membrane formation (Lee et al.,

2005; Bauer et al., 2009). Coupled with no change in phosphorylation status of either AKT and/or GSK3β, canonical downstream effectors (McDonald et al., 2008), we strongly suspect phenotypic outcome in ILK-depleted OLs is predominantly a result of cytoskeletal dysfunction leading to gross morphological deficits.

Interestingly, as we move from simple cell culture to mouse model, there appears to be a correlative mitigation in defect severity. As discussed, ILK-depleted OLs cultured on a single substrate, Ln-2, are grossly abnormal. By eliminating the OLs need for Ln-2 signaling (through introduction of an inert PLL substrate) we demonstrate clear phenotypic amelioration, though not complete recovery. In DRGN co-cultures, phenotypic manifestation is delayed, and finally, *in vivo*, the phenotype – amyelination of small caliber axons – is transient, with full recovery in the aged animal. Why the discrepancy? Why do we not observe a more severe phenotype *in vivo*? Moving from isolated cultures, wherein a single substrate is provided, to DRGN co-cultures and finally, a living organism, we exponentially increase environmental complexity; a plethora of integrin binding ECM substrates (for example, vitronectin, fibronectin, and collagen) as well as many other extracellular signaling cues, are now made available, augmenting the probability for compensatory pathway activation (O'meara et al., 2011a). Furthermore, the very nature of integrin-based signaling differs for cells in 2 or 3 dimensions, with complex formation or protein activation often unique to the given dimensionality (DeMali et al., 2003). It also suggests the OL, similar to its ability to adapt and accommodate increased axon number (to a point), can also conform to a shift (or loss) in environmental cues (Burne et al., 1996; Almeida et al., 2011; Chong et al., 2012). This fits the picture of Ln-2, and the pathway it activates, as myelination enhancers. We know

the OL will myelinate in Ln-2's absence, as seen when cultured on PLL, or, for example, when introduced to inert nanofibers (Lee et al., 2012a). Rather, Ln-2 ensures maximal myelin potential, pushing the OL's boundaries for extension and sheath formation, a critical process given the temporal restrictions placed on the OLs myelinating window (Czopka et al., 2013). Therefore, by disrupting the Ln-2/β1 integrin/ILK pathway, we render the system inefficient. It suggests a model with no single master switch (none have been found for OLs), but rather a multitude of smaller overlapping and cumulative signals, which, together, sculpt myelin in the CNS.

But what of the phenotype that does arise *in vivo* – transient amyelination of small fibers. In Chapter 3, we proposed two primary defects as phenotypically responsible: (1) an inability of the OL to extend a sufficient number of processes and (2) a failure to initiate myelin membrane formation upon axonal contact. These two appeared specific for the Ln-2/ILK pathway, as ILK-depleted OLs grown on PLL had a complex morphology and formed myelin membrane in culture. However, the same studies also demonstrated defects in ILK-depleted OLs independent of Ln-2 signaling: decreased process length and outgrowth as well as sluggish and bloated OL growth cones. Together, the data paint ILK-depleted OLs as lethargic, limited in their ability to sample the environment and extend processes to distant axons, followed by an inability to initiate myelination in response to surface ligand (Figure 5.1). We know sheath generation occurs in a limited time window, and once finished, *de novo* myelination by the same OL is rare (Czopka et al., 2013). So rather than ILK-depleted OLs beginning to myelinate and then stalling, we suggest the OLs first stall (again, decreased process growth, branching, milieu sampling and failing to initiate a wrapping response), before they are able to kick

start sheath formation, possibly through a compensatory and/or adaptive response. Such a scenario would shift the whole course of myelination backwards as OLs take longer to initiate myelinogenesis and commit to the myelination process. Evidence suggests large diameter axons are myelinated prior to smaller (Almeida et al., 2011; Lee et al., 2012a; Simons and Lyons, 2013). As we are only afforded a glance at a specific temporal window with fixed tissue (in our case, P14) we may be seeing the delayed ILK-depleted OLs as they finish myelinating the largest axons while, in the WT, OLs have already moved onto smaller fibers. If we were to examine earlier time points, we may well observe amyelination of larger axons in the ILK-depleted animals. While the hypothesis presented here differs from that first presented in Chapter 3 – loss in process number and inability to overcome ligand thresholds as cause for amyelination of small diameter axons (see Chapter 3, Discussion) – the two are not mutually exclusive. Hopefully, with the help of *in vivo* live imaging, we will soon have a full and complete picture as to how the system adapts in a living organism.

Our work also suggests possible differences in lateral (lateral edges) versus radial (inner tongue) membrane expansion (see Figures 1.2 and 1.3 in the Introduction), as myelin internodes generated by ILK-depleted OLs are shorter than WT, but myelin thickness is unchanged. As β1 integrin mutants do not share a similar loss in internode length (Câmara et al., 2009), the defect may be Ln-2 and/or β1 integrin independent. In support, ILK-depleted OLs fail to extend the same volume of membrane relative to WT on PLL. Perhaps tongue and lateral edge (future paranode) growth is regulated by distinct cytoskeletal complexes, as has previously been shown for the small Rho GTPases Cdc42 and Rac1 (loss of either results in inner tongue swelling, while paranodes appear normal)

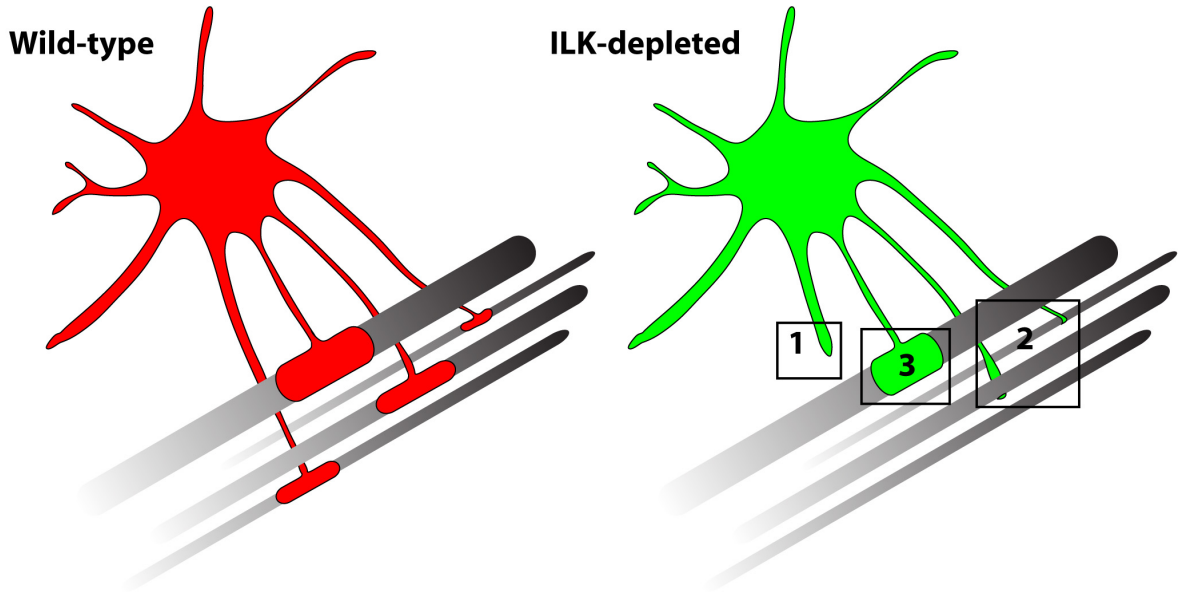

Figure 5.1. ILK-depleted OLs suffer multiple morphological defects. A simplified schematic depicting wild-type (WT) OLs on the left and ILK-depleted on the right. ILK-depleted OLs are lethargic: [1] they fail to extend processes or the process is sluggish in finding appropriate axonal targets and [2] they do not trigger a myelinating event even if contact is made. Once myelination is finally triggered, internodes formed are also [3] shorter than WT. As discussed in the main text, the ILK-depleted OL is not stalled during active myelination, but rather, stalled before. Therefore, boxes [1] and [2] represent ILK-depleted OLs prior to triggering myelination, and [3] the internodes once sheath generation begins.

(Thurnherr et al., 2006). As such, future studies should focus on possible defects in either uncompacted compartment following ILK loss, the study of which could provide valuable insight into shared and unique aspects of the underlying cytoskeleton.

Finally, as noted above, when cultured on PLL, the tips of ILK deficient OLs were characterized by extremely bloated lamella. When stained for F-actin and tubulin, cytoskeletal architecture highly reminiscent of a neuronal growth cone's emerged. These results not only suggest a role for ILK, independent of Ln-2, in maintaining OL growth cone dynamics, but also reinforce the idea of OLs as growth cone bearing. As we have stated many times throughout, while not a novel concept, these structures have received little attention as growth cones per se, and are usually referred to simply in passing. Our hope, by furthering the connection between OL and neuron, is to drive interest in the structure, as it is responsible for guiding OL processes in search of bare axons, contacting the axon, and initiating myelination. We know, for example, upon axonal contact, the growth cone flattens and becomes triangular in shape, but we have little knowledge as to the mechanisms involved or how this structure communicates with the axon (or even if it does) (Snaidero et al., 2014). Some have begun to liken the interaction between OL growth cone and axon to the formation of synapses between axons and dendrites, suggesting many of the molecular mechanisms necessary for the initiation of neuronal junctions may be at play in the initial contact (Almeida and Lyons, 2013). These are new and radical ideas for OL biology, and, as we move forward, we must begin to piece together how they are regulated, in part by making a real push for a better understanding of the OL's growth cone.

Concluding remarks

The body of work presented herein demonstrates ILK as important for OL mediated myelination of the CNS. In response to Ln-2 signaling, ILK governs multiple aspects of OL development, including, but not limited to, adhesion, morphological maturation and myelin membrane production. Independently, ILK also regulates process outgrowth and growth cone dynamics. In vivo, the two regulatory modes give rise to an amyelination phenotype, with recovery in the aged animal. ILK's necessity in the spectrum of OL maturation clearly depends on matrix complexity, showcasing the OLs inherent ability to adapt and compensate. And yet questions remain. How does ILK regulate growth cone size and dynamics? Or, importantly, how, precisely, do OLs overcome ILK loss *in vivo*. As a similar adaptive response is often lacking when OLs stall in a diseased brain, parsing apart compensatory mechanisms involving ECM/OL interactions could provide insight when designing future therapeutic strategies.

This is an exciting time for OL biology. New models, techniques, and modes of imaging allow unprecedented access to the cells inner workings. We have come so far in such a short period of time and the future looks bright and promising.

References

Aggarwal S, Snaidero N, Pähler G, Frey S, Sánchez P, Zweckstetter M, Janshoff A, Schneider A, Weil M-T, Schaap IAT, Görlich D, Simons M (2013) Myelin membrane assembly is driven by a phase transition of myelin basic proteins into a cohesive protein meshwork. PLoS Biol 11:e1001577.

Aggarwal S, Yurlova L, Snaidero N, Reetz C, Frey S, Zimmermann J, Pähler G, Janshoff A, Friedrichs J, Müller DJ, Goebel C, Simons M (2011) A size barrier limits protein diffusion at the cell surface to generate lipid-rich myelin-membrane sheets. Dev Cell 21:445–456.

Akhtar N, Streuli CH (2013) An integrin-ILK-microtubule network orients cell polarity and lumen formation in glandular epithelium. Nat Cell Biol 15:17–27.

Almeida RG, Czopka T, Ffrench-Constant C, Lyons DA (2011) Individual axons regulate the myelinating potential of single oligodendrocytes in vivo. Development 138:4443–4450.

Almeida RG, Lyons DA (2013) On the resemblance of synapse formation and CNS myelination. Neuroscience.

Attwell S, Mills J, Troussard A, Wu C, Dedhar S (2003) Integration of cell attachment, cytoskeletal localization, and signaling by integrin-linked kinase (ILK), CH-ILKBP, and the tumor suppressor PTEN. Mol Biol Cell 14:4813–4825.

Bacon C, Lakics V, Machesky L, Rumsby M (2007) N-WASP regulates extension of filopodia and processes by oligodendrocyte progenitors, oligodendrocytes, and Schwann cells-implications for axon ensheathment at myelination. Glia 55:844–858.

Bakhti M, Aggarwal S, Simons M (2014) Myelin architecture: zippering membranes tightly together. Cell Mol Life Sci 71:1265–1277.

Baron W, Bijlard M, Nomden A, de Jonge JC, Teunissen CE, Hoekstra D (2014) Sulfatide-mediated control of extracellular matrix-dependent oligodendrocyte maturation. Glia 62:927–942.

Barres BA, Hart IK, Coles HS, Burne JF, Voyvodic JT, Richardson WD, Raff MC (1992) Cell death and control of cell survival in the oligodendrocyte lineage. Cell 70:31–46.

Barres BA, Raff MC (1999) Axonal control of oligodendrocyte development. J Cell Biol 147:1123–1128.

Barros CS, Nguyen T, Spencer KSR, Nishiyama A, Colognato H, Müller U (2009) Beta1 integrins are required for normal CNS myelination and promote AKT-dependent myelin outgrowth. Development 136:2717–2724.

Bauer NG, Ffrench-Constant C (2009) Physical forces in myelination and repair: a question of balance? J Biol 8:78.

Bauer NG, Richter-Landsberg C, Ffrench-Constant C (2009) Role of the oligodendroglial cytoskeleton in differentiation and myelination. Glia 57:1691–1705.

Baumann N, Pham-Dinh D (2001) Biology of oligodendrocyte and myelin in the mammalian central nervous system. Physiol Rev 81:871–927.

Benninger Y, Colognato H, Thurnherr T, Franklin RJM, Leone DP, Atanasoski S, Nave K-A, Ffrench-Constant C, Suter U, Relvas JB (2006) Beta1-integrin signaling mediates premyelinating oligodendrocyte survival but is not required for CNS myelination and remyelination. J Neurosci 26:7665–7673.

Blakemore WF, Murray JA (1981) Quantitative examination of internodal length of remyelinated nerve fibres in the central nervous system. J Neurol Sci 49:273–284.

Boggs JM, Wang H (2001) Effect of liposomes containing cerebroside and cerebroside sulfate on cytoskeleton of cultured oligodendrocytes. J Neurosci Res 66:242–253.

Boggs JM, Wang H (2004) Co-clustering of galactosylceramide and membrane proteins in oligodendrocyte membranes on interaction with polyvalent carbohydrate and prevention by an intact cytoskeleton. J Neurosci Res 76:342–355.

Bongarzone ER, Campagnoni CW, Kampf K, Jacobs EC, Handley VW, Schonmann V, Campagnoni AT (1999) Identification of a new exon in the myelin proteolipid protein gene encoding novel protein isoforms that are restricted to the somata of oligodendrocytes and neurons. J Neurosci 19:8349–8357.

Boulter E, Grall D, Cagnol S, Van Obberghen-Schilling E (2006) Regulation of cell-matrix adhesion dynamics and Rac-1 by integrin linked kinase. FASEB J 20:1489–1491.

Brakebusch C, Fässler R (2003) The integrin-actin connection, an eternal love affair. Eur Mol Biol Organ J 22:2324–2333.

Brinkmann BG, Agarwal A, Sereda MW, Garratt AN, Müller T, Wende H, Stassart RM, Nawaz S, Humml C, Velanac V, Radyushkin K, Goebbels S, Fischer TM, Franklin RJ, Lai C, Ehrenreich H, Birchmeier C, Schwab MH, Nave KA (2008) Neuregulin-1/ErbB signaling serves distinct functions in myelination of the peripheral and central nervous system. Neuron 59:581–595.

Bunge RP (1968) Glial cells and the central myelin sheath. Physiol Rev 48:197–251.

Burne JF, Staple JK, Raff MC (1996) Glial cells are increased proportionally in transgenic optic nerves with increased numbers of axons. J Neurosci 16:2064–2073.

Burnette DT, Ji L, Schaefer AW, Medeiros NA, Danuser G, Forscher P (2008) Myosin II activity facilitates microtubule bundling in the neuronal growth cone neck. Dev Cell 15:163–169.

Butt AM, Berry M (2000) Oligodendrocytes and the control of myelination in vivo: new insights from the rat anterior medullary velum. J Neurosci Res 59:477–488.

Buttery PC, Ffrench-Constant C (1999) Laminin-2/integrin interactions enhance myelin membrane formation by oligodendrocytes. Mol Cell Neurosci 14:199–212.

Cai J, Qi Y, Hu X, Tan M, Liu Z, Zhang J, Li Q, Sander M, Qiu M (2005) Generation of oligodendrocyte precursor cells from mouse dorsal spinal cord independent of Nkx6 regulation and Shh signaling. Neuron 45:41–53.

Câmara J, Wang Z, Nunes-Fonseca C, Friedman HC, Grove M, Sherman DL, Komiyama NH, Grant SG, Brophy PJ, Peterson A, ffrench-Constant C (2009) Integrin-mediated axoglial interactions initiate myelination in the central nervous system. J Cell Biol 185:699–712.

Campagnoni CW, Garbay B, Micevych P, Pribyl T, Kampf K, Handley VW, Campagnoni AT (1992) DM20 mRNA splice product of the myelin proteolipid protein gene is expressed in the murine heart. J Neurosci Res 33:148–155.

Chang A, Tourtellotte WW, Rudick R, Trapp BD (2002) Premyelinating oligodendrocytes in chronic lesions of multiple sclerosis. N Engl J Med 346:165–173.

Charles P, Hernandez MP, Stankoff B, Aigrot MS, Colin C, Rougon G, Zalc B, Lubetzki C (2000) Negative regulation of central nervous system myelination by polysialylated-neural cell adhesion molecule. Proc Natl Acad Sci U S A 97:7585–7590.

Chong SYC, Rosenberg SS, Fancy SPJ, Zhao C, Shen Y-AA, Hahn AT, McGee AW, Xu X, Zheng B, Zhang LI, Rowitch DH, Franklin RJM, Lu QR, Chan JR (2012) Neurite outgrowth inhibitor Nogo-A establishes spatial segregation and extent of oligodendrocyte myelination. Proc Natl Acad Sci U S A 109:1299–1304.

Chun SJ, Rasband MN, Sidman RL, Habib AA, Vartanian T (2003) Integrin-linked kinase is required for laminin-2-induced oligodendrocyte cell spreading and CNS myelination. J Cell Biol 163:397–408.

Colognato H, Baron W, Avellana-Adalid V, Relvas JB, Baron-Van Evercooren A, Georges-Labouesse E, ffrench-Constant C (2002) CNS integrins switch growth factor signalling to promote target-dependent survival. Nat Cell Biol 4:833–841.

Colognato H, Galvin J, Wang Z, Relucio J, Nguyen T, Harrison D, Yurchenco PD, Ffrench-Constant C (2007) Identification of dystroglycan as a second laminin receptor in oligodendrocytes, with a role in myelination. Development 134:1723–1736.

Colognato H, Ramachandrappa S, Olsen IM, ffrench-Constant C (2004) Integrins direct Src family kinases to regulate distinct phases of oligodendrocyte development. J Cell Biol 167:365–375.

Colognato H, Tzvetanova ID (2011) Glia unglued: how signals from the extracellular matrix regulate the development of myelinating glia. Dev Neurobiol 71:924–955.

Czopka T, Ffrench-Constant C, Lyons DA (2013) Individual oligodendrocytes have only a few hours in which to generate new myelin sheaths in vivo. Dev Cell 25:599–609.

Dawson MRL, Polito A, Levine JM, Reynolds R (2003) NG2-expressing glial progenitor cells: an abundant and widespread population of cycling cells in the adult rat CNS. Mol Cell Neurosci 24:476–488.

Delaunay D, Heydon K, Cumano A, Schwab MH, Thomas J-L, Suter U, Nave K-A, Zalc B, Spassky N (2008) Early neuronal and glial fate restriction of embryonic neural stem cells. J Neurosci 28:2551–2562.

Delcommenne M, Tan C, Gray V, Rue L, Woodgett J, Dedhar S (1998) Phosphoinositide-3-OH kinase-dependent regulation of glycogen synthase kinase 3 and protein kinase B/AKT by the integrin-linked kinase. Proc Natl Acad Sci U S A 95:11211–11216.

DeMali KA, Wennerberg K, Burridge K (2003) Integrin signaling to the actin cytoskeleton. Curr Opin Cell Biol 15:572–582.

Dickinson PJ, Fanarraga ML, Griffiths IR, Barrie JM, Kyriakides E, Montague P (1996) Oligodendrocyte progenitors in the embryonic spinal cord express DM-20. Neuropathol Appl Neurobiol 22:188–198.

Dickinson PJ, Griffiths IR, Barrie JM, Kyriakides E, Pollock GF, Barnett SC (1997) Expression of the dm-20 isoform of the plp gene in olfactory nerve ensheathing cells: evidence from developmental studies. J Neurocytol 26:181–189.

Doerflinger NH, Macklin WB, Popko B (2003) Inducible site-specific recombination in myelinating cells. Genesis 35:63–72.

Dyer CA, Benjamins JA (1989a) Organization of oligodendroglial membrane sheets: II. Galactocerebroside:antibody interactions signal changes in cytoskeleton and myelin basic protein. J Neurosci Res 24:212–221.

Dyer CA, Benjamins JA (1989b) Organization of oligodendroglial membrane sheets. I: Association of myelin basic protein and 2',3'-cyclic nucleotide 3'-phosphohydrolase with cytoskeleton. J Neurosci Res 24:201–211.

Eyermann C, Czaplinski K, Colognato H (2012) Dystroglycan promotes filopodial formation and process branching in differentiating oligodendroglia. J Neurochem 120:928–947.

Flores AI, Narayanan SP, Morse EN, Shick HE, Yin X, Kidd G, Avila RL, Kirschner DA, Macklin WB (2008) Constitutively active Akt induces enhanced myelination in the CNS. J Neurosci 28:7174–7183.

Fogarty M, Richardson WD, Kessaris N (2005) A subset of oligodendrocytes generated from radial glia in the dorsal spinal cord. Development 132:1951–1959.

Forrest AD, Beggs HE, Reichardt LF, Dupree JL, Colello RJ, Fuss B (2009) Focal adhesion kinase (FAK): A regulator of CNS myelination. J Neurosci Res 87:3456–3464.

Fox MA, Afshari FS, Alexander JK, Colello RJ, Fuss B (2006) Growth conelike sensorimotor structures are characteristic features of postmigratory, premyelinating oligodendrocytes. Glia 53:563–566.

Franklin RJM, Ffrench-Constant C (2008) Remyelination in the CNS: from biology to therapy. Nat Rev Neurosci 9:839–855.

Fukuda K, Knight JDR, Piszczek G, Kothary R, Qin J (2011) Biochemical, proteomic, structural, and thermodynamic characterizations of integrin-linked kinase (ILK): cross-validation of the pseudokinase. J Biol Chem 286:21886–21895.

Fukuda T, Chen K, Shi X, Wu C (2003) PINCH-1 is an obligate partner of integrin-linked kinase (ILK) functioning in cell shape modulation, motility, and survival. J Biol Chem 278:51324–51333.

Fünfschilling U, Supplie LM, Mahad D, Boretius S, Saab AS, Edgar J, Brinkmann BG, Kassmann CM, Tzvetanova ID, Möbius W, Diaz F, Meijer D, Suter U, Hamprecht B, Sereda MW, Moraes CT, Frahm J, Goebbels S, Nave K-A (2012) Glycolytic oligodendrocytes maintain myelin and long-term axonal integrity. Nature 485:517–521.

Fuss B, Afshari FS, Colello RJ, Macklin WB (2001) Normal CNS myelination in transgenic mice overexpressing MHC class I H-2L(d) in oligodendrocytes. Mol Cell Neurosci 18:221–234.

Fuss B, Mallon B, Phan T, Ohlemeyer C, Kirchhoff F, Nishiyama A, Macklin WB (2000) Purification and analysis of in vivo-differentiated oligodendrocytes expressing the green fluorescent protein. Dev Biol 218:259–274.

Geren BB (1954) The formation from the Schwann cell surface of myelin in the peripheral nerves of chick embryos. Exp Cell Res 7:558–562.

Geren BB, Raskind J (1953) Development of the Fine Structure of the Myelin Sheath in Sciatic Nerves of Chick Embryos. Proc Natl Acad Sci U S A 39:880–884.

Ghatak S, Morgner J, Wickström SA (2013) ILK: a pseudokinase with a unique function in the integrin-actin linkage. Biochem Soc Trans 41:995–1001.

Gibson EM, Purger D, Mount CW, Goldstein AK, Lin GL, Wood LS, Inema I, Miller SE, Bieri G, Zuchero JB, Barres BA, Woo PJ, Vogel H, Monje M (2014) Neuronal activity promotes oligodendrogenesis and adaptive myelination in the mammalian brain. Science 344:1252304.

Goebbels S, Oltrogge JH, Kemper R, Heilmann I, Bormuth I, Wolfer S, Wichert SP, Möbius W, Liu X, Lappe-Siefke C, Rossner MJ, Groszer M, Suter U, Frahm J, Boretius S, Nave K-A (2010) Elevated phosphatidylinositol 3,4,5-trisphosphate in glia triggers cell-autonomous membrane wrapping and myelination. J Neurosci 30:8953–8964.

Goold RG, Owen R, Gordon-Weeks PR (1999) Glycogen synthase kinase 3beta phosphorylation of microtubule-associated protein 1B regulates the stability of microtubules in growth cones. J Cell Sci 112 (Pt 1:3373–3384.

Govek E-E, Newey SE, Van Aelst L (2005) The role of the Rho GTPases in neuronal development. Genes Dev 19:1–49.

Graness A, Giehl K, Goppelt-Struebe M (2006) Differential involvement of the integrin-linked kinase (ILK) in RhoA-dependent rearrangement of F-actin fibers and induction of connective tissue growth factor (CTGF). Cell Signal 18:433–440.

Gravel M, Peterson J, Yong VW, Kottis V, Trapp B, Braun PE (1996) Overexpression of 2',3'-cyclic nucleotide 3'-phosphodiesterase in transgenic mice alters oligodendrocyte development and produces aberrant myelination. Mol Cell Neurosci 7:453–466.

Greenfield EA, Reddy J, Lees A, Dyer CA, Koul O, Nguyen K, Bell S, Kassam N, Hinojoza J, Eaton MJ, Lees MB, Kuchroo VK, Sobel RA (2006) Monoclonal antibodies to distinct regions of human myelin proteolipid protein simultaneously recognize central nervous system myelin and neurons of many vertebrate species. J Neurosci Res 83:415–431.

Guo F, Ma J, McCauley E, Bannerman P, Pleasure D (2009) Early postnatal proteolipid promoter-expressing progenitors produce multilineage cells in vivo. J Neurosci 29:7256–7270.

Haber M, Vautrin S, Fry EJ, Murai KK (2009) Subtype-specific oligodendrocyte dynamics in organotypic culture. Glia 57:1000–1013.

Hanna S, El-Sibai M (2013) Signaling networks of Rho GTPases in cell motility. Cell Signal 25:1955–1961.

Hannigan GE, Leung-Hagesteijn C, Fitz-Gibbon L, Coppolino MG, Radeva G, Filmus J, Bell JC, Dedhar S (1996) Regulation of cell adhesion and anchorage-dependent growth by a new b1-integrin-linked protein kinase. Nature 379:91–96.

Hannigan GE, McDonald PC, Walsh MP, Dedhar S (2011) Integrin-linked kinase: Not so "pseudo" after all. Oncogene 30:4375–4385.

Harlow DE, Saul KE, Culp CM, Vesely EM, Macklin WB (2014) Expression of proteolipid protein gene in spinal cord stem cells and early oligodendrocyte progenitor cells is dispensable for normal cell migration and myelination. J Neurosci 34:1333–1343.

Hoshina N, Tezuka T, Yokoyama K, Kozuka-Hata H, Oyama M, Yamamoto T (2007) Focal adhesion kinase regulates laminin-induced oligodendroglial process outgrowth. Genes Cells 12:1245–1254.

Hughes EG, Kang SH, Fukaya M, Bergles DE (2013) Oligodendrocyte progenitors balance growth with self-repulsion to achieve homeostasis in the adult brain. Nat Neurosci 16:668–676.

Hynes RO (2002) Integrins: bidirectional, allosteric signaling machines. Cell 110:673–687.

Ikenaka K, Kagawa T, Mikoshiba K (1992) Selective expression of DM-20, an alternatively spliced myelin proteolipid protein gene product, in developing nervous system and in nonglial cells. J Neurochem 58:2248–2253.

Jacobs EC, Bongarzone ER, Campagnoni CW, Campagnoni AT (2004) Embryonic expression of the soma-restricted products of the myelin proteolipid gene in motor neurons and muscle. Neurochem Res 29:997–1002.

Jacobs EC, Bongarzone ER, Campagnoni CW, Kampf K, Campagnoni AT (2003) Soma-restricted products of the myelin proteolipid gene are expressed primarily in neurons in the developing mouse nervous system. Dev Neurosci 25:96–104.

Jarjour AA, Kennedy TE (2004) Oligodendrocyte precursors on the move: mechanisms directing migration. Neuroscientist 10:99–105.

Kang SH, Fukaya M, Yang JK, Rothstein JD, Bergles DE (2010) NG2+ CNS glial progenitors remain committed to the oligodendrocyte lineage in postnatal life and following neurodegeneration. Neuron 68:668–681.

Kessaris N, Fogarty M, Iannarelli P, Grist M, Wegner M, Richardson WD (2006) Competing waves of oligodendrocytes in the forebrain and postnatal elimination of an embryonic lineage. Nat Neurosci 9:173–179.

Kilpatrick TJ, Ortuño D, Bucci T, Lai C, Lemke G (2000) Rat oligodendroglia express c-met and focal adhesion kinase, protein tyrosine kinases implicated in regulating epithelial cell motility. Neurosci Lett 279:5–8.

Kim H-J, DiBernardo AB, Sloane JA, Rasband MN, Solomon D, Kosaras B, Kwak SP, Vartanian TK (2006) WAVE1 is required for oligodendrocyte morphogenesis and normal CNS myelination. J Neurosci 26:5849–5859.

Kippert A, Fitzner D, Helenius J, Simons M (2009) Actomyosin contractility controls cell surface area of oligodendrocytes. BMC Cell Biol 10:71.

Kirby BB, Takada N, Latimer AJ, Shin J, Carney TJ, Kelsh RN, Appel B (2006) In vivo time-lapse imaging shows dynamic oligodendrocyte progenitor behavior during zebrafish development. Nat Neurosci 9:1506–1511.

Klugmann M, Schwab MH, Pühlhofer A, Schneider A, Zimmermann F, Griffiths IR, Nave KA (1997) Assembly of CNS myelin in the absence of proteolipid protein. Neuron 18:59–70.

Kogata N, Tribe RM, Fässler R, Way M, Adams RH (2009) Integrin-linked kinase controls vascular wall formation by negatively regulating Rho/ROCK-mediated vascular smooth muscle cell contraction. Genes Dev 23:2278–2283.

Lafrenaye AD, Fuss B (2010) Focal adhesion kinase can play unique and opposing roles in regulating the morphology of differentiating oligodendrocytes. J Neurochem 115:269–282.

Lang J, Maeda Y, Bannerman P, Xu J, Horiuchi M, Pleasure D, Guo F (2013) Adenomatous polyposis coli regulates oligodendroglial development. J Neurosci 33:3113–3130.

Lau LW, Cua R, Keough MB, Haylock-Jacobs S, Yong VW (2013) Pathophysiology of the brain extracellular matrix: a new target for remyelination. Nat Rev Neurosci 14:722–729.

Laursen LS, Chan CW, ffrench-Constant C (2009) An integrin-contactin complex regulates CNS myelination by differential Fyn phosphorylation. J Neurosci 29:9174–9185.

Le Bras B, Chatzopoulou E, Heydon K, Martínez S, Ikenaka K, Prestoz L, Spassky N, Zalc B, Thomas J-L (2005) Oligodendrocyte development in the embryonic brain: the contribution of the plp lineage. Int J Dev Biol 49:209–220.

Lee J, Gravel M, Zhang R, Thibault P, Braun PE (2005) Process outgrowth in oligodendrocytes is mediated by CNP, a novel microtubule assembly myelin protein. J Cell Biol 170:661–673.

Lee KK, de Repentigny Y, Saulnier R, Rippstein P, Macklin WB, Kothary R (2006) Dominant-negative beta1 integrin mice have region-specific myelin defects accompanied by alterations in MAPK activity. Glia 53:836–844.

Lee S, Chong SYC, Tuck SJ, Corey JM, Chan JR (2013) A rapid and reproducible assay for modeling myelination by oligodendrocytes using engineered nanofibers. Nat Protoc 8:771–782.

Lee S, Leach MK, Redmond SA, Chong SYC, Mellon SH, Tuck SJ, Feng Z-Q, Corey JM, Chan JR (2012a) A culture system to study oligodendrocyte myelination processes using engineered nanofibers. Nat Methods 9:917–922.

Lee Y, Morrison BM, Li Y, Lengacher S, Farah MH, Hoffman PN, Liu Y, Tsingalia A, Jin L, Zhang P-W, Pellerin L, Magistretti PJ, Rothstein JD (2012b) Oligodendroglia metabolically support axons and contribute to neurodegeneration. Nature 487:443–448.

Legate KR, Montañez E, Kudlacek O, Fässler R (2006) ILK, PINCH and parvin: the tIPP of integrin signalling. Nat Rev Mol Cell Biol 7:20–31.

Li W, Zhang B, Tang J, Cao Q, Wu Y, Wu C, Guo J, Ling E-A, Liang F (2007) Sirtuin 2, a mammalian homolog of yeast silent information regulator-2 longevity regulator, is an oligodendroglial protein that decelerates cell differentiation through deacetylating alpha-tubulin. J Neurosci 27:2606–2616.

Liang X, Draghi NA, Resh MD (2004) Signaling from integrins to Fyn to Rho family GTPases regulates morphologic differentiation of oligodendrocytes. J Neurosci 24:7140–7149.

Liu J, Dietz K, DeLoyht JM, Pedre X, Kelkar D, Kaur J, Vialou V, Lobo MK, Dietz DM, Nestler EJ, Dupree J, Casaccia P (2012) Impaired adult myelination in the prefrontal cortex of socially isolated mice. Nat Neurosci 15:1621–1623.

Lowery LA, Van Vactor D (2009) The trip of the tip: understanding the growth cone machinery. Nat Rev Mol Cell Biol 10:332–343.

Lu QR, Sun T, Zhu Z, Ma N, Garcia M, Stiles CD, Rowitch DH (2002) Common developmental requirement for Olig function indicates a motor neuron/oligodendrocyte connection. Cell 109:75–86.

Lucas FR, Goold RG, Gordon-Weeks PR, Salinas PC (1998) Inhibition of GSK-3beta leading to the loss of phosphorylated MAP-1B is an early event in axonal remodelling induced by WNT-7a or lithium. J Cell Sci 111 (Pt 1:1351–1361.

Lunn KF, Baas PW, Duncan ID (1997) Microtubule organization and stability in the oligodendrocyte. J Neurosci 17:4921–4932.

Machesky LM, Hall A (1997) Role of actin polymerization and adhesion to extracellular matrix in Rac- and Rho-induced cytoskeletal reorganization. J Cell Biol 138:913–926.

Macklin WB, Campagnoni CW, Deininger PL, Gardinier M V (1987) Structure and expression of the mouse myelin proteolipid protein gene. J Neurosci Res 18:383–394.

Maier O, van der Heide T, van Dam A-M, Baron W, de Vries H, Hoekstra D (2005) Alteration of the extracellular matrix interferes with raft association of neurofascin in oligodendrocytes. Potential significance for multiple sclerosis? Mol Cell Neurosci 28:390–401.

Makinodan M, Rosen KM, Ito S, Corfas G (2012) A critical period for social experience-dependent oligodendrocyte maturation and myelination. Science 337:1357–1360.

Mallon BS, Shick HE, Kidd GJ, Macklin WB (2002) Proteolipid promoter activity distinguishes two populations of NG2-positive cells throughout neonatal cortical development. J Neurosci 22:876–885.

Marcos S, Moreau J, Backer S, Job D, Andrieux A, Bloch-Gallego E (2009) Tubulin tyrosination is required for the proper organization and pathfinding of the growth cone. PLoS One 4:e5405.

McDonald PC, Fielding AB, Dedhar S (2008) Integrin-linked kinase--essential roles in physiology and cancer biology. J Cell Sci 121:3121–3132.

Medeiros NA, Burnette DT, Forscher P (2006) Myosin II functions in actin-bundle turnover in neuronal growth cones. Nat Cell Biol 8:215–226.

Mi S, Miller RH, Lee X, Scott ML, Shulag-Morskaya S, Shao Z, Chang J, Thill G, Levesque M, Zhang M, Hession C, Sah D, Trapp B, He Z, Jung V, McCoy JM, Pepinsky RB (2005) LINGO-1 negatively regulates myelination by oligodendrocytes. Nat Neurosci 8:745–751.

Michailov G V, Sereda MW, Brinkmann BG, Fischer TM, Haug B, Birchmeier C, Role L, Lai C, Schwab MH, Nave K-A (2004) Axonal neuregulin-1 regulates myelin sheath thickness. Science 304:700–703.

Michalski J-P, Anderson C, Beauvais A, De Repentigny Y, Kothary R (2011) The proteolipid protein promoter drives expression outside of the oligodendrocyte lineage during embryonic and early postnatal development. PLoS One 6:e19772.

Miller MJ, Kangas CD, Macklin WB (2009) Neuronal expression of the proteolipid protein gene in the medulla of the mouse. J Neurosci Res 87:2842–2853.

Milner R, Ffrench-Constant C (1994) A developmental analysis of oligodendroglial integrins in primary cells: changes in alpha v-associated beta subunits during differentiation. Development 120:3497–3506.

Milner R, Frost E, Nishimura S, Delcommenne M, Streuli C, Pytela R, Ffrench-Constant C (1997) Expression of alpha vbeta3 and alpha vbeta8 integrins during oligodendrocyte precursor differentiation in the presence and absence of axons. Glia 21:350–360.

Mishima W, Suzuki A, Yamaji S, Yoshimi R, Ueda A, Kaneko T, Tanaka J, Miwa Y, Ohno S, Ishigatsubo Y (2004) The first CH domain of affixin activates Cdc42 and Rac1 through alphaPIX, a Cdc42/Rac1-specific guanine nucleotide exchanging factor. Genes Cells 9:193–204.

Mitra SK, Hanson DA, Schlaepfer DD (2005) Focal adhesion kinase: in command and control of cell motility. Nat Rev Mol Cell Biol 6:56–68.

Montanez E, Wickström SA, Altstätter J, Chu H, Fässler R (2009) Alpha-parvin controls vascular mural cell recruitment to vessel wall by regulating RhoA/ROCK signalling. EMBO J 28:3132–3144.

Muzumdar MD, Tasic B, Miyamichi K, Li L, Luo L (2007) A global double-fluorescent Cre reporter mouse. Genesis 45:593–605.

Nadon NL, Miller S, Draeger K, Salvaggio M (1997) Myelin proteolipid DM20: evidence for function independent of myelination. Int J Dev Neurosci 15:285–293.

Nadon NL, West M (1998) Myelin proteolipid protein: function in myelin structure is distinct from its role in oligodendrocyte development. Dev Neurosci 20:533–539.

Narayanan SP, Flores AI, Wang F, Macklin WB (2009) Akt signals through the mammalian target of rapamycin pathway to regulate CNS myelination. J Neurosci 29:6860–6870.

Nave K-A (2010a) Myelination and support of axonal integrity by glia. Nature 468:244–252.

Nave K-A (2010b) Myelination and the trophic support of long axons. Nat Rev Neurosci 11:275–283.

Nave KA, Lai C, Bloom FE, Milner RJ (1987) Splice site selection in the proteolipid protein (PLP) gene transcript and primary structure of the DM-20 protein of central nervous system myelin. Proc Natl Acad Sci U S A 84:5665–5669.

O'Meara RW, Michalski J-P, Anderson C, Bhanot K, Rippstein P, Kothary R (2013) Integrin-linked kinase regulates process extension in oligodendrocytes via control of actin cytoskeletal dynamics. J Neurosci 33:9781–9793.

O'Meara RW, Michalski J-P, Kothary R (2011a) Integrin signaling in oligodendrocytes and its importance in CNS myelination. J Signal Transduct 2011:354091.

O'Meara RW, Ryan SD, Colognato H, Kothary R (2011b) Derivation of Enriched Oligodendrocyte Cultures and Oligodendrocyte/Neuron Myelinating Co-cultures from Post-natal Murine Tissues. J Vis Exp JoVE:1–9.

Pedraza L, Huang JK, Colman D (2009) Disposition of axonal caspr with respect to glial cell membranes: Implications for the process of myelination. J Neurosci Res 87:3480–3491.

Peitz M, Pfannkuche K, Rajewsky K, Edenhofer F (2002) Ability of the hydrophobic FGF and basic TAT peptides to promote cellular uptake of recombinant Cre recombinase: a tool for efficient genetic engineering of mammalian genomes. Proc Natl Acad Sci U S A 99:4489–4494.

Pereira JA, Benninger Y, Baumann R, Gonçalves AF, Ozçelik M, Thurnherr T, Tricaud N, Meijer D, Fässler R, Suter U, Relvas JB (2009) Integrin-linked kinase is required for radial sorting of axons and Schwann cell remyelination in the peripheral nervous system. J Cell Biol 185:147–161.

Pribyl TM, Campagnoni C, Kampf K, Handley VW, Campagnoni AT (1996a) The major myelin protein genes are expressed in the human thymus. J Neurosci Res 45:812–819.

Pribyl TM, Campagnoni CW, Kampf K, Kashima T, Handley VW, McMahon J, Campagnoni AT (1996b) Expression of the myelin proteolipid protein gene in the human fetal thymus. J Neuroimmunol 67:125–130.

Puckett C, Hudson L, Ono K, Friedrich V, Benecke J, Dubois-Dalcq M, Lazzarini RA (1987) Myelin-specific proteolipid protein is expressed in myelinating Schwann cells but is not incorporated into myelin sheaths. J Neurosci Res 18:511–518.

Purro SA, Ciani L, Hoyos-Flight M, Stamatakou E, Siomou E, Salinas PC (2008) Wnt regulates axon behavior through changes in microtubule growth directionality: a new role for adenomatous polyposis coli. J Neurosci 28:8644–8654.

Rajasekharan S, Baker KA, Horn KE, Jarjour AA, Antel JP, Kennedy TE (2009) Netrin 1 and Dcc regulate oligodendrocyte process branching and membrane extension via Fyn and RhoA. Development 136:415–426.

Rajasekharan S, Bin JM, Antel JP, Kennedy TE (2010) A central role for RhoA during oligodendroglial maturation in the switch from netrin-1-mediated chemorepulsion to process elaboration. J Neurochem 113:1589–1597.

Readhead C, Popko B, Takahashi N, Shine HD, Saavedra RA, Sidman RL, Hood L (1987) Expression of a myelin basic protein gene in transgenic shiverer mice: correction of the dysmyelinating phenotype. Cell 48: 703-12.

Relucio J, Menezes MJ, Miyagoe-Suzuki Y, Takeda S, Colognato H (2012) Laminin regulates postnatal oligodendrocyte production by promoting oligodendrocyte progenitor survival in the subventricular zone. Glia 60:1451–1467.

Relucio J, Tzvetanova ID, Ao W, Lindquist S, Colognato H (2009) Laminin alters fyn regulatory mechanisms and promotes oligodendrocyte development. J Neurosci 29:11794–11806.

Relvas JB, Setzu A, Baron W, Buttery PC, LaFlamme SE, Franklin RJ, ffrench-Constant C (2001) Expression of dominant-negative and chimeric subunits reveals an essential role for beta1 integrin during myelination. Curr Biol 11:1039–1043.

Richardson WD, Kessaris N, Pringle N (2006) Oligodendrocyte wars. Nat Rev Neurosci 7:11–18.

Ridley AJ (2011) Life at the leading edge. Cell 145:1012–1022.

Rivers LE, Young KM, Rizzi M, Jamen F, Psachoulia K, Wade A, Kessaris N, Richardson WD (2008) PDGFRA/NG2 glia generate myelinating oligodendrocytes and piriform projection neurons in adult mice. Nat Neurosci 11:1392–1401.

Rosenberg SS, Kelland EE, Tokar E, De la Torre AR, Chan JR (2008) The geometric and spatial constraints of the microenvironment induce oligodendrocyte differentiation. Proc Natl Acad Sci U S A 105:14662–14667.

Rosenberger G, Jantke I, Gal A, Kutsche K (2003) Interaction of alphaPIX (ARHGEF6) with beta-parvin (PARVB) suggests an involvement of alphaPIX in integrin-mediated signaling. Hum Mol Genet 12:155–167.

Roussarie J-P, Ruffié C, Brahic M (2007) The role of myelin in Theiler's virus persistence in the central nervous system. PLoS Pathog 3:e23.

Rumsby M, Afsari F, Stark M, Hughson E (2003) Microfilament and microtubule organization and dynamics in process extension by central glia-4 oligodendrocytes: evidence for a microtubule organizing center. Glia 42:118–129.

Sakai T, Li S, Docheva D, Grashoff C, Sakai K, Kostka G, Braun A, Pfeifer A, Yurchenco PD, Fässler R (2003) Integrin-linked kinase (ILK) is required for polarizing the epiblast, cell adhesion, and controlling actin accumulation. Genes Dev 17:926–940.

Sarret C, Combes P, Micheau P, Gelot A, Boespflug-Tanguy O, Vaurs-Barriere C (2010) Novel neuronal proteolipid protein isoforms encoded by the human myelin proteolipid protein 1 gene. Neuroscience 166:522–538.

Schain AJ, Hill RA, Grutzendler J (2014) Label-free in vivo imaging of myelinated axons in health and disease with spectral confocal reflectance microscopy. Nat Med 20:443–449.

Sevc J, Matiašová A, Kútna V, Daxnerová Z (2014) Evidence that the central canal lining of the spinal cord contributes to oligodendrogenesis during postnatal development and adulthood in intact rats. J Comp Neurol.

Simons M, Lyons DA (2013) Axonal selection and myelin sheath generation in the central nervous system. Curr Opin Cell Biol 25:512–519.

Sisková Z, Yong VW, Nomden A, van Strien M, Hoekstra D, Baron W (2009) Fibronectin attenuates process outgrowth in oligodendrocytes by mislocalizing MMP-9 activity. Mol Cell Neurosci 42:234–242.

Snaidero N, Möbius W, Czopka T, Hekking LHP, Mathisen C, Verkleij D, Goebbels S, Edgar J, Merkler D, Lyons DA, Nave K-A, Simons M (2014) Myelin membrane wrapping of CNS axons by PI(3,4,5)P3-dependent polarized growth at the inner tongue. Cell 156:277–290.

Sobel RA, Mitchell ME (1989) Fibronectin in multiple sclerosis lesions. Am J Pathol 135:161–168.

Sobottka B, Ziegler U, Kaech A, Becher B, Goebels N (2011) CNS live imaging reveals a new mechanism of myelination: the liquid croissant model. Glia 59:1841–1849.

Song J, Goetz BD, Baas PW, Duncan ID (2001) Cytoskeletal reorganization during the formation of oligodendrocyte processes and branches. Mol Cell Neurosci 17:624–636.

Soriano P (1999) Generalized lacZ expression with the ROSA26 Cre reporter strain. Nat Genet 21:70–71.

Spassky N, Goujet-Zalc C, Parmantier E, Olivier C, Martinez S, Ivanova A, Ikenaka K, Macklin W, Cerruti I, Zalc B, Thomas JL (1998) Multiple restricted origin of oligodendrocytes. J Neurosci 18:8331–8343.

Spassky N, Olivier C, Perez-Villegas E, Goujet-Zalc C, Martinez S, Thomas J l, Zalc B (2000) Single or multiple oligodendroglial lineages: a controversy. Glia 29:143–148.

Stoffels JMJ, de Jonge JC, Stancic M, Nomden A, van Strien ME, Ma D, Sisková Z, Maier O, Ffrench-Constant C, Franklin RJM, Hoekstra D, Zhao C, Baron W (2013) Fibronectin aggregation in multiple sclerosis lesions impairs remyelination. Brain 136:116–131.

Tang D, Goldberg DJ (2000) Bundling of microtubules in the growth cone induced by laminin. Mol Cell Neurosci 15:303–313.

Taveggia C, Zanazzi G, Petrylak A, Yano H, Rosenbluth J, Einheber S, Xu X, Esper RM, Loeb JA, Shrager P, Chao M V, Falls DL, Role L, Salzer JL (2005) Neuregulin-1 type III determines the ensheathment fate of axons. Neuron 47:681–694.

Terpstra L, Prud'homme J, Arabian A, Takeda S, Karsenty G, Dedhar S, St-Arnaud R (2003) Reduced chondrocyte proliferation and chondrodysplasia in mice lacking the integrin-linked kinase in chondrocytes. J Cell Biol 162:139–148.

Thomson CE, Vouyiouklis DA, Barrie JA, Wease KN, Montague P (2005) Plp gene regulation in the developing murine optic nerve: correlation with oligodendroglial process alignment along the axons. Dev Neurosci 27:27–36.

Thurnherr T, Benninger Y, Wu X, Chrostek A, Krause SM, Nave K-A, Franklin RJM, Brakebusch C, Suter U, Relvas JB (2006) Cdc42 and Rac1 signaling are both required for and act synergistically in the correct formation of myelin sheaths in the CNS. J Neurosci 26:10110–10119.

Timsit S, Martinez S, Allinquant B, Peyron F, Puelles L, Zalc B (1995) Oligodendrocytes originate in a restricted zone of the embryonic ventral neural tube defined by DM-20 mRNA expression. J Neurosci 15:1012–1024.

Timsit SG, Bally-Cuif L, Colman DR, Zalc B (1992) DM-20 mRNA is expressed during the embryonic development of the nervous system of the mouse. J Neurochem 58:1172–1175.

Tomassy GS, Berger DR, Chen H-H, Kasthuri N, Hayworth KJ, Vercelli A, Seung HS, Lichtman JW, Arlotta P (2014) Distinct profiles of myelin distribution along single axons of pyramidal neurons in the neocortex. Science 344:319–324.

Trapp BD, Nishiyama A, Cheng D, Macklin W (1997) Differentiation and death of premyelinating oligodendrocytes in developing rodent brain. J Cell Biol 137:459–468.

Tuason MC, Rastikerdar A, Kuhlmann T, Goujet-Zalc C, Zalc B, Dib S, Friedman H, Peterson A (2008) Separate proteolipid protein/DM20 enhancers serve different lineages and stages of development. J Neurosci 28:6895–6903.

Umemori H, Sato S, Yagi T, Aizawa S, Yamamoto T (1994) Initial events of myelination involve Fyn tyrosine kinase signalling. Nature 367:572–576.

Vallstedt A, Klos JM, Ericson J (2005) Multiple dorsoventral origins of oligodendrocyte generation in the spinal cord and hindbrain. Neuron 45:55–67.

Van Horssen J, Bö L, Vos CMP, Virtanen I, de Vries HE (2005) Basement membrane proteins in multiple sclerosis-associated inflammatory cuffs: potential role in influx and transport of leukocytes. J Neuropathol Exp Neurol 64:722–729.

Van Horssen J, Dijkstra CD, de Vries HE (2007) The extracellular matrix in multiple sclerosis pathology. J Neurochem 103:1293–1301.

Vitriol EAA, Zheng JQQ (2012) Growth Cone Travel in Space and Time: the Cellular Ensemble of Cytoskeleton, Adhesion, and Membrane. Neuron 73:1068–1081.

Wake H, Lee PR, Fields RD (2011) Control of local protein synthesis and initial events in myelination by action potentials. Science 333:1647–1651.

Wang H, Rusielewicz T, Tewari A, Leitman EM, Einheber S, Melendez-Vasquez C V (2012) Myosin II is a negative regulator of oligodendrocyte morphological differentiation. J Neurosci Res 90:1547–1556.

Wang H, Tewari A, Einheber S, Salzer JL, Melendez-Vasquez C V (2008) Myosin II has distinct functions in PNS and CNS myelin sheath formation. J Cell Biol 182:1171–1184.

Watanabe T, Wang S, Noritake J, Sato K, Fukata M, Takefuji M, Nakagawa M, Izumi N, Akiyama T, Kaibuchi K (2004) Interaction with IQGAP1 links APC to Rac1, Cdc42, and actin filaments during cell polarization and migration. Dev Cell 7:871–883.

Wickström SA, Lange A, Hess MW, Polleux J, Spatz JP, Krüger M, Pfaller K, Lambacher A, Bloch W, Mann M, Huber LA, Fässler R (2010a) Integrin-linked kinase controls microtubule dynamics required for plasma membrane targeting of caveolae. Dev Cell 19:574–588.

Wickström SA, Lange A, Montanez E, Fässler R (2010b) The ILK/PINCH/parvin complex: the kinase is dead, long live the pseudokinase! EMBO J 29:281–291.

Wight PA, Duchala CS, Readhead C, Macklin WB (1993) A myelin proteolipid protein-LacZ fusion protein is developmentally regulated and targeted to the myelin membrane in transgenic mice. J Cell Biol 123:443–454.

Wolf RM, Wilkes JJ, Chao M V, Resh MD (2001) Tyrosine phosphorylation of p190 RhoGAP by Fyn regulates oligodendrocyte differentiation. J Neurobiol 49:62–78.

Yamaguchi Y, Katoh H, Yasui H, Mori K, Negishi M (2001) RhoA inhibits the nerve growth factor-induced Rac1 activation through Rho-associated kinase-dependent pathway. J Biol Chem 276:18977–18983.

Ye P, Bagnell R, D'Ercole AJ (2003) Mouse NG2+ oligodendrocyte precursors express mRNA for proteolipid protein but not its DM-20 variant: a study of laser microdissection-captured NG2+ cells. J Neurosci 23:4401–4405.

Yin X, Peterson J, Gravel M, Braun PE, Trapp BD (1997) CNP overexpression induces aberrant oligodendrocyte membranes and inhibits MBP accumulation and myelin compaction. J Neurosci Res 50:238–247.

Young KM, Psachoulia K, Tripathi RB, Dunn S-J, Cossell L, Attwell D, Tohyama K, Richardson WD (2013) Oligodendrocyte dynamics in the healthy adult CNS: evidence for myelin remodeling. Neuron 77:873–885.

Zhou F-Q, Zhou J, Dedhar S, Wu Y-H, Snider WD (2004) NGF-induced axon growth is mediated by localized inactivation of GSK-3beta and functions of the microtubule plus end binding protein APC. Neuron 42:897–912.